THE UNIVERSITY
of EDINBURGH

Stochastic reaction-diffusion models in biology

Stephen Smith

Doctor of Philosophy
University of Edinburgh
September 10, 2018

Declaration

I declare that this thesis was composed by myself and that the work contained therein is my own, except where explicitly stated otherwise in the text. The work has not been submitted for any other degree or professional qualification except as specified. Any included publications are my own work, except where indicated.

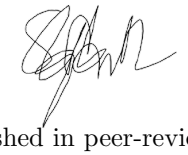

This thesis contains work previously published in peer-reviewed journals, specifically:

- Smith, S. and Grima, R., *Breakdown of the reaction-diffusion master equation with nonelementary rates*, Phys. Rev. E (2016), in Chapter 2.
- Smith, S., Cianci, C. and Grima, R., *Analytical approximations for spatial stochastic gene expression in single cells and tissues*, J. R. Soc. Interface (2016), in Chapter 3.
- Smith, S. and Grima, R., *Single-cell variability in multicellular organisms*, Nat. Comm., (2018), in Chapter 4.
- Smith, S. and Grima, R., *Fast simulation of Brownian dynamics in a crowded environment*, J. Chem. Phys. (2017), in Chapter 5.
- Smith, S., Cianci, C. and Grima, R., *Macromolecular crowding directs the motion of small molecules inside cells*, J. R. Soc. Interface, (2017), in Chapter 6

In addition, the following articles were completed during the work on this thesis, but are not directly related to its contents:

- Smith, S. and Shahrezaei, V., *General transient solution of the one-step master equation in one dimension*, Phys. Rev. E (2015),
- Smith, S., Cianci, C. and Grima, R., *Model reduction for stochastic chemical systems with abundant species*, J. Chem. Phys. (2015),
- Cianci, C., Smith, S. and Grima, R., *Molecular finite-size effects in stochastic models of equilibium chemical systems*, J. Chem. Phys. (2016),
- Cianci, C., Smith, S. and Grima, R., *Capturing Brownian dynamics with an on-lattice model of hard-sphere diffusion*, Phys. Rev. E, (2017),
- Smith, S. and Grima, R., *Model reduction for stochastic reaction systems*, chapter in *Stochastic Processes, Multiscale Modeling, and Numerical Methods for Computational Cellular Biology*, Springer (2017),
- Smith, S. and Dalchau, N., *Model reduction enables Turing instability analysis of large reaction-diffusion models*, J. R. Soc. Interface, (2018).

I would like to express my gratitude to Pippa Mitchell, Fred Smith, and Lucy McGovern for their continuous and unconditional support. I am indebted to my supervisor, Dr Ramon Grima, for his support, guidance and dedication to my project, and also to my committee members, Dr Baojun Wang and Dr Nikola Popovic, for their advice and assistance. I am grateful to Dr Vahid Shahrezaei, for his support during the earlier stages of my PhD, and to Dr Neil Dalchau, during the later stages. I thank the members of our group, Dr Harriet Jones, Dr Philipp Thomas, Dr Claudia Cianci, Dr David Schnoerr, Abhishek Gupta, and Dr Edward Cao, for sharing their time and wisdom with me over the last four years. I would finally like to thank Dr. Konstantinos Zygalakis and Prof. Radek Erban for their time spent in reviewing this thesis, and their comments which have signifcantly improved it.

Abstract

Every cell contains several millions of diffusing and reacting biological molecules. The interactions between these molecules ultimately manifest themselves in all aspects of life, from the smallest bacterium to the largest whale. One of the greatest open scientific challenges is to understand how the microscopic chemistry determines the macroscopic biology.

Key to this challenge is the development of mathematical and computational models of biochemistry with molecule-level detail, but which are sufficiently coarse to enable the study of large systems at the cell or organism scale. Two such models are in common usage: the reaction-diffusion master equation, and Brownian dynamics. These models are utterly different in both their history and in their approaches to chemical reactions and diffusion, but they both seek to address the same reaction-diffusion question.

Here we make an in-depth study into the physical validity of these models under various biological conditions, determining when they can reliably be used. Taking each model in turn, we propose modifications to the models to better model the realities of the cellular environment, and to enable more efficient computational implementations. We use the models to make predictions about how and why cells behave the way they do, from mechanisms of self-organisation to noise reduction. We conclude that both models are extremely powerful tools for clarifying the details of the mysterious relationship between chemistry and biology.

Lay Summary

Chemical reactions inside cells are influenced both by the diffusion of the reactants (spatial effects) and the random timing of reactions (stochastic effects). Spatial stochastic mathematical models of biochemistry are consequently an important research area for understanding what goes on inside cells.

In this thesis, we perform an in-depth study of the two most popular spatial stochastic models: the reaction-diffusion master equation (RDME), and Brownian dynamics (BD). We ask questions about when it is appropriate to use these models, and what the relative advantages of each model are. We use both models to make testable predictions about real biology, and test them with experimental data and computer simulations.

We conclude that both RDME and BD are extremely useful approaches for understanding biology, and will grow in popularity as computational power increases.

Contents

Abstract **5**

Lay Summary **7**

1 Introduction **11**
1.1 The reaction-diffusion master equation . . . 12
1.2 Brownian dynamics . . . 23
1.3 Summary . . . 31

2 The validity of the reaction-diffusion master equation **33**
2.1 Convergence of the RDME . . . 33
2.1.1 The CME . . . 34
2.1.2 The RDME . . . 34
2.1.3 The RDME in the limit of fast diffusion . . . 35
2.1.4 The RDME and the CME in the limits of fast diffusion and large volumes 36
2.2 Examples of convergent and non-convergent propensities . . . 37
2.2.1 Convergent propensities . . . 37
2.2.2 Non-convergent propensities . . . 38
2.3 Simple convergent and non-convergent example systems . . . 39
2.3.1 A convergent example . . . 39
2.3.2 A non-convergent example . . . 40
2.4 Summary . . . 42

3 Analytical approaches to the reaction-diffusion master equation **45**
3.1 Effective mesoscopic rate equations (EMRE) . . . 45
3.2 The spatial EMRE (sEMRE) . . . 47
3.3 Application . . . 53
3.3.1 Comparison of BD with sEMRE . . . 56
3.3.2 sEMRE of the volume-excluded RDME . . . 57
3.4 Summary . . . 59

4 The reaction-diffusion master equation as a tissue model **61**
4.1 Illustratory examples . . . 61
4.2 Theory . . . 64
4.3 Verification of theory using stochastic simulations . . . 66
4.4 Application to experimental data . . . 68
4.5 Summary . . . 71

5 Accelerated Brownian dynamics using implicit crowder molecules **73**
5.1 Point particles in a crowded environment . . . 73
5.1.1 Derivation . . . 74
5.1.2 Comparative tests . . . 78
5.1.3 A note on more complex systems . . . 82
5.2 Finite-size particles in a crowded environment . . . 83
5.2.1 Derivation . . . 84
5.2.2 Comparative tests . . . 85

5.3 Summary 90

6 Analytical approaches to Brownian dynamics **91**
6.1 Diffusion equations with macromolecular crowding 91
6.2 Applications 94
6.3 Summary 98

7 Discussion **99**

Chapter 1

Introduction

Chemical reactions are the building blocks of biology. Substrates bind to enzymes, messenger RNA binds to ribosomes, proteins bind to DNA, amino acids bind to each other – the cumulative effect is ultimately life as we know it. It is perhaps unintuitive to think in these terms, but any observable behaviour of a living organism (e.g. a human reading this sentence) can be understood as a series of interactions between molecules. The question of how microscopic chemistry gives rise to macroscopic biology is one of the greatest open scientific problems. Modelling is key to answering this question: our understanding of the underlying chemistry is good, as is our knowledge of the observable biology; what is missing is a model linking the distinct scales together.

A system can be modelled in a great variety of ways, but not all models are equally useful. It is theoretically possible to model the biochemistry in an entire cell using Schrödinger's equation, but it would not be appropriate. The challenge is to select a model incorporating the salient details of a system, while leaving out the extraneous ones.

For instance, consider a simple molecule like carbon dioxide, CO_2. At the coarsest level, we could model the *concentration* of CO_2, which refers to the total number of carbon dioxide molecules divided by the volume of whatever container the molecules are in (such as a cell, or a test tube). The numerical value which we assign to the concentration will depend on the concentrations of other chemical species in the container, and the rates of any reactions which involve these species. For instance, there might be some molecules of carbon monoxide, CO, and some molecules of oxygen, O, and there might be a reaction of the form:

$$CO + O \xrightarrow{k} CO_2, \tag{1.1}$$

where k denotes the rate at which CO and O are converted into CO_2. The basic model which describes chemical kinetics at this level of complexity is the rate equations (REs) [1].

Alternatively at a considerably more complex level we could model each atom of each molecule individually, by considering the forces exerted by each atom in the volume on every other atom. The three atoms which make up any single CO_2 molecule are bonded together and so will exert very strong forces on each other (these forces are traditionally modelled as springs), but they will also experience weaker forces from the rest of the atoms (e.g. electrostatic forces). This is a more complex model because if our container contains, say, 1000 C atoms and 2000 O atoms we will need to keep track of 9000 distinct quantities (the locations of each atom in 3 spatial dimensions) as well as physical properties of the system (the volume of the container, the nature of its boundaries, the temperature, etc.) rather than 3 in the REs (the concentrations of each species). The basic model which describes chemical kinetics at this level of complexity is molecular dynamics (MD) [2].

There are a huge variety of models spanning the range of complexity from the REs to MD. We can imagine these models as points on a "complexity scale", ranging from the coarsest (the REs) to the extremely complex (the Schrödinger equation), as shown in Fig. 1.1. On the left, we find the REs. As we move up the complexity scale, we gain microscopic detail at the cost of more difficult mathematics or longer computation times, ultimately resulting in MD. For example, one of the main assumptions behind the REs is that the diffusion coefficients of all

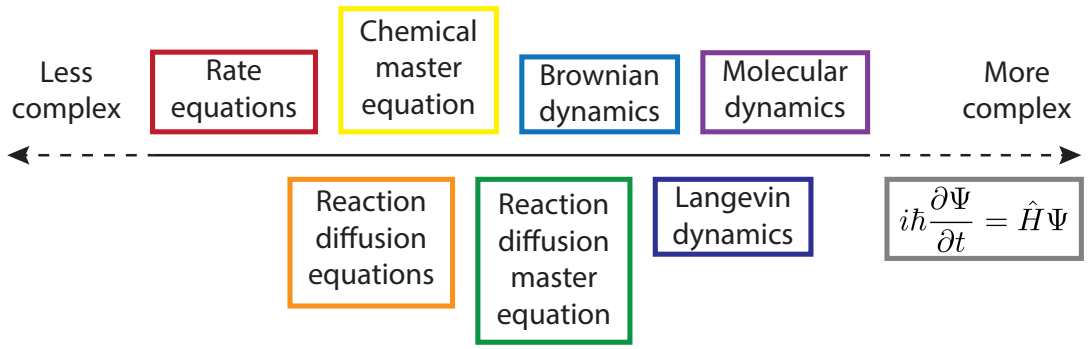

Figure 1.1: The scale of model complexity, ranging from coarse to extremely complex. Between the extremes are the models of interest in chemical kinetics, ranging from the rate equations (red) to molecular dynamics (violet). Reviews of the models *not* studied in-depth in this thesis can be found in Refs. [3, 4, 5].

molecules are infinitely fast – relaxing this assumption pushes us up the complexity scale to a model known as the reaction-diffusion equations (RDEs) [3], which is always going to be more accurate than the REs, but correspondingly will always incur a greater computational cost.

The two models which are the subject of this thesis are at an intermediate level of complexity: the reaction-diffusion master equation (RDME) [6] and Brownian dynamics (BD) [7]. As we will go on to show, these models are very different, though they both model the same kinds of processes at roughly the same level of detail. Unlike the REs, the RDME and BD both acknowledge that molecules are discrete entities, but they do not go down to atomic-level resolution like MD. The RDME and BD do not explicitly model water molecules (unlike MD), but they do model the *effect* of water molecules (diffusion) which is beyond the scope of the REs.

The reason for focussing on the RDME and BD is that they are likely to be the appropriate level of modelling detail for understanding the link between microscopic chemistry and macroscopic biology [8]. They are the simplest models which explicitly model individual reactions and the diffusion of individual molecules, and so are not too distant from chemistry as we understand it intuitively. Yet they are not too computationally intensive: both models have already been used to study systems on the scale of an entire cell [9, 10, 11, 12], and it is surely only a matter of time until multicellular organisms are within their scope.

In the remainder of this introduction, we lay out the the derivations of the RDME and BD starting from basic physical principles, setting the groundwork for the main sections to follow.

1.1 The reaction-diffusion master equation

Consider the following chemical reaction system:

$$A + B \underset{k_2}{\overset{k_1}{\rightleftharpoons}} C. \tag{1.2}$$

This denotes that a molecule of type A can bind to a molecule of type B to create a molecule of type C, and that this process occurs with rate k_1. Furthermore, a molecule of type C can spontaneously unbind into one molecule of type A and one molecule of type B, a process which occurs with rate k_2. As already mentioned, the simplest method of modelling systems like (1.2) is to describe the concentrations (number of molecules per unit volume) of A, B, and C as differentiable functions of time, denoted $[A]$, $[B]$, and $[C]$ respectively. These functions are

implictly defined as the solutions to a set of ordinary differential equations, the REs:

$$\begin{aligned}\frac{d[A]}{dt} &= -k_1[A][B] + k_2[C], \\ \frac{d[B]}{dt} &= -k_1[A][B] + k_2[C], \\ \frac{d[C]}{dt} &= k_1[A][B] - k_2[C].\end{aligned} \tag{1.3}$$

The equation for $\frac{d[A]}{dt}$, for example, states that the rate of change of $[A]$ is equal to minus the rate at which A molecules are removed from the system (the rate of the binding reaction, k_1, multiplied by the product of concentrations of the reactants, $[A][B]$) plus the rate at which A molecules are added to the system (the rate of the unbinding reaction, k_2, multiplied by the concentration of the reactant, $[C]$). The functional form of these rates follows from the principle of mass action kinetics [13], which states that the rate of a reaction is proportional to the product of concentrations of the reactants.

Eq. (1.3) can be solved exactly, given initial concentrations of species A, B, and C, say, $[A]_0$, $[B]_0$, and $[C]_0$ respectively. The solution proceeds by noting that two quantities are conserved, no matter which reactions take place. First, $[A] - [B]$ must remain constant, since any change in $[A]$ can occur when and only when $[B]$ changes by an identical amount; therefore $[A] - [B] = [A]_0 - [B]_0$. Second, $[A] + [B] + 2[C]$ must remain constant, since any change in $[A]$ and $[B]$ occurs when and only when an opposite change occurs in $[C]$; therefore $[A]+[B]+2[C] = [A]_0 + [B]_0 + 2[C]_0$. Substituting these conservation laws into Eq. (1.3), leads to a simplified ODE for $[A]$ alone:

$$\frac{d[A]}{dt} = -k_1[A]^2 + (k_1[A]_0 - k_1[B]_0 - k_2)[A] + k_2([A]_0 + [C]_0). \tag{1.4}$$

The solution to Eq. (1.4)is:

$$[A] = \frac{-1}{2k_1}\left(-[A]_0k_1 + [B]_0k_1 + k_2 + K\tan\left[\frac{1}{2}Kt - \arctan\left[\frac{([A]_0 + [B]_0)k_1 + k_2}{K}\right]\right]\right), \tag{1.5}$$

where $K = \sqrt{-([A]_0 - [B]_0)^2k_1^2 - 2([A]_0 + [B]_0 + 2[C]_0)k_1k_2 - k_2^2}$. Eq. (1.5) gives the value of $[A]$ at any point in the future, and simple manipulation with the conservation laws gives equivalent expressions for $[B]$ and $[C]$. These, or more difficult ODEs, can also be solved using a numerical ODE solver [14].

The REs are simple to derive for any system, simple to understand, and easy to solve with a computer, and therefore they remain by far the most common model of chemical kinetics in use today, in fields ranging from physical chemistry [15] to cell biology [16].

However, the RE model relies heavily on the assumption that concentrations are differentiable functions of time, which is clearly untrue since numbers of molecules must be integer-valued, and therefore discrete. This assumption becomes particularly egregious when the concentrations are small, so that a system may contain only a few tens or hundreds of molecules of each species. In addition to this, it must be noted that chemical kinetics is inherently probabilistic, for a variety of reasons. For one, chemical reactions are quantum mechanical events [17], though the details of this are beyond the scope of this thesis. Another reason is that bimolecular reactions occur only when the two reactants diffuse close enough together to react, and diffusion (the cumulative effect of huge numbers of collisions with water molecules) is such a complex process that it is typically modelled as random [18].

Thinking along the lines of discreteness and randomness leads us to consider not concentrations $[A]$, $[B]$ and $[C]$, but rather the joint probability mass function $P(n_A, n_B, n_C; t)$, the probability that the system contains exactly n_A molecules of A, n_B molecules of B and n_C molecules of C at time t. Though this quantity may seem hopelessly complicated, it turns out that we can say quite a lot about it.

Consider a very short time period Δt, so short that at most one reaction can happen in it, then consider what we can say about $P(n_A, n_B, n_C; t + \Delta t)$ in terms of $P(n_A, n_B, n_C; t)$.

We can end up with exactly n_A, n_B, n_C molecules at time $t + \Delta t$ in three different ways: (I) if there were $n_A + 1, n_B + 1, n_C - 1$ molecules at time t and a binding reaction happened in the interval $[t, t + \Delta t)$; (II) if there were $n_A - 1, n_B - 1, n_C + 1$ molecules at time t and an unbinding reaction happened in $[t, t + \Delta t)$; (III) if there were n_A, n_B, n_C molecules at time t and no reactions happened in $[t, t + \Delta t)$. So we can write:

$$P(n_A, n_B, n_C; t + \Delta t) = P(\mathrm{I}) + P(\mathrm{II}) + P(\mathrm{III}), \tag{1.6}$$

where $P(i)$ represents the probability that scenario (i) happened. By the definition of conditional probability [19], we can write the following for $P(\mathrm{I})$:

$$\begin{aligned} P(\mathrm{I}) &= P(n_A + 1, n_B + 1, n_C - 1 \text{ molecules at time } t \text{ and a binding reaction happened}) \\ &= P(n_A + 1, n_B + 1, n_C - 1; t) \times P(\text{a binding reaction happened in time } \Delta t \\ &\qquad \mid n_A + 1, n_B + 1, n_C - 1 \text{ molecules at time } t), \end{aligned} \tag{1.7}$$

where the conditional symbol $\mid$ means "given that".

At this point in the analysis we need to make an assumption, namely that the waiting times between chemical reactions are exponentially distributed. For unimolecular reactions (i.e. unbinding), Fermi's golden rule implies that waiting times are very close to exponential [20, 21]. For bimolecular reactions (i.e. binding) the reality is more complicated: reacting molecules must diffuse close together, then collide with a sufficiently high energy, at the correct orientation [17]. Although the underlying processes involved here are ultimately deterministic (at least at the level we go to in this thesis), they are so complex that they appear to be random, and the overall waiting time will appear to follow some probability distribution. The exponential distribution is chosen because of the assumption of *memorylessness*, meaning that the future of the system depends only on the current state (i.e. molecule numbers) and not on the states which preceded it. Exponential waiting times are a direct consequence of this assumption.

Though it is a straightforward assumption, it is not strictly true, for instance imagine that a system is currently in the state $(n_A = 10,\ n_B = 10,\ n_C = 10)$. According to the memorylessness assumption, the probability that a binding reaction happens next is independent of how the system got into its current state, whether from state $(n_A = 11,\ n_B = 11,\ n_C = 9)$ and a binding reaction, or from state $(n_A = 9,\ n_B = 9,\ n_C = 11)$ and an unbinding reaction. Yet if an unbinding reaction happened very recently, then we know that the products of that reaction will be close together, and so will be significantly more likely to bind than a typical pair of reactants. In other words, binding reactions are more likely in the immediate aftermath of an unbinding, violating the memorylessness assumption. Choosing the exponential distribution essentially amounts to ignoring this rather subtle effect, but in its favour the exponential distribution has very useful mathematical properties.

One of the nice mathematical properties of exponentially distributed events is that the probability of the event happening in a short interval Δt is proportional to Δt. By the principle of mass action, this probability is also proportional to the number of molecules of the reactants. It follows that we can write:

$$P(\text{binding in time } \Delta t \mid n_A + 1, n_B + 1, n_C - 1 \text{ molecules at } t) = \frac{k_1}{V}(n_A + 1)(n_B + 1)\Delta t, \tag{1.8}$$

where V is the reaction volume.

Why do we write k_1/V instead of just k_1? This is quite a subtle point of statistical physics [22], but it can be intuitively justified by a dimensional argument. Concentrations have units of *inverse volume*, so in order for Eq. (1.3) to be dimensionally consistent, k_1 must have units of *volume per time*, whereas k_2 simply has units of *inverse time*. The extra V is thus required to make Eq. (1.8) dimensionally consistent. It can generally be shown that reactions with n reactants will have their rates scaled by V^{1-n} [22]. This can be intuitively justified by observing that bimolecular reactions will tend to happen less frequently in larger volumes, since it is harder for particles to find each other.

Applying the same arguments to scenarios (II) and (III), we find that we can write Eq.

(1.6) as:

$$\begin{aligned} P(n_A, n_B, n_C; t+\Delta t) =& \frac{k_1}{V}(n_A+1)(n_B+1)\Delta t P(n_A+1, n_B+1, n_C-1; t) \\ &+ k_2(n_C+1)\Delta t P(n_A-1, n_B-1, n_C+1; t) \\ &+ \left(1 - \frac{k_1}{V} n_A n_B \Delta t - k_2 n_C \Delta t\right) P(n_A, n_B, n_C; t). \end{aligned} \tag{1.9}$$

This equation simplifies very nicely to give:

$$\begin{aligned} &\frac{P(n_A, n_B, n_C; t+\Delta t) - P(n_A, n_B, n_C; t)}{\Delta t} = \\ &\quad \frac{k_1}{V}\left[(n_A+1)(n_B+1)P(n_A+1, n_B+1, n_C-1; t) - n_A n_B P(n_A, n_B, n_C; t)\right] \\ &\quad + k_2\left[(n_C+1)P(n_A-1, n_B-1, n_C+1; t) - n_C P(n_A, n_B, n_C; t)\right]. \end{aligned} \tag{1.10}$$

The left-hand side of Eq. (1.10), in the limit of small Δt, is the definition of a derivative, and the right-hand side has no Δt dependence, so we get:

$$\begin{aligned} &\frac{d}{dt}P(n_A, n_B, n_C; t) = \\ &\quad \frac{k_1}{V}\left[(n_A+1)(n_B+1)P(n_A+1, n_B+1, n_C-1; t) - n_A n_B P(n_A, n_B, n_C; t)\right] \\ &\quad + k_2\left[(n_C+1)P(n_A-1, n_B-1, n_C+1; t) - n_C P(n_A, n_B, n_C; t)\right], \end{aligned} \tag{1.11}$$

which is known as the chemical master equation (CME) [22].

As with the REs, Eq. (1.3), Eq. (1.11) can be solved analytically, given initial molecule numbers of species A, B, and C, say, $n_A^{(0)}$, $n_B^{(0)}$, and $n_C^{(0)}$ respectively. Again, the solution proceeds by noting the presence of the same two conservation laws as were used in solving Eq. (1.3): $n_A - n_B = n_A^{(0)} - n_B^{(0)}$, and $n_A + n_B + 2n_C = n_A^{(0)} + n_B^{(0)} + 2n_C^{(0)}$. Substituting these conservation laws into Eq. (1.11), leads to a simplified CME for n_A alone:

$$\begin{aligned} \frac{d}{dt}P(n_A; t) = &\frac{k_1}{V}\left[(n_A+1)(n_A - n_A^{(0)} + n_B^{(0)} + 1)P(n_A+1; t) - n_A(n_A - n_A^{(0)} + n_B^{(0)})P(n_A; t)\right] \\ &+ k_2\left[(n_A^{(0)} + n_C^{(0)} - (n_A-1))P(n_A-1; t) - (n_A^{(0)} + n_C^{(0)} - n_A)P(n_A; t)\right]. \end{aligned} \tag{1.12}$$

The time-dependent solution to Eq. (1.12) can be obtained using a matrix exponential method, such as Ref. [23], however, this does not admit a neat analytical expression, so we will leave it out here. However, the steady-state solution to Eq. (1.12) can be written relatively straighforwardly, using the method outlined in Ref. [24] :

$$P(n_A) = \frac{k_2^{n_A}(n_A^{(0)} + n_C^{(0)})!(-n_A^{(0)} + n_B^{(0)})!}{(k_1/V)^{n_A} n_A!(n_A - n_A^{(0)} + n_B^{(0)})!(n_A^{(0)} + n_C^{(0)} - n_A)!} \tag{1.13}$$

In general, CMEs can be solved numerically using a variety of methods, the most well-known being the finite-state projection method (FSP) [23] in which the problem of solving the CME is mapped on the evaluation of a (typically very large) matrix exponential. Since this approach can become computationally expensive for systems with more than one or two species, simplifications have been developed, such as those based on tensor trains, an analogue of the singular value deocompostion (SVD) for matrices [25]. The CME can also be mapped onto a drift-diffusion equation called the Chemical Fokker Planck Equation (CFPE), for which standard PDE solvers can be used. More recently tensor-based methods [26] and adaptive finite-element methods [27] have been developed to improve speed and accuracy of the solutions.

In special case, simple CMEs can be solved analytically [28, 29, 30, 31, 32, 24, 28, 33, 34]. A

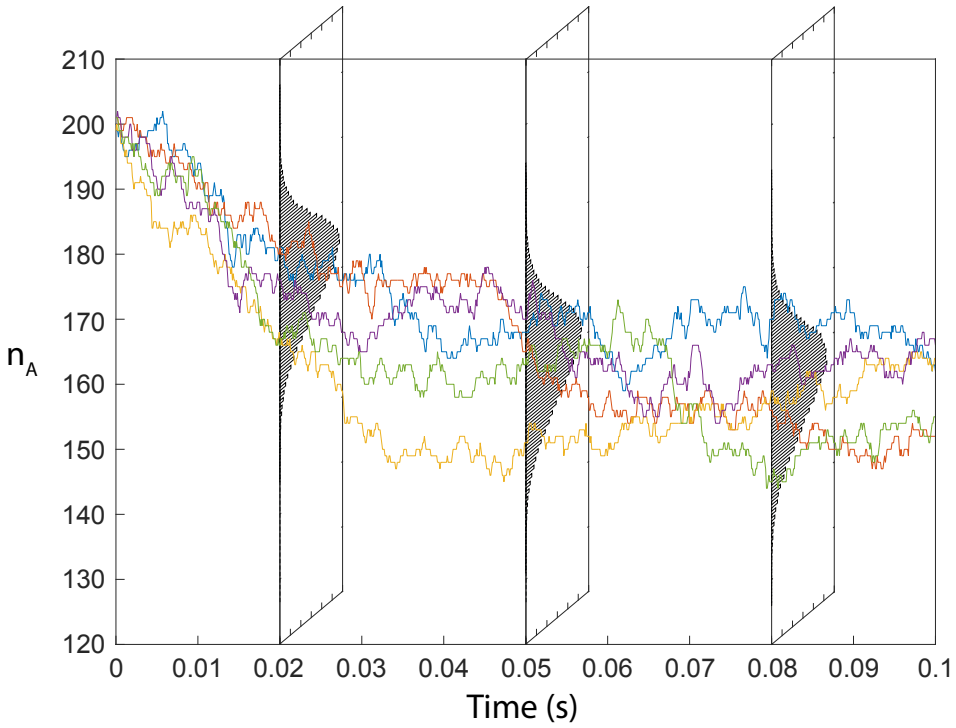

Figure 1.2: Stochastic simulations and analytical solutions of Eq. (1.11). The 5 multicoloured trajectories are independent simulations made using the SSA. Marginal distributions of the exact probability distributions solving Eq. (1.11) are shown as perpendicular grey histograms at $t = 0.02$, 0.05 and 0.08. This makes clear that at each time point t the numerical value of each trajectory is a sample from the probability distribution solving the CME.

less intensive appoach is to approximate either the distribution [35, 36, 37, 38], or the moments (e.g. the mean or variance) of $P(n_A, n_B, n_C; t)$, and a variety of methods are popular such as the Van Kampen approximation [22, 39], moment-closure approximations [40, 41, 42, 43, 44], or the chemical Langevin equation [45, 46]. For a recent review see Ref. [47].

There is an alternative (and much more popular) approach to the CME, which has no analog corresponding to the REs. This approach notes that $P(n_A, n_B, n_C; t)$ is not just any function, but is a probability distribution, and therefore pseudo-random samples can be drawn from it exactly as one might sample from a Gaussian or a Poisson distribution [48]. In fact, $P(n_A, n_B, n_C; t)$ is actually an infinite set of related probability distributions indexed by t, and so a sample will be an entire trajectory of molecule numbers over time. Such trajectories are much more intuitive than the CME itself, because each trajectory represents a particular realisation of what we might actually see if we observed a system in real time. Furthermore, it turns out it is typically computationally much easier to sample from the CME than to solve the CME, and if we take a large number of sample trajectories we can use them to estimate $P(n_A, n_B, n_C; t)$. The reason for this computational difference is that the cost of numerical solution of the CME scales with the number of possible system states (i.e. the number of permissible combinations of molecule numbers), while the cost of sampling scales with the frequency of reactions. Numerically solving the CME will typically only be worthwhile for systems with a small number of states and fast reaction rates.

Sampling trajectories of the CME is typically referred to as "simulating" the underlying system, for obvious reasons. The most common way to simulate is to use Gillespie's stochastic simulation algorithm (SSA) [49], because this algorithm gives statistically exact trajectories, by taking advantage of the fact that the waiting times between reactions are exponentially distributed. The SSA can be quite slow, because it explicitly simulates every reaction, so a huge

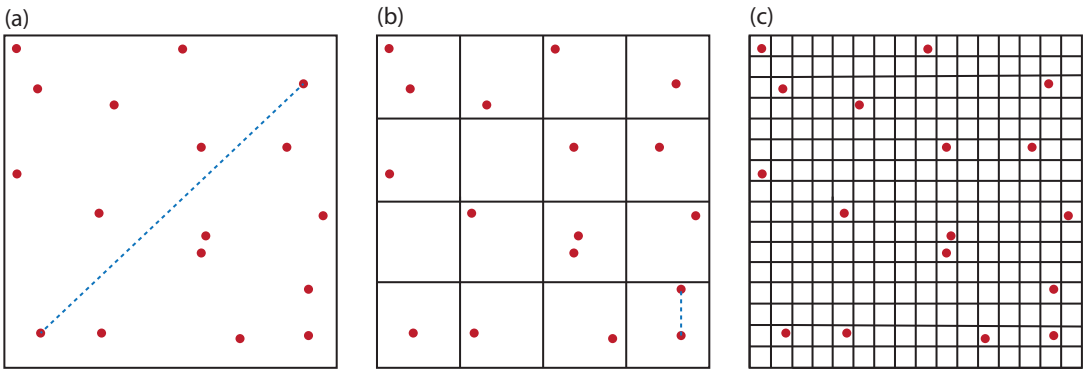

Figure 1.3: The rationale behind dividing a volume into subvolumes. (a) The principle of mass action claims that every reacting pair of molecules is equally likely to react in any time period, including pairs which might be very distant (blue dotted line). (b) One solution is to divide the volume into M subvolumes, and only allow molecules in the same subvolume to react, so reacting pairs are now close together (blue dotted line). (c) If M is too large, then there will very rarely be pairs in the same subvolume, and bimolecular reactions will tend not to happen at all.

number of approximate simulation algorithms has been developed. The most popular is a time-discretised algorithm called τ-leaping, also by Gillespie [50], but new algorithms are proposed every year that typically sacrifice a degree of accuracy for an increase in speed. These include timescale-separation algorithms which simulate "fast" species with the SSA and "slow" species with a CFPE solver [51], or abundance separation algorithms which treat low-concentration species using the SSA, and high-concentration species using the CLE [52], amongst many others [53, 54, 55]. For a recent review see Ref. [56].

The relationship between individual sample trajectories and the CME solution is quite unintuitive, so we have shown an example in Fig. 1.2. The main graph shows 5 independent sample trajectories of the CME Eq. (1.11), showing the number of A molecules n_A over a short time period. Perpendicular to the main graph are three histograms showing the marginal probability distribution $P(n_A;t)$ at three time points $t = 0.02$, 0.05, and 0.08. This representation makes it clear that the values of the trajectories of n_A at $t = 0.02$ (for example) are independent samples of the distribution $P(n_A;0.02)$. There is a one-to-one correspondence between the distributions $P(n_A,n_B,n_C;t)$ and the sample trajectories: if we know the distributions then we can sample trajectories; if we have enough independent trajectories we can approximate the distributions to an arbitrarily high degree of accuracy.

One point that we have not satisfactorily addressed so far is the validity of the principle of mass action, the principle which underpins fundamental equations such as (1.8). The principle of mass action is based on combinatorial arguments: if a reaction has two reactants, A and B say, then the probability of a reaction must be proportional to the number of ways a reacting pair can be made up, i.e. n_An_B different ways; similarly, if a reaction involves two molecules of A reacting with each other, then we would expect the reaction probability to scale as $n_A(n_A-1)/2$.

These arguments are not particularly satisfactory when considered from a microscopic point of view: if no pair of molecules is sufficiently close together to collide and react in a short time Δt, then a reaction will not happen, no matter how many molecules there are over all; or if only 2 (or 3 or 4 or...) pairs is sufficiently close together, then the probability of reaction will be roughly proportional to 2 (or 3 or 4 or...) rather than the total number of pairs. The principle of mass action surely amounts to assuming (nonsensically) that *all* the pairs are sufficiently close together to potentially react in a short time Δt. The absurdity of this assumption is demonstrated graphically in Fig. 1.3 (a). A counter-argument to this is that we have no way of knowing how many pairs are close together, so we stick to assuming that a fixed proportion of them are close together, and absorb the proportionality constant into the reaction rate. But this again is not truly satisfactory because the true proportion of pairs that are close together is itself a random variable and not a constant.

It turns out that the principle of mass action is closely related to the *diffusion* of the reacting molecules. The diffusion coefficient is essentially a measure of the rate at which a randomly diffusing particle moves around the reaction volume. A particle with a very high diffusion coefficient could have diffused all over the volume in a short time Δt, whereas a particle with a small diffusion coefficient may only have covered a small region of space (the average distance covered by a diffusing molecule before it reacts is known as the *Kuramoto length*, see Ref. [57]). It follows that the principle of mass action could plausibly apply if particles have very high diffusion coefficients, so that any pair could potentially collide in a short time Δt. This idea can actually be proved from a microscopic point-of-view (and we will demonstrate this later), but *only if* we assume all particles have infinite (or practically infinite) diffusion coefficients. (Of course the concept of an "infinite diffusion coefficient" is physically impossible, and we will address this point shortly.) Doubting the principle of mass action is then essentially equivalent to believing that the diffusion coefficients might not be high enough for the reaction volume to be well-mixed, and this is a sensible belief as far as cell biology is concerned [58]. Clearly an alternative approach is needed: in particular, we want a model which can tell us how many pairs of particles are "close together" at any given time.

The simplest way to go about this is to subdivide the entire reaction volume into small subvolumes, with the implication that we will consider molecules in the same subvolume to be "close together", while molecules in different subvolumes are not. Suppose we have chosen to divide our volume into M subvolumes, which for simplicity we assume are equally-sized; then the probability of a reaction involving A and B in subvolume i will be proportional to $n_A^{(i)} n_B^{(i)}$, where $n_X^{(i)}$ denotes the number of molecules of species X is subvolume i. This idea is shown in Fig. 1.3 (b).

While superficially satisfying, this description actually raises more questions than it answers, at least at first. Principally, how should we choose M? Clearly we should choose $M > 1$, otherwise the description is identical to the CME, and generally if M is small we will tend to have the same issues with the principle of mass action that the CME had, and which drove us to seek a new model. On the other hand, if we make M very large, the subvolumes will become very small (possibly smaller than the physical size of a molecule) and the probability of two reacting molecules being in the same subvolume at a given time becomes negligible. As shown in Fig. 1.3 (c), this results in bimolecular reactions simply not happening, which is clearly something we would like to avoid.

Choosing the correct partition of the volume into subvolumes requires us to be more specific about what we truly mean by "close together", a phrase about which we have thus far been deliberately vague. To do this we would need to propose a physical model for how chemical reactions occur, including molecular sizes and shapes, how they diffuse, whether they react immediately upon collision or whether they need a sufficiently large kinetic energy, and how electrostatic and hydrodynamic interactions impact on the reaction. These are questions that go far beyond the scope of our models, and which would significantly detract from their simplicity. As a result, the standard response is to be vague about the value of M, suggesting that it should be neither too small nor too large. Though this is not a very satisfying answer, it highlights that there is no value of M which can be pre-specified for all situations: the correct M will depend on a number of factors and will likely be different for different situations, such as different diffusion coefficients.

Another significant issue with this model is how we decide how many molecules are in the i^{th} subvolume. This is an issue because molecules, in reality, do not remain in the same location forever, but diffuse throughout the reaction volume – indeed, it was the issue of diffusion which led us to seek out a new model. To address this issue, drawing on the argument in Ref. [6], we will consider a simplified one-dimensional volume and a single diffusing molecule currently located at a point x. It is well known that the probability density functions of diffusing point-particles obey a partial differential equation (PDE) called the diffusion equation:

$$\frac{\partial}{\partial t} p(x,t) = D \frac{\partial}{\partial x^2} p(x,t), \tag{1.14}$$

where $p(x,t)$ is the probability density of finding the particle at location x at time t, and D is the particle's diffusion coefficient. We can rewrite Eq. (1.14) in terms of small increments Δt

and Δx, and rearrange to get:

$$p(x, t + \Delta t) = p(x, t) + \frac{D\Delta t}{\Delta x^2} [p(x + \Delta x, t) - 2p(x, t) + p(x - \Delta x, t)] + o(\Delta t). \tag{1.15}$$

Now, consider a partition of the total volume into M subvolumes of incremental width Δx, and let subvolume k be centered around the point x. If we denote by $q(k, t)$ the probability that the molecule is in subvolume k at time t, then we will have that:

$$q(k, t) = \int_{x-\Delta x/2}^{x+\Delta x/2} p(y, t)dy \approx p(x, t)\Delta x, \tag{1.16}$$

where the approximation will tend to hold when Δx is small. It follows that we can write:

$$q(k, t + \Delta t) = q(k, t) + \frac{D\Delta t}{\Delta x^2} [q(k + 1, t) - 2q(k, t) + q(k - 1, t)] . \tag{1.17}$$

In other words, in a short time Δt, the probability that the molecule moves from subvolume k to subvolume $k + 1$ is equal to $D\Delta t/\Delta x^2$, provided that Δt is sufficiently small to make this expression a strict probability. Eq. (1.17) has the form of a master equation, which implies that the waiting time for a molecule diffusing between subvolumes is approximately exponential, at least when the subvolumes are small, but it is a reasonable approximation even when the subvolumes are quite large.

This leads us to a model in which particles "hop" between neighbouring subvolumes at random times, and the waiting times between hoppings are exponentially distributed. This means that we can represent hopping events as just another type of reaction event. This seems a little counter-intuitive, but makes sense when studied in detail. Let us consider the system (1.2) again under this model. We can write $X^{(i)}$ to denote the species X in subvolume i. Then we can write the new system in the following way:

$$\begin{aligned}
&A^{(i)} + B^{(i)} \underset{k_2}{\overset{k_1}{\rightleftharpoons}} C^{(i)} && \text{for } i = 1, ..., M, \\
&A^{(i)} \underset{k_D^{(A,j,i)}}{\overset{k_D^{(A,i,j)}}{\rightleftharpoons}} A^{(j)} && \text{for } i, j = 1, ..., M, \\
&B^{(i)} \underset{k_D^{(B,j,i)}}{\overset{k_D^{(B,i,j)}}{\rightleftharpoons}} B^{(j)} && \text{for } i, j = 1, ..., M, \\
&C^{(i)} \underset{k_D^{(C,j,i)}}{\overset{k_D^{(C,i,j)}}{\rightleftharpoons}} C^{(j)} && \text{for } i, j = 1, ..., M,
\end{aligned} \tag{1.18}$$

where $k_D^{(X,i,j)}$ is the "hopping rate"at which a molecule of type X in subvolume i will hop into subvolume j, which will be equal to zero if i and j are not neighbouring subvolumes. Note that we do not use the specific rate obtained in Eq. (1.17), because that rate is derived assuming that the subvolumes are arranged in a particular regular manner, and we would like to retain generality for the time being. Clearly system (1.18) is much more complicated than (1.2), but there is little actual difference in principle. Both systems comprise species, reactions and rates – it just happens that the "species" in system (1.18) are not just the types of molecules (A, B, C) but the types of molecules in a particular subvolume ($A^{(i)}$, $B^{(i)}$, $C^{(i)}$). This might be unintuitive, but it makes no difference mathematically. It follows, then, that any technique which can be applied to system (1.2), can also be applied to system (1.18).

For example, analogously to the REs (1.3), we can write equations for the concentrations

$[A^{(i)}]$, $[B^{(i)}]$ and $[C^{(i)}]$ (intuitively, the local concentrations of A, B and C in subvolume i):

$$\begin{aligned}
\frac{d[A^{(i)}]}{dt} &= -k_1[A^{(i)}][B^{(i)}] + k_2[C^{(i)}] + \sum_{j=1}^{M}\left[-k_D^{(A,i,j)}[A^{(i)}] + k_D^{(A,j,i)}[A^{(j)}]\right], \\
\frac{d[B^{(i)}]}{dt} &= -k_1[A^{(i)}][B^{(i)}] + k_2[C^{(i)}] + \sum_{j=1}^{M}\left[-k_D^{(B,i,j)}[B^{(i)}] + k_D^{(B,j,i)}[B^{(j)}]\right], \\
\frac{d[C^{(i)}]}{dt} &= k_1[A^{(i)}][B^{(i)}] - k_2[C^{(i)}] + \sum_{j=1}^{M}\left[-k_D^{(C,i,j)}[C^{(i)}] + k_D^{(C,j,i)}[C^{(j)}]\right],
\end{aligned} \tag{1.19}$$

where, as before, M is the number of subvolumes. Eq. (1.19) is the analogue of the REs with spatial resolution, but it would be helpful if we had a better idea of the form of the hopping rates $k_D^{(X,i,j)}$. Calculating the hopping rates from microscopic principles is an extremely challenging problem, and in fact is still an open research question. In the simplest case, where each subvolume is an equally-sized cube (or square, or line segment) of side-length h arranged in a cartesian grid, then we have already seen that there is a simple expression:

$$k_D^{(X,i,j)} = \begin{cases} \frac{D_X}{h^2} & \text{if } i \text{ neighbours } j, \\ 0 & \text{otherwise,} \end{cases} \tag{1.20}$$

where D_X is the diffusion coefficient associated with particles of type X.

If we imagine a one-dimensional array of subvolumes of equal size arranged in a line of length L, such that subvolume 1 neighbours subvolume 2, subvolume 2 neighbours subvolumes 1 and 3, subvolume 3 neighbours 2 and 4, etc, then Eq. (1.19) becomes:

$$\begin{aligned}
\frac{d[A^{(i)}]}{dt} &= -k_1[A^{(i)}][B^{(i)}] + k_2[C^{(i)}] + \frac{D_A}{(L/M)^2}\left[[A^{(i-1)}] - 2[A^{(i)}] + [A^{(i+1)}]\right], \\
\frac{d[B^{(i)}]}{dt} &= -k_1[A^{(i)}][B^{(i)}] + k_2[C^{(i)}] + \frac{D_B}{(L/M)^2}\left[[B^{(i-1)}] - 2[B^{(i)}] + [B^{(i+1)}]\right], \\
\frac{d[C^{(i)}]}{dt} &= k_1[A^{(i)}][B^{(i)}] - k_2[C^{(i)}] + \frac{D_C}{(L/M)^2}\left[[C^{(i-1)}] - 2[C^{(i)}] + [C^{(i+1)}]\right],
\end{aligned} \tag{1.21}$$

for $i = 2, ..., M-1$ with small modifications for the end subvolumes 1 and M depending on the boundary conditions. We can now imagine taking the limit $M \to \infty$. There are a couple of issues with this. First, we already noted that choosing subvolumes too small could be a problem because the probability of two molecules being in the same subvolume would become negligibly small, thus making bimolecular reactions unsually rare events. We will bypass this issue by saying that the limit $M \to \infty$ is simply an approximation, which we expect to be accurate when concentrations are high. The second issue is that the notation $[A^{(i)}]$ becomes meaningless when M is infinite. This we will solve by replacing $[A^{(i)}]$ with $[A]$ which we consider to be a function of location $x = \frac{iL}{M}$ as well as time. In the limit $M \to \infty$, x approaches a continuous quantity, so that differentiation with respect to x becomes valid. For example, $\frac{D_A}{(L/M)^2}\left[[A^{(i-1)}] - 2[A^{(i)}] + [A^{(i+1)}]\right]$ converges to $D_A\frac{\partial^2[A]}{\partial x^2}$ in the limit $M \to \infty$. As a result, we get the following PDEs:

$$\begin{aligned}
\frac{\partial[A]}{\partial t} &= -k_1[A][B] + k_2[C] + D_A\frac{\partial^2[A]}{\partial x^2}, \\
\frac{\partial[B]}{\partial t} &= -k_1[A][B] + k_2[C] + D_B\frac{\partial^2[B]}{\partial x^2}, \\
\frac{\partial[C]}{\partial t} &= k_1[A][B] - k_2[C] + D_C\frac{\partial^2[C]}{\partial x^2}.
\end{aligned} \tag{1.22}$$

These PDEs are the well-known reaction-diffusion equations (RDEs), ubiquitous in mathematical biology [3], and popularised by Alan Turing in his seminal paper Ref. [59]. Turing famously

demonstrated that certain systems [60] could be unstable when modelled with the RDEs, but stable when modelled with the REs: this kind of instability manifests itself as visual patterns (e.g. spots, stripes) in an RDE simulation. The Turing instability (as it is now known) is believed by some to be the cause of biological patterns such as zebrafish stripes [61] or the regular spacing between mammalian digits (fingers and toes) [62, 63], but there is still controversy around whether the Turing mechanism is really behind these phenomena [64]. One of the biggest current challenges in synthetic biology is therefore to synthesise a Turing patterning network in living cells [65, 66, 67, 68, 69, 70], which would provide convincing evidence of Turing's theory. Furthermore, recent theoretical work has suggested that stochasticity may be important to Turing pattern formation, allowing for patterns in regions of parameter space where the RDEs predict homogeneous concentrations [71], though the choice of subvolume size in these stochastic models remains an important question [72].

As well as the REs, we can also apply the CME methodology to system (1.18). Instead of the probability mass function $P(n_A, n_B, n_C; t)$, we now consider a new probability mass function $P(\vec{n}_A, \vec{n}_B, \vec{n}_C; t)$, where $\vec{n}_X = (n_X^{(1)}, ..., n_X^{(M)})$ is a vector of molecule numbers, with one entry for each subvolume. Because of the complexity of the RDME, we have to introduce some new notation to be able to write it down compactly: we let $E_{(X,i)}$ be the shift operator which replaces any instance of $n_X^{(i)}$ with $n_X^{(i)} + 1$. For example: $E_{(X,i)} n_X^{(i)} = n_X^{(i)} + 1$, and, $E_{(X,i)}^{-1} n_X^{(i)} = n_X^{(i)} - 1$, and for any function $f(\cdot)$, $E_{(X,i)} f(n_X^{(i)}) = f(n_X^{(i)} + 1)$.

Following the argument for the CME, we consider a time step Δt, sufficiently short that at most one reaction (including hopping events) can occur. Then, we consider the ways we can end up with $\vec{n}_A, \vec{n}_B, \vec{n}_C$ molecules at time $t + \Delta t$. This can happen if: (I) a binding reaction happens in subvolume i, for some $i = 1, ..., M$, in the time interval $[t, t + \Delta t)$; (II) an unbinding reaction happens in subvolume i, for some $i = 1, ..., M$, in $[t, t + \Delta t)$; (III) a particle of type X hops from subvolume i to subvolume j, for some $i, j = 1, ..., M$ and $X \in \{A, B, C\}$, in $[t, t + \Delta t)$; (IV) no reactions happen in the time interval $[t, t + \Delta t)$. Clearly this is much more complicated than for the CME, but exactly the same principles apply, and after some simplification we obtain the following equation:

$$\begin{aligned}
\frac{d}{dt} P(\vec{n}_A, \vec{n}_B, \vec{n}_C; t) = & \sum_{i=1}^{M} \frac{k_1 M}{V} \left[E_{(A,i)} E_{(B,i)} E_{(C,i)}^{-1} - 1 \right] n_A^{(i)} n_B^{(i)} P(\vec{n}_A, \vec{n}_B, \vec{n}_C; t) \\
& + \sum_{i=1}^{M} k_2 \left[E_{(A,i)}^{-1} E_{(B,i)}^{-1} E_{(C,i)} - 1 \right] n_C^{(i)} P(\vec{n}_A, \vec{n}_B, \vec{n}_C; t) \\
& + \sum_{i=1}^{M} \sum_{j=1}^{M} k_D^{(A,i,j)} \left[E_{(A,i)} E_{(A,j)}^{-1} - 1 \right] n_A^{(i)} P(\vec{n}_A, \vec{n}_B, \vec{n}_C; t) \\
& + \sum_{i=1}^{M} \sum_{j=1}^{M} k_D^{(B,i,j)} \left[E_{(B,i)} E_{(B,j)}^{-1} - 1 \right] n_B^{(i)} P(\vec{n}_A, \vec{n}_B, \vec{n}_C; t) \\
& + \sum_{i=1}^{M} \sum_{j=1}^{M} k_D^{(C,i,j)} \left[E_{(C,i)} E_{(C,j)}^{-1} - 1 \right] n_C^{(i)} P(\vec{n}_A, \vec{n}_B, \vec{n}_C; t),
\end{aligned} \tag{1.23}$$

noting the correct volume scaling $\frac{k_1 M}{V}$ for the bimolecular reaction. This equation is known as the reaction-diffusion master equation (RDME). The first two lines correspond to the two reactions in each subvolume, while the final three lines correspond to the hopping of particles of type A, B and C respectively between neighbouring subvolumes.

Now that we have the RDME (which is really just a special type of CME) we can do to it anything that we could do to the CME. For instance, it is possible to solve RDMEs analytically, if they are composed exclusively of certain types of linear reactions [30, 29] or purely reversible reactions [34]. The example (1.18) is actually solvable, as long as the hopping events are reversible (i.e. as long as $k_D^{(X,i,j)} = k_D^{(X,j,i)}$, for all $X = A, B, C$ and $i, j = 1, ..., M$). Other analytical approximation techniques for the CME (e.g. the van Kampen approximation [22],

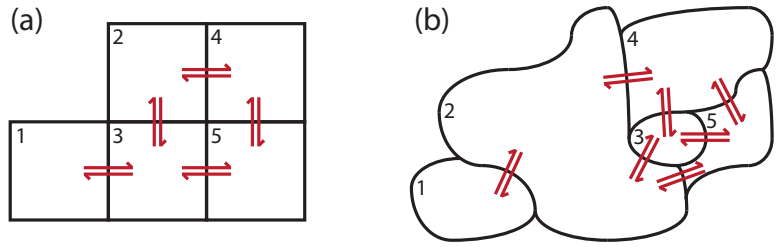

Figure 1.4: (a) If subvolumes are arranged in a grid, all hopping rates are straightforwadly given by Eq. (1.20). (b) If subvolumes are irregular shapes, and boundaries between subvolumes are different sizes, it is not clear how to best choose hopping rates.

and the chemical Langevin equation [45]) can also be applied to the RDME, and have been, with interesting results [73, 74], as we will see in chapter 3.

Any stochastic simulation algorithm designed for the CME can also naturally be applied to the RDME [75, 76, 77, 78]. Several new issues arise when simulating the RDME however. For example, stochastic simulation algorithms tend to have computation time proportional to the frequency of reaction events [49]. If the hopping rates are quite large, then an RDME simulation may take substantially longer than an equivalent CME simulation – it is not uncommon for upwards of 99% of the simulation time to be spent simulating hopping events rather than chemical reactions. This issue in particular has driven a huge amount of research into fast and accurate simulation of the RDME [79, 80, 81, 82].

It is worth going into a little more detail now about the hopping rates $k_D^{(X,i,j)}$. In the simplest case where each subvolume is the same size, Eq. (1.20) can be used. This case is demonstrated in Fig. 1.4 (a): neighbouring subvolumes (such as 1 and 3) all have the same hopping rates between them, whereas non-neighbouring subvolumes (such as 1 and 2) have zero hopping rates. More generally, subvolumes can be any shape and size, and the size of the boundaries where two neighbouring subvolumes join can vary greatly as well. Such a case is shown in Fig. 1.4 (b): neighbouring subvolumes (such as 1 and 2) tend to be different sizes, so the hopping rate in one direction will generally be different from the other; moreover, boundaries between neighbours are not necessarily the same length (such as the boundaries between 2 and 4, and 2 and 5), and shorter boundaries will tend to be crossed by fewer molecules, and so should have correspondingly lower hopping rates. In these cases, the hopping rate should (in principle) be calculated using a first passage time approach with the diffusion equation [83], but this is often computationally unfeasible and in practice there is no easy answer. Some authors have proposed techniques for choosing these rates in a manner which agrees optimally with Brownian diffusion [84, 85, 86, 87, 88, 89, 90], but these are typically simulation-based and not analytically straightforward.

For the time being, we assume that molecules do not occupy any volume themselves (i.e. they are point-particles), but relaxing this assumption leads to even more complex hopping rates, and we will discuss this further in chapters 3, 5 and 6. These rates typically depend on the concentrations of the various species in the destination subvolume j, so that a subvolume with a high concentration of molecules is less likely to be able to accomodate a new molecule hopping into it [91, 92, 93, 34]. Writing the hopping rate as a linear function of the concentrations is a popular choice, but when concentrations are very high certain non-linear functions have been shown to be more accurate [94, 95, 96].

When diffusion coefficients are large, simulations of the RDME can become very slow (because molecules will hop around many times between reactions) [80], and significant modifications to the hopping rates have been introduced to address this issue. In particular, it is common to allow particles to hop between non-neighbouring subvolumes i and j [97]. The implication is that the particle did in fact follow a neighbour-to-neighbour path from i to j, but the intermediate steps are eliminated for speed: a very careful choice of the hopping rates is required in these cases to correctly model diffusion.

We have seen how the RDME was obtained as an extension of the CME, to address the

problem of mass action kinetics. In this sense, the RDME is a *top-down* model, since it is not a simplification of a more detailed microscopic model like Brownian dynamics. The risk with top-down models is that the new components (the hopping rates, in the case of the RDME) could be added in a flawed manner, making the model inconsistent with other well-established models. In short, the RDME is just the CME with some additional terms to explicitly model diffusion, but how do we know that these additional terms are correct?

This question has plagued users of the RDME for decades. A whole subgenre of the reaction-diffusion field is dedicated to comparing the RDME with microscopic models, including various types of Brownian dynamics and molecular dynamics, which are taken to be the "ground truth". Almost invariably, because of the complexities of the models involved, it is stochastic simulations of models which are compared, rather than the actual equations which make up the models [98, 99, 100]. As a result, the outcome of these comparisons is typically to suggest optimal values of the various RDME model parameters (reaction rates, hopping rates, number and size of subvolumes) to get best agreement with the "ground truth" model, for a particular reaction-diffusion system. Such comparisons are therefore very limited in their applicability: there is no reason to believe that the optimal hopping rates (for example) for one system will be the same for another system, even if they are quite similar.

An alternative (though much trickier) approach is to directly compare the RDME with the "ground truth" model by writing out equations for both and discerning to what extent they agree [101, 100, 102]. This kind of comparison will provide general rules about when models agree, and will not generally be limited by system specifics. The challenge is that "ground truth" models tend to be very hard to write down, since they are very complex and are usually conceived as models for simulation rather than mathematical analysis. A pioneer in this kind of comparison is Isaacson, who has published several articles analytically comparing the RDME with a variety of "ground truth" models [103, 104, 105]. Two principal results emerge from Isaacson's work. First, the RDME can be thought of as an approximation to a particular BD model known as the Smoluchowski model [106] (more on this later), but there is no limit in which one converges to the other [104]. It can be rigorously proved that as M increases, the approximation first gets better, then gets worse (while never actually showing perfect agreement), and it is hard to know in general which M is the optimal one. In a similar vein, Hellander et. al. have shown that there exists a hard upper limit on M, above which the RDME cannot agree with the Smoluchowski model because the subvolumes become unphysically smaller than the size of a molecule [107]. Isaacson's second principal result is that the RDME can be modified to create a new model (known as the "convergent RDME", or CRDME) in which molecules can react with molecules in different subvolumes, according to certain strict rules [105]. The CRDME was shown to converge precisely to another BD model known as the $\lambda - \rho$ model [108] (more on this later). Over all, it seems that the RDME never quite sits comfortably with BD, and potentially this could call its accuracy into question. However, as well will see in chapters 3 and 4, the RDME provides an elment of analytical tractability which is absent from BD, and furthermore may be the appropriate description for modelling multicellular systems, such as tissues and biofilms, as we will see in chapter 5.

We have seen how the RDME was derived as an extension of the CME, allowing stochastic models to incorporate diffusion in a logical manner. BD achieves the same goal, but addresses the problem from a completely different point-of-view. While the RDME is a top-down model (formed by systematically adding features to a simple model), BD is a bottom-up model (obtained by systematically simplifying a complex model). In the next section, we study the derivation of BD to understand its assumptions and properties.

1.2 Brownian dynamics

The theory of molecular dynamics (MD) considers systems consisting of particles, each of which exerts forces on the surrounding space, including Van der Waals and electrostatic forces [2, 17]. Imagining a system of N particles, and a particle i with position $\mathbf{x}_i$, we can add up the forces at that point caused by all other particles in the system to get $\mathbf{F}_i(\mathbf{x}_i)$, which is the force that would be felt by particle i.

It is worth going into some detail about what is meant by "particle" in MD. In the most

complex forms of MD, "particle" means "atom" [109, 110, 111]. Atoms which are bonded together into molecules experience spring-like forces between each other, ensuring that their average separation is equal to the empirically calculated bond-length. Alternatively, at the simplest level, each molecule is considered a single particle, and so forces act on the centre of mass of the molecule rather than its constituent atoms [112, 113]. Naturally there are no spring-like forces in this description since there are no chemical bonds between particles. In between these two extremes are descriptions of intermediate complexity, where each particle represents a handful of atoms. For instance, one or more water molecules could be treated as a single particle [114, 115], or a protein molecule could be treated as a chain of particles (up to amino acids) connected by spring-like forces (bonds) [116, 117, 118]. In the remainder of this discussion we will, for simplicity, assume the simplest form of MD: "particle" means "molecule". Since all forces act on molecule centres of mass, issues such as molecular shape, molecular orientation and rotation are all absorbed into the force term $\mathbf{F}_i(\mathbf{x}_i)$. It may be simpler henceforth to think of molecules as spheres.

It is also worth saying something initially about how chemical reactions occur in MD. Reactions are typically beyond the capabilities of MD simulators: the reasons for this are complex but fundamentally it is because reactions are quantum mechanical [17] while MD uses classical mechanics. There are quantum mechanical versions of MD but they are well beyond the scope of this thesis, and besides, are extremely computationally intensive [119]. We will therefore postpone discussion of chemical reactions until a later point in this section.

We will now consider what we can say about the dynamics of our system of N particles. By Newton's second law, the change in momentum of particle i is equal to $\mathbf{F}_i(\mathbf{x}_i)$. We can therefore write:

$$m_i \frac{\partial^2 \mathbf{x}_i}{\partial t^2} = \mathbf{F}_i(\mathbf{x}_i), \tag{1.24}$$

where m_i is particle i's mass. This model is perfectly good in theory, but there is an issue of scale. A system of N particles consists of N coupled versions of Eq. (1.24), each of which is really 3 equations (assuming a 3 dimensional system volume), so we end up with $3N$ coupled equations. In the vast majority of systems of interest to biologists, water molecules are by far the most numerous particles: a simple calculation shows that a typical $1\mu m^3$ *Eschericia coli* cell contains upwards of 10^{10} molecules of water alone. Trying to solve Eq. (1.24) with N on that kind of scale is simply impossible, even for the best computers. One solution to this is to study only a very small subvolume, much smaller than a cell, possibly containing only one protein [120]. But unfortunately the most interesting biochemistry concerns interactions between several different biological molecules, possibly located in several different parts of the cell, and systems of this kind are beyond the capabilities of molecular dynamics. An alternative approach is to use a multi-resolution approach with detailed molecular dynamics simulations in some regions of space, and more coarse-grained models in others [121]: such methods have recently been applied to solutions of ions [122] and DNA [123].

The issue, in essence, is that in order to simulate a useful number of interesting molecules a much greater number of water molecules must also be simulated. It was realised that a way around this problem might be to not simulate the water molecules explicitly, but rather to approximate the effect of water molecules on the other molecules by adding terms to Eq. (1.24) [124]. This would dramatically reduce N, and so dramatically increase the size of systems we could plausibly simulate.

The approximation of the water molecules has three components, which have an intuitive justification. We will use the word "collide" to refer to a steric (Van der Waals) interaction between particles, this can be thought of as a usual collision between hard objects (or, for simplicity, hard spheres). A graphical explanation of these effects is shown in Fig. 1.5

(I) When water molecules collide with a larger molecule, X, they will apply a force and thereby induce a change in X's velocity. This is simply due to the conservation of momentum and the conservation of energy. The direction and magnitude of this change are highly variable, and are well-approximated by a random quantity. If X is much larger in diameter than the water molecules there will be a huge number of collisions even in a very short time, and so irrespective of the actual distributions of the individual collisions (as long as they have finite variance), the central limit theorem implies that their sum (and thus the over all random force)

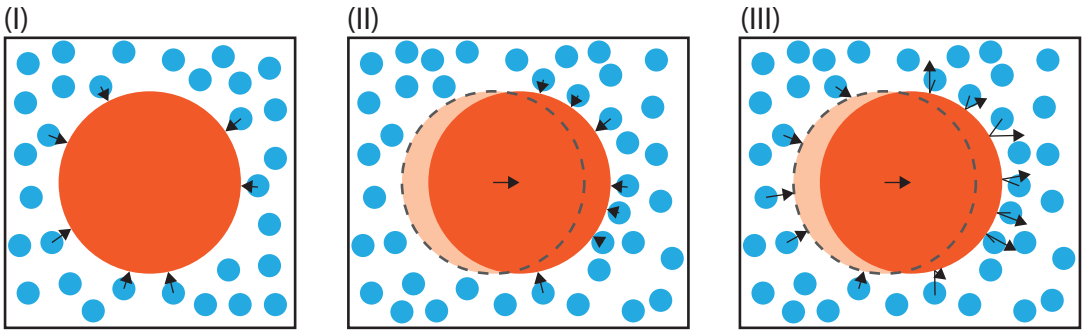

Figure 1.5: Three effects of water molecules (blue) on the motion of a large particle X (orange). (I) Water molecules collide on all sides of the large particle apparently at random (black arrows). If X is stationary, there is no directional bias to the random collisions. (II) If X is moving right, water molecules will collide more frequently on the particle's right side and less frequently on its left. There will be a deterministic force opposing X's velocity. (III) The arrows show how the water molecules might move in the time it would have taken them to collide with X had X been stationary (dotted circle). The water molecules on the left have not yet collided with anything, while the molecules on the right have collided and reflected away with higher speeds. They are all further to the right than they would have been otherwise, causing a net flow of water to the right.

will be approximately Gaussian [19, 125]. See Fig. 1.5 (I).

(II) When X moves with some non-zero velocity, it will tend to collide more frequently with water molecules in its direction of travel. That is, if X is moving to the right, it will tend to experience more collisions on its right side, and fewer on its left side, than the average predicted by (I). The number of collisions will scale with the magnitude of X's velocity (since faster moving particles will experience more such collisions in a fixed time period). See Fig. 1.5 (II).

(III) This component is much more subtle and takes some explaining. Let's say X is initially stationary, and is hit on the left by a water molecule. Now X starts to move to the right with a fixed speed. After a short time, before it collides with anything else, it will have moved a short distance. Now we think about a potential water molecule which might be about to collide with X. If it is about to collide from above, below, the front or the back, then the fact that X has moved makes essentially no difference to its behaviour. If it is about to collide from the left, it will have to travel slightly further before it collides than it would have if X had not moved. If it is about to collide from the right, it will have to travel slightly less far before it collides. Now suppose the water molecule has collided, and been reflected, and is now travelling away from X. *On average*, the water molecule will be slightly further to the right than it would have been if X had been stationary. Furthermore, a post-collision water molecule moving right will be moving faster than it otherwise would have been, thanks to the extra energy from the moving X; similarly a post-collision left-moving water molecule will be moving more slowly. Now imagine another large stationary molecule, Y, to the right of X. It is now slightly more likely to be hit on the left and by a faster-moving water molecule. Another large stationary molecule, Z, to the left of X, is slightly less likely to be hit on the right, and if it is hit it will likely be by a slower-moving water molecule. These two molecules will now both be slightly more likely to move right. Large molecules above, below, in front of and behind X will tend to be unaffected.

Perhaps a more intuitive – though less microscopic – way to think of this is in terms of pressure. If X moves slightly to the right, it will vacate some volume to its left, so there will be a slightly lower water pressure to its left, and water molecules will rush to fill the void. It will also occupy some volume to its right, so there will be a slightly higher water pressure to its right, and water molecules will be pushed out. There will therefore be a net flow of water molecules to the right in the vicinity of X, and so Y and Z will tend to be moved slightly right by the flow.

Mathematically, this manifests itself in a peculiar way: when effects (I) or (II) induce a force on a particle j, effect (III) ensures that all other particles in the system also experience a small force as a result. These forces will be separation dependent, so that two nearby particles will experience strongly correlated forces, while distant particles are weakly correlated. This effect is known as a "hydrodynamic" interaction between particles, because it is really a fluid dynamical effect [126].

(I), (II) and (III) all refer to forces induced by steric interactions (collisions) between water molecules and the larger molecule i, but (I) is a random component, (II) is a deterministic component, and (III) is the consequence experienced by molecule i of components (I) and (II) acting on all other molecules in the system. The new version of Eq. (1.24), implementing all the components, is known as the Langevin equation, and it has the following form:

$$m_i \frac{\partial^2 \mathbf{x}_i}{\partial t^2} = \mathbf{F}_i(\mathbf{x}_i) + \sum_{j=1}^{N} \sqrt{2k_B T} \left(\Gamma^{\frac{1}{2}}\right)_{ij} \xi_j - \sum_{j=1}^{N} \Gamma_{ij} \frac{\partial \mathbf{x}_j}{\partial t}, \tag{1.25}$$

where k_B is the Boltzmann constant, T is the temperature, ξ_i is a standard Gaussian random vector, and Γ is a $3N \times 3N$ matrix known as the "friction tensor". The matrix Γ can be split into 3×3 blocks: the term Γ_{ij} refers to the 3×3 submatrix corresponding to the effect of particle j's motion on particle i. The matrix $\Gamma^{\frac{1}{2}}$ is the square-root of the friction tensor. Note that, strictly speaking, Eq. (1.25) will consist of time integrals rather than Gaussian random vectors, due to the short-time correlations between the force terms. The Gaussians arise from assuming the timescale of interest to be significantly larger than the the timescale over which the correlations exist. See [127] for a nice summary.

Effect (I) is described by the term $\sqrt{2k_B T} \left(\Gamma^{\frac{1}{2}}\right)_{ii} \xi_i$, i.e. the component of the square-root friction tensor for the effect of particle i on itself. Similarly, effect (II) is described by $-\Gamma_{ii} \frac{\partial \mathbf{x}_i}{\partial t}$. Effect (III) is incorporated in two distinct ways: first, any random force felt by any particle j, ξ_j, has a hydrodynamic effect on particle i – this is the reason for the first sum in Eq. (1.25); secondly the velocity of any particle j induces a hydrodynamic force on particle i – this is the reason for the second sum in Eq. (1.25). The hydrodynamic friction tensor Γ mediates these two hydrodynamic contributions, and it is a complicated function of the relative positions of all the particles in the system. The details of the hydrodynamic implementations are well beyond the scope of this thesis; for a nice summary see Ref. [126] which gives examples of the Oseen [128] and Rotne-Prager [129] implementations. For more recent discussions of hydrodynamic implementations, using a variety of approximations to speed-up the computation time, see e.g. Refs. [130, 131, 132, 133, 134].

The hydrodynamic effect (III) is often left out of the Langevin equation, because it is subtle and complicated to implement. In that case, instead of Eq. (1.25) we get the much simpler form:

$$m_i \frac{\partial^2 \mathbf{x}_i}{\partial t^2} = \mathbf{F}_i(\mathbf{x}_i) + \sqrt{2\gamma_i k_B T} \xi_i - \gamma_i \frac{\partial \mathbf{x}_i}{\partial t}, \tag{1.26}$$

where ξ_i is now an uncorrelated Gaussian random vector, and the scalar $\gamma_i = \Gamma_{ii}$ is the "friction coefficient". It is easy to see the differential contributions of effects (I) and (II) in Eq. (1.26). However, there is no physically valid reason to eliminate the hydrodynamic effects at this stage, so we will leave it in for now, and discuss when it may be appropriate to remove it later.

Eq. (1.25) is a significant improvement on Eq. (1.24), and for computational simulations it does well, but the presence of second derivatives makes it somewhat difficult to study analytically. However, a simplification can be made due to the fact that molecules in water exist in low Reynolds number conditions, which implies that viscous effects dominate and inertial forces are negligible [135]. The result is that $\frac{\partial^2 \mathbf{x}_i}{\partial t^2} = 0$ and so Eq. (1.25) is simplified.

This is quite complicated so it worth exploring what is actually happening. Let us temporarily ignore the random collisions with water molecules and think about what happens to a molecule moving through water at a constant velocity. Intuition is not very helpful here, since we are used to thinking about water from a human point-of-view: if a human is swimming in water at a constant speed, then stops swimming, their motion will slow until they stop completely, i.e. there is a (relatively) lengthy period of decreasing speed (acceleration). This is

not what happens to a molecule (e.g. a protein) in water. A closer analogy would be a human swimming though a viscous fluid, such as treacle: when the human stops swimming, they simply stop moving instantly, there is no notable period of decreasing speed (of course, there is one, but it happens over such a short timescale that it is negligible). Water from the point-of-view of a protein is just like this: it stops moving instantly, there is no protracted period of slowing down. This is the intuitive reason why we can set the acceleration term to zero in Eq. (1.25). See Ref. [135] for an interesting discussion of this effect.

It follows that Eq. (1.25) becomes:

$$\mathbf{0} = \mathbf{F}_i(\mathbf{x}_i) + \sum_{j=1}^{N} \sqrt{2k_BT} \left(\Gamma^{\frac{1}{2}}\right)_{ij} \xi_j - \sum_{j=1}^{N} \Gamma_{ij} \frac{\partial \mathbf{x}_j}{\partial t}. \tag{1.27}$$

Using linear algebra techniques, this set of equations (for $i = 1, ..., N$) can be rearranged to give expressions for the velocity of each particle:

$$\frac{\partial \mathbf{x}_i}{\partial t} = \sum_{j=1}^{N} \left(\Gamma^{-1}\right)_{ij} \mathbf{F}_j(\mathbf{x}_j) + \sqrt{\frac{2k_BT}{\gamma_i}} \zeta_i, \tag{1.28}$$

where Γ^{-1} is the matrix inverse of the hydrodynamic friction tensor Γ, and ζ_i is a standard Gaussian random vector which (unlike ξ_i) is *correlated* with ζ_j (for all $j = 1, ..., N$) according to a complicated hydrodynamic function [126]. The effect of the linear algebraic rearrangement is to replace the sum of *velocities* in Eq. (1.27) with a sum of *forces* in Eq. (1.28). The implication is that any force between two particles (such as a steric repulsion) will induce a (typically miniscule) change in the velocity of every other particle in the system, even if the force does not affect them directly.

Eq. (1.28) is known as Brownian dynamics [136], and in essence it says that the large molecule's velocity has a deterministic component (due to the forces between each pair of large molecules) and a random component due to random collisions with the water molecules. It is tempting to think that individual collisions with the water molecules induce a random change in the large molecule's position, and that is what Eq. (1.28) seems to imply, but this is not quite correct. The individual water molecules actually induce random changes in the large molecule's *velocity*, and these changes will tend to happen extremely frequently, so in reality several water molecules contribute to each substantive change in the large molecule's position. This may seem like a semantic distinction, but it is worth bearing in mind that each random position increment corresponds to a large number of actual collisions.

The next simplifying step we can make is to assume that $\mathbf{F}_i(\mathbf{x}_i) = \mathbf{0}$ everywhere and to decorrelate the random vectors ζ_i, which essentially amounts to ignoring steric (Van der Waals), electrostatic and hydrodynamic interactions. This may seem to be a preposterous approximation to make , given that Eq. (1.28) is already quite simple, but there is a logic behind it. If we were trying to simulate (i.e. solve) Eq. (1.28) on a computer, we would most likely use an Euler scheme such as the one used in Ref. [126]. To do this, we would pick a small time step Δt and apply the update rule:

$$\mathbf{x}(t + \Delta t) = \mathbf{x}(t) + \sum_{j=1}^{N} \left(\Gamma^{-1}\right)_{ij} \mathbf{F}_j(\mathbf{x}_j)\Delta t + \sqrt{\frac{2k_BT}{\gamma_i}} \zeta_i \Delta t \tag{1.29}$$

to each particle at each time-step. This is not too computationally intensive in itself, but the problem is that for each particle both the associated force function $\mathbf{F}_i(\cdot)$, the matrix Γ^{-1}, and the size of the correlation in ζ_i depends on the relative locations of all the other particles in the system. All the different $\mathbf{F}_i$'s, $\left(\Gamma^{-1}\right)_{ij}$'s and correlations must be re-evaluated at every time-step, and this is what seriously slows down the computation. So it is clearly going to be useful to assume $\mathbf{F}_i(\mathbf{x}_i) = \mathbf{0}$, and that the ζ_i's are uncorrelated, but how can we justify this physically? If the concentrations of molecules are quite dilute, so that pairs of molecules rarely come close enough to interact sterically, electrostatically or hydrodynamically, then $\mathbf{F}_i(\mathbf{x}_i)$ would genuinely be equal to zero and ζ_i's would be genuinely uncorrelated, for the vast majority of particles,

the vast majority of the time.

We can then use the following equation for BD:

$$\mathbf{x}_i = \sqrt{2D_i}\mathbf{W}_t, \tag{1.30}$$

where $\mathbf{W}_t$ is a 3-dimensional Wiener process (confusingly also known as Brownian motion) and $D_i = \frac{k_B T}{\gamma_i}$ is the diffusion coefficient of particle i. The Wiener process, $\mathbf{W}_t = (W_t^{(1)}, W_t^{(2)}, W_t^{(3)})^T$, is a stochastic process defined by making $W_{t+\Delta t}^{(i)}$ a Normal$\left(W_t^{(i)}, \Delta t\right)$ random variable, for $i = 1, 2, 3$. Mathematically, $\mathbf{W}_t$ is the time integral of ξ [137].

It is worth considering the assumption of diluteness that lies behind Eq. (1.30). Until very recently, and to a large extent currently, diluteness was the *sine qua non* of modelling biochemistry. This was partly due to the modeller's preference for simple models like the REs and the RDEs, which implicitly assume diluteness, but also due to cell biologists' incomplete knowledge about the cellular environment. Then seminal work by Zimmerman and coworkers [138, 139] introduced both modellers and cell biologists to the idea of "macromolecular crowding" [140], an idea which has since become extremely fashionable in fields ranging from computational physics [141, 142] to bioengineering [143, 144].

The basic idea is that the cell contains high concentrations of large molecules. Zimmerman estimated that up to 30% of the internal volume of an *Eschericia coli* cell could actually be occupied by large molecules rather than water [138]. Under these conditions, the behaviour of an individual molecule will be seriously affected by the other large molecules in its vicinity, even if they do not interact chemically. There is an open question of how we might accurately modify Eq. (1.30) to account for this effect. Perhaps the obvious answer is to take a step backwards and bring the $\mathbf{F}(\cdot)$ back into the equation, and this is a common approach [145, 146, 147], but then we again have the problem of computational efficiency.

There are two other modifications to Eq. (1.30) which are currently in common usage. The first is to replace the diffusion coefficient D with a modified diffusion coefficient $\tilde{D}$, typically $\tilde{D} = D(1 - \alpha\phi)$ where ϕ is the local fraction of volume occupied by large molecules and α is a constant [148, 149, 93, 150, 96], an approach which we discuss in detail in chapter 6. The rationale is that diffusing through a crowded medium might be analogous to diffusing through a viscous medium, and so reducing the diffusion coefficient accounts for an increase in viscosity. There is some computational evidence to back this up, but insufficient for the matter to be considered solved [151, 152].

Many scientists believe the effect of crowding is more complex than a modification of the diffusion coefficient, and so the second modification is correspondingly less simple. The idea is to replace the Wiener process $\mathbf{W}_t$ with another process with non-Gaussian increments. The rationale is that the variance of a Wiener process is proportional to t, and some experiments appear to show that the variance of diffusion in a crowded environment is proportional more generally to t^α, an effect known as "anomalous diffusion". Generally it is observed that $\alpha < 1$ inside cells, which is known as "subdiffusion" [153, 154], however $\alpha \approx 1$ ("diffusion") [155] and $\alpha > 1$ ("superdiffusion") [156] have also been observed. Variants of the Wiener process for prespecified values of α are commonly used in simulations [157, 158], but the idea behind this is not uncontroversial and it raises questions [159]. For example, how do we know which value of α to pick in any given simulation? The debate around anomalous diffusion in the cytoplasm is still very much open, and much more experimental evidence will be needed to reach a satisfactory conclusion.

The question of how to modify Eq. (1.30) to include hydrodynamic effects is a difficult one, and has not been studied in significant detail. It is common to either just use Eq. (1.28) and live with the computational cost [126], or else to simply ignore hydrodynamic effects [160, 161, 145]. There is some evidence that steric effects and hydrodynamic effects could simply cancel each other out [162] – so potentially including both or neither in a model might be OK, while including just one might be a bad idea – but much more evidence is needed for this to be a practical solution. Alternatively, some authors have attempted to calculate the effect of hydrodynamic interactions on diffusion coefficients [162, 163] and reaction rates [164] – then it might be possible to modify them accordingly and claim that hydrodynamics have been taken into account. This is probably the most plausible approach, but again considerably more work

is needed to make this method practical.

To bring the discussion back to Brownian dynamics, there is still something missing from our model Eq. (1.30): how do reactions happen? Reactions with 1 reactant (i.e. unbinding reactions) are easy: each molecule which can unbind has an internal clock, and the time until unbinding is generated as an exponentially distibuted random time in the future – when the clock exceeds this time, the reaction occurs. There is a question of where the daughter molecules (i.e. the products of the unbinding) should be placed, and several different methods are in use. Perhaps the simplest method is to place them both at the same location, where the parent particle was before it unbound: this is unphysical but straightforward and requires no new parameters [7]. An alternative is to propose an "unbinding distance", σ, and place them randomly opposite each other on a sphere of diameter σ centered around the location of the parent particle [165].

On the other hand, modelling *bimolecular* reactions is a complicated question with a very long history. The original method, still popular today, was devised by Marian Smoluchowski [106], who incidentally was one of the originators of the physical theory of Brownian motion, along with Albert Einstein [166, 136]. Smoluchowski's idea was a simple one: each molecule is assigned a "reaction radius", and two reacting particles will react immediately if they are brought close enough together that their reaction radii overlap (see Fig. 1.6). This model has advantages and disadvantages.

The advantages are that it is simple to understand, and computationally and mathematically very straightforward. The most popular Brownian dynamics software, *Smoldyn* [165], uses the Smoluchowski model because it is so much faster than the alternatives. Mathematically, it is possible to write down the expected time until a reaction between two particles, μ, as a simple function of their reaction radii (r_1, r_2), their diffusion coefficients (D_1, D_2), and the reaction volume V:

$$\mu = \frac{V}{4\pi(r_1 + r_2)(D_1 + D_2)}. \tag{1.31}$$

Eq. (1.31) is obtained from the diffusion equation, and a derivation can be found in Ref. [167]. In principle μ^{-1} could be put into the CME as the rate of a reaction, although this would be an approximation because the actual waiting time for Brownian collisions is not exponential [83].

The disadvantages of Smoluchowski's approach are slightly more complicated. Principally, the Smoluchowski model is not a particularly accurate model of how bimolecular reactions actually happen. Reacting molecules must approach each other in the correct orientation and with sufficient combined kinetic energy to exceed the activation energy of the reaction, otherwise they will simply collide without reacting [17]. Smoluchowski does not allow for these kinds of collisions, which can occur much more frequently than successful reactions.

The second issue is a modelling issue rather than a physical one. In the limiting case where diffusion is very fast relative to reactions, we would ideally like our BD model to converge to the CME. In the Smoluchowski model, the expected time until a reaction scales as the inverse of the diffusion coefficient, and so when diffusion is infinitely fast bimolecular reactions happen infinitely quickly. It may appear that Smoluchowski has it right here because we know from basic chemistry that if we increase the temperature of a system (and therefore the diffusion coefficients) the reactions will tend to occur more quickly [17]. But the reality is not quite so simple.

A significant source of confusion arises from the fact that a generalised bimolecular reaction rate k (such as the rate in the REs) really incorporates two distinct processes: a diffusive process which brings two molecules together; and a reactive process which causes them to react with some probability. Collins and Kimball go into considerable detail on this subject in Ref. [101], as well as Gillespie later in Ref. [167]. They consider a physically plausible system in which hard sphere particles diffuse by Brownian motion, but over very short timescales (shorter than the time between collisions with solvent molecules) they have instantaneous random velocities given by the Maxwell-Boltzmann distribution. In this description, a reaction occurs when the instantaneous velocities of a very close pair of particles combine in such a way that they collide with an energy greater than the intrinsic activation energy of the reaction. Under these

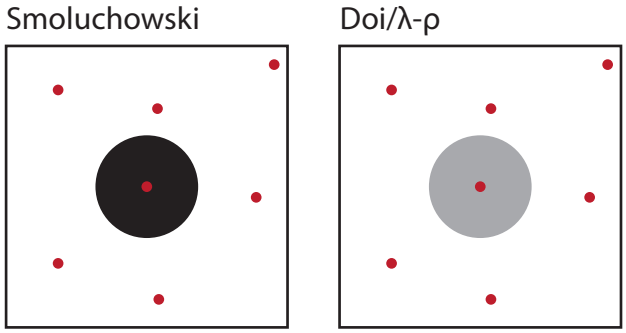

Figure 1.6: Two methods of implementing bimolecular reactions in BD. The Smoluchowski model allows particles to react immediately when the distance between the particle centres equals the sum of the particles' reaction radii. This radius of certain interaction is shown as a solid black circle. The Doi/$\lambda - \rho$ model allows particles to react with probability λ per unit time when the distance between the particle centres is less than a distance ρ. This radius of probabilistic interaction is shown as a solid grey circle. Note that the particle centres are denoted in red.

conditions, Collins and Kimball observe that the reaction rate k satisfies:

$$\frac{1}{k} = \frac{1}{k_d} + \frac{1}{k_b}, \tag{1.32}$$

where k_d is the *diffusive rate* and k_b is the *ballistic rate*. In other words, the expected time until a reaction between a given pair of particles is the sum of the expected time until they are brought together by diffusion and the expected time until they subsequently collide with sufficient energy.

According to Collins' and Kimball's model [101], the role of diffusion is to bring reactive molecules together, whereupon they can react according to some diffusion-independent process. In other words, the probability of a reaction between a sufficiently close pair of particles (in a sufficiently short time that they cannot diffuse away again) is not a function of the diffusion coefficient. When the diffusion coefficient is infinitely fast the time until a reaction, $\frac{1}{k}$, approaches $\frac{1}{k_b}$ rather than 0, and so infinite diffusion seems not to pose a problem. Unfortunately, again, it is not so simple.

Since Collins' and Kimball's k_d is a linear fuction of the diffusion coefficient D, while k_b has no D-dependence, our assumption may seem to be straightforwardly valid. However, both D and k_b are functions of temperature, via the Stokes-Einstein relation and the Arrhenius equation respectively [17]. It follows that k_b has an implicit D-dependence - e.g. if D is large, there is a possibility that this may be due to the temperature being large, so k_b may also be large. In biology (unlike chemistry) this is not a serious problem, since temperature is essentially constant for living beings. Our assumption amounts to ignoring this subtle implicit dependence, and thereby restricting our models to biological systems. We assume that it is possible to freely vary D without affecting the reactive component of the bimolecular reaction rate – we can think of this as varying D by tuning the viscosity of the solvent, which does not directly affect the reaction rate.

In this spirit, a popular alternative to the Smoluchowski model was proposed by Doi [168], building on the work of Teramoto and Shigesada [169]. He suggests that we should associate with each pair of reacting particles a reaction rate λ and a reaction distance ρ, then we assume again that waiting times between reactions are exponential, so that two particles will react in a short timestep Δt with a probability $\lambda \Delta t$ if they are separated by a distance less than ρ. In other words, if two particles are sufficiently close they react with a rate λ, otherwise they do not react (see Fig. 1.6). In practice, at each timestep Δt particle positions are updated according to Eq. (1.29) (typically minus the force term), whereupon the distances between each pair of potentially-reacting particles is calculated. For each pair, if this distance is less than the

ρ associated with the reaction, then the reaction occurs with probability $\lambda\Delta t$, the particles are removed from the system, and the product particles (if there are any) are put in their place.

Doi's model, which has come to be known as the $\lambda - \rho$ model [108], is actually a generalisation of the Smoluchowski model, which would have $\lambda = \infty$ and ρ equal to the sum of the reactants' reaction radii [170]. Overall, the $\lambda - \rho$ model seems to be an optimal trade-off between model simplicity and physical accuracy. The process we want to model explicitly (diffusion) is modelled explicitly, while more complex processes (reactant orientation, kinetic energy, etc) are lumped into the rate λ. The main disadvantage is that we are assuming exponential waiting times between reactions, but this cannot really be helped without going into significantly more modelling detail and thereby incurring a significantly higher computational cost.

One alternative to both Smoluchowski and Doi is to use a Robin boundary condition where a reaction occurs immediately upon collision with a finite rate: such a model has been shown to agree with finer-grained Langevin dynamics with a reaction potential, though is correspondingly more analytically complex [171].

1.3 Summary

We have seen how the two most common stochastic reaction diffusion models (RDME and BD) originated, and how they attempt to model both reactions and diffusion. In the ensuing sections we will go into much greater detail to analyse these models, propose fast algorithms for them, and make biological predictions using them. The remainder of this thesis will have the following form.

In chapter 2, we study the validity of the RDME, and the extent to which it agrees with the CME. In chapter 3, we derive analytical approximations for the RDME, allowing fast computation of relevant statistics beyond the CME level. In chapter 4 we study the RDME as a model for multicellular dynamics, an alternative usage which solves many of the RDME's problems. In chapter 5 we propose a fast algorithm for BD in the presence of crowder molecules, allowing large-scale simulation of realistic, detailed biochemical systems. In chapter 6, we derive partial differential equations to describe BD at the macroscopic level, incorporating crowding effects, which leads to interesting testable predictions about real biological behaviour. We conclude with a discussion in chapter 7.

Chapter 2

The validity of the reaction-diffusion master equation

As discussed in chapter 1, the CME describes the fluctuations of molecule numbers in reactive chemical systems which are dilute and well-mixed. In particular, it assumes that the probability of two particles reacting with each other is independent of their relative positions in space, which is strictly true only if diffusion rates are infinitely large, i.e., well-mixed conditions. The CME has in fact been derived from a microscopic physical description under these conditions, if mass-action kinetics are assumed [172], and is also known to be correct for non-elementary reaction in quasi-equilibrium conditions [173, 174]. When diffusion coefficients are not fast, the RDME is a natural extension allowing us to treat diffusion explicitly.

The RDME and the CME describe the same systems, but the RDME claims greater accuracy in the sense that it contains all the information of the CME while incorporating local spatial effects which are beyond its scope. Since we know the CME to be valid if diffusion rates are fast [172], a useful test of the validity of the RDME is that it should converge to the CME in the limit of infinite diffusion rates. This convergence seems intuitively likely: if diffusion rates are fast then particles hop between subvolumes much more frequently than they react, and so the well-mixedness assumption of the CME should be recovered.

In this chapter, we show that the RDME converges to *a* master equation in the limit of fast diffusion, but remarkably, under certain conditions, this master equation is not the CME. The accuracy of the RDME under these conditions is therefore called into question. The chapter is organised in the following way. In section 2.1 we derive an expression for the master equation to which the RDME converges in the limit of fast diffusion. We subsequently define a class of reaction types (and their corresponding propensity functions) which we call *convergent propensity functions* with the following property: *if a chemical system has exclusively convergent propensity functions, then the RDME will converge to the CME of the same system in the limit of fast diffusion.* If a chemical system has any non-convergent propensity functions, then it will almost surely not converge to the correct CME. In section 2.2 we show that elementary reactions (including zero, first and second-order reactions) are in the convergent class, while more complex reactions (including Michaelis-Menten and Hill-type) are of the non-convergent class. In section 2.3 we illustrate our results by applying them to two simple systems: one convergent and one non-convergent. We conclude with a summary in section 2.4.

2.1 Convergence of the RDME

In chapter 1 we defined the CME and RDME for the specific system $A + B \rightleftharpoons C$ (Eqs. (1.11) and (1.23) respectively). In this section we define the CME and the RDME in general, and prove that the latter may or may not converge to the former in the limit of fast diffusion. We further prove that independent of the type of propensity, the RDME still converges to the CME

in the limit of fast diffusion and of large volumes, taken simultaneously.

2.1.1 The CME

The CME defined in Eq. (1.11) can be generalised for any chemical system of N species $X_1, ..., X_N$ and R reactions, where the j^{th} reaction has the form:

$$s_{1j}X_1 + ... + s_{Nj}X_N \to r_{1j}X_1 + ... + r_{Nj}X_N, \tag{2.1}$$

where r_{ij} and s_{ij} are known as the *stoichiometric coefficients*. The CME then has the form

$$\frac{d}{dt}P(\vec{n},t) = \sum_{j=1}^{R}\left(\prod_{i=1}^{N} E_i^{s_{ij}-r_{ij}} - 1\right)\hat{a}_j(\vec{n},V)P(\vec{n},t), \tag{2.2}$$

where we recall that V is the reaction volume, $\vec{n} = (n_1, ..., n_N)^T$ is the vector of molecule numbers of species $X_1, ..., X_N$ respectively, $P(\vec{n},t)$ is the probability that the system is in the state $\vec{n}$ at time t, and E_i^x is again the shift operator. Finally, the notation $\hat{a}_j(\vec{n},V)$ denotes the *propensity function* of reaction j. Note that we do not use the mass-action propensities based on rates k_j, since we would like to retain generality about the functional form of the propensities for the time being, though it should noted that all biological reactions are in fact bimolecular, yet may be better described by other propensity functions.

The propensity function is formally defined as follows: given that the system is in state $\vec{n}$, then $\hat{a}_j(\vec{n},V)\Delta t$ is the probability that a reaction of index j occurs somewhere in the volume V in the next infinitesimal time interval $[t, t+\Delta t)$ [175].

2.1.2 The RDME

Just as with the CME, the RDME defined in Eq. (1.23) can be generalised for the chemical system (2.1). For simplicity, we divide the volume V into M equally-sized subvolumes. The j^{th} chemical reaction in subvolume k will now have the form:

$$s_{1j}X_1^{(k)} + ...s_{Nj}X_N^{(k)} \to r_{1j}X_1^{(k)} + ... + r_{Nj}X_N^{(k)}, \tag{2.3}$$

where we recall that $X_i^{(k)}$ refers to species X_i locally in subvolume k. As explained in Eq. (1.18), the diffusive interchange of chemicals between neighbouring subvolumes is modelled by the reactions:

$$X_i^{(k)} \underset{k_D^{(i,k',k)}}{\overset{k_D^{(i,k,k')}}{\rightleftharpoons}} X_i^{(k')}, \quad k' \in \mathcal{N}(k), \tag{2.4}$$

where we recall that $k_D^{(i,k,k')}$ is the hopping rate of species X_i from subvolume k to subvolume k', and $\mathcal{N}(k)$ is the set of indices of subvolumes neighbouring subvolume k. The specific neighbours of a subvolume depend on the topology of the lattice, though for the purposes of this chapter it does not matter what this is, as long as every subvolume is indirectly connected to every other by some path. For simplicity, we will assume that the hopping rates do not vary between subvolumes, that is:

$$k_D^{(i,k,k')} = \begin{cases} k_D^{(i)} & \text{if } k' \in \mathcal{N}(k), \\ 0 & \text{otherwise,} \end{cases} \tag{2.5}$$

for some $k_D^{(i)}$. Since all subvolumes are equally-sized and hopping rates are constant across space, the set of reactions (2.4) accurately models unbiased diffusion.

The stochastic dynamics of this system is then described by the RDME:

$$\frac{d}{dt}P(\vec{n}^{(1)},...,\vec{n}^{(M)},t) = \sum_{k=1}^{M}\sum_{j=1}^{R}\left(\prod_{i=1}^{N}E_{i,k}^{s_{ij}-r_{ij}}-1\right)\hat{a}_j(\vec{n}^{(k)},V/M)P(\vec{n}^{(1)},...,\vec{n}^{(M)},t) + \sum_{k=1}^{M}\sum_{k'\in Ne(k)}\sum_{i=1}^{N}\left(E_{i,k}^{1}E_{i,k'}^{-1}-1\right)k_D^{(i)}n_i^{(k)}P(\vec{n}^{(1)},...,\vec{n}^{(M)},t), \quad (2.6)$$

where we recall $n_i^{(k)}$ is the number of molecules of species $X_i^{(k)}$, $\vec{n}^{(k)} = (n_1^{(k)},...,n_N^{(k)})^T$, $P(\vec{n}^{(1)},...,\vec{n}^{(M)},t)$ is the probability of the system being in state $(\vec{n}^{(1)},...,\vec{n}^{(M)})$ at time t, and $E_{i,k}^{x}$ is the shift operator which replaces $n_i^{(k)}$ with $n_i^{(k)}+x$. Note that the first line of Eq. (2.6) refers to the chemical reactions while the second line refers to the diffusive reactions. The local propensity function is defined as: given that the state of subvolume k is $\vec{n}^{(k)}$, then $\hat{a}_j(\vec{n}^{(k)},V/M)\Delta t$ is the probability that one reaction of index j occurs somewhere inside this subvolume in the next infinitesimal time interval $[t,t+\Delta t)$.

2.1.3 The RDME in the limit of fast diffusion

We now investigate what happens to the RDME in the limit where $k_D^{(i)}\to\infty$ for all $i=1,...,N$. Suppose that the system is in state $(\vec{n}^{(1)},...,\vec{n}^{(M)})$ at time t, and define $n_i = n_i^{(1)}+...+n_i^{(M)}$ as the global molecule number of the species X_i. Each time a chemical reaction occurs somewhere in space, the local molecule number of one or more species changes leading to a corresponding change in the global number of molecules of the concerned species. Before the next chemical reaction occurs, diffusive reactions will happen a very large number of times such that the system will approach the steady-state of the purely diffusive system (2.4). Specifically suppose that a chemical reaction just occurred somewhere in space and that the global state vector is $(n_1,n_2,...,n_N)$. Then it follows that due to the effect of infinitely fast diffusion, the probability of having $n_i^{(k)}$ molecules of species X_i in subvolume k, conditional on the fact that there are n_i molecules of the same species in all of space, is given by the binomial distribution:

$$P(n_i^{(k)}|n_i) = \frac{n_i!}{n_i^{(k)}!(n_i-n_i^{(k)})!}\left(\frac{1}{M}\right)^{n_i^{(k)}}\left(1-\frac{1}{M}\right)^{n_i-n_i^{(k)}}, \quad i=1,...,N. \quad (2.7)$$

It also follows that the distribution of molecule numbers of all chemical species in subvolume k, conditional on the global state vector, is given by:

$$P(\vec{n}^{(k)}|\vec{n}) = \prod_{i=1}^{N}P(n_i^{(k)}|n_i). \quad (2.8)$$

Now starting from the RDME, we want to calculate the probability $a_j(\vec{n},V)dt$, in the limit of fast diffusion, that the j^{th} chemical reaction occurs somewhere in the space of volume V in the next infinitesimal time interval $[t,t+dt)$, conditional on the global state vector, $\vec{n}=(n_1,n_2,...,n_N)$. This reaction can occur in either subvolume 1 or subvolume 2 or ... or subvolume M and hence we must sum the propensities of the j^{th} chemical reaction in each subvolume. Furthermore we must also sum over all possible different states in each subvolume which are compatible with the global state vector, $\vec{n}$. Hence it follows that:

$$a_j(\vec{n},V) = \sum_{k=1}^{M}\sum_{n_1^{(k)}=0}^{n_1}...\sum_{n_N^{(k)}=0}^{n_N}\hat{a}_j(\vec{n}^{(k)},V/M)P(\vec{n}^{(k)}|\vec{n}). \quad (2.9)$$

In the limit of fast diffusion, the average propensity of the j^{th} chemical reaction in a given subvolume is the same as that in any other subvolume and hence Eq. (2.9) further simplifies

to:

$$a_j(\vec{n},V) = M \sum_{n_1^{(k)}=0}^{n_1} ... \sum_{n_N^{(k)}=0}^{n_N} \hat{a}_j(\vec{n}^{(k)},V/M)P(\vec{n}^{(k)}|\vec{n}), \tag{2.10}$$

for some $k = 1, ..., M$. This can be written conveniently as an expected value under the Binomial distribution defined by Eq. (2.8):

$$a_j(\vec{n},V) = M\mathbb{E}\left[\hat{a}_j(\vec{n}^{(k)},V/M)\right]. \tag{2.11}$$

By the definition of the propensity function $a_j(\vec{n},V)$, it follows immediately from the laws of probability that the master equation to which the RDME converges to, in the limit of fast diffusion, is:

$$\frac{d}{dt}P(\vec{n},t) = \sum_{j=1}^{R}\left(\prod_{i=1}^{N} E_i^{s_{ij}-r_{ij}} - 1\right) a_j(\vec{n},V)P(\vec{n},t). \tag{2.12}$$

Note that this equation is identical to Eq. (2.2) except that $\hat{a}_j$ is replaced with a_j. The main result follows: *The RDME converges to the CME in the limit of fast diffusion if* $a_j(\vec{n},V) = \hat{a}_j(\vec{n},V)$ for all $j = 1, ..., R$ (note that this limit is taken with the volume V and all rate constants held constant).

With this in mind, we can define a class of propensities which we call *convergent propensities*. A propensity function $\hat{a}_j(\vec{n},V)$ is convergent if $a_j(\vec{n},V) = \hat{a}_j(\vec{n},V)$. A system consisting exclusively of convergent propensities will have the satisfying property of convergence of the RDME to the CME, in the fast diffusion limit. A system with at least one non-convergent propensity will almost surely not have this property, though this possibility cannot be generally excluded. For instance there could exist two non-convergent propensity functions which perfectly cancel out each others' effects, leading to convergence over all.

2.1.4 The RDME and the CME in the limits of fast diffusion and large volumes

We now briefly show that a non-convergent RDME can still converge to the correct CME in the limit of fast diffusion, if we also take the macroscopic limit of large volumes. The proof is based on the fact that in the macroscopic limit, the solution of a master equation is approximated by the chemical Langevin equation whose solution has sharp peaks centred on the solution of the corresponding REs [176].

The REs have already been defined for the specific system $A + B \rightleftharpoons C$ in Eq. (1.2), but they too can be written for the general system Eq. (2.1):

$$\frac{d}{dt}\vec{\phi} = \sum_{j=1}^{R}(r_{ij} - s_{ij})f_j(\vec{\phi}), \tag{2.13}$$

where $\vec{\phi} = \langle\vec{n}\rangle/V$ is the vector of deterministic concentrations of species $X_1, ..., X_N$ (the angled brackets signify the average taken in the macroscopic limit), and $f_j(\vec{\phi})$ is the *macroscopic propensity function* of reaction j defined as:

$$f_j(\vec{\phi}) = \lim_{V\to\infty}\frac{\hat{a}_j(\vec{n} = V\vec{\phi},V)}{V}. \tag{2.14}$$

Similary, the REs of the system given by Eqs. (2.3) and (2.4), described stochastically by the RDME, are given by:

$$\frac{d}{dt}\phi_i^{(k)} = \sum_{j=1}^{R}(r_{ij} - s_{ij})f_j(\vec{\phi}^{(k)}) + k_D^{(i)}\left(\sum_{k'\in\mathcal{N}(k)}\phi_i^{(k')} - z\phi_i^{(k)}\right), \tag{2.15}$$

where $\vec{\phi}^k = \langle \vec{n}^k \rangle / (V/M)$ is the vector of deterministic concentrations in subvolume k, f_j is the same f_j as defined in Eq. (2.14), and z is the number of neighbours of a subvolume for a particular RDME topology. Clearly in the limit of fast diffusion, the deterministic concentration of each species is the same in all subvolumes, i.e., $\phi_i^{(k)} = \phi_i^{(k')}$ at all times. Hence the second term on the right hand side of Eq. (2.15) equals zero and the rate equations of the RDME simplify to:

$$\frac{d}{dt}\phi_i^{(k)} = \sum_{j=1}^{R}(r_{ij} - s_{ij}) f_j(\vec{\phi}^{(k)}). \tag{2.16}$$

Now to compare with the REs of the CME, we need to use Eq. (2.16) derive the REs for the global concentration ϕ_i, which follows from the definition of the global molecule numbers and is given by $\phi_i = \frac{1}{M}(\phi_i^{(1)} + ... + \phi_i^{(M)})$. These are given by:

$$\frac{d}{dt}\phi_i = \frac{1}{M}\frac{d}{dt}\sum_{k=1}^{M}\phi_i^{(k)} = \frac{1}{M}\sum_{k=1}^{M}\sum_{j=1}^{R}(r_{ij} - s_{ij}) f_j(\vec{\phi}^{(k)}) = \sum_{j=1}^{R}(r_{ij} - s_{ij}) f_j(\vec{\phi}), \tag{2.17}$$

where the last equation follows from the fact that in the fast diffusion limit, $\phi_i^{(k)} = \phi_i$ at all times. The RE of the global concentrations of the RDME given by Eq. (2.17) is therefore equal to Eq. (2.13), the RE of the global concentrations of the CME. In summary, *in the combined limits of fast diffusion and large volumes, the RDME of a system converges to the CME of the same system, regardless of whether the propensities are convergent.*

It can also be straightforwardly shown using the linear noise approximation (LNA) that for deterministically monostable systems, the solution of the RDME and CME, in the macroscopic and fast diffusion limits, tends to the same Gaussian centred on the RE solution [22]. This follows from the fact that the variance and covariance of the Gaussian are functions of the RE solution and which, as we have shown, is one and the same for the RDME and CME.

2.2 Examples of convergent and non-convergent propensities

In this section we test whether some commonly-used propensities are in the convergent or non-convergent class.

2.2.1 Convergent propensities

Consider mass-action kinetics, as discussed at length in chapter 1. It then follows [22] that the propensity of the j^{th} chemical reaction in the CME and of the j^{th} chemical reaction in subvolume k of the RDME are respectively given by:

$$\hat{a}_j(\vec{n}, V) = V k_j \prod_{z=1}^{N} V^{-s_{zj}} \frac{n_z!}{(n_z - s_{zj})!}, \tag{2.18}$$

$$\hat{a}_j(\vec{n}^k, V/M) = (V/M) k_j \prod_{z=1}^{N} (V/M)^{-s_{zj}} \frac{n_z^{(k)}!}{(n_z^{(k)} - s_{zj})!}. \tag{2.19}$$

The most commonly used types of reactions following mass-action kinetics are the zero order reaction, first order reaction, second-order reactions between similar reactants and second-order reaction with different reactants which have CME propensities $\hat{a}_j(\vec{n}, V)$ equal to $k_j V$, $k_j n_i$, $(k_j/V) n_i(n_i - 1)$ and $(k_j/V) n_i n_j$ respectively, for some integers i and j.

Substituting Eq. (2.19) in Eq. (2.10), we have that in the fast diffusion limit, the RDME

converges to a master equation with a propensity for the j^{th} chemical reaction equal to:

$$a_j(\vec{n},V) = M\prod_{z=1}^{N}\sum_{n_z^{(k)}=0}^{n_z}\hat{a}_j(\vec{n}^{(k)},V/M)P(n_z^{(k)}|n_z), \tag{2.20}$$

$$= M(V/M)k_j\prod_{z=1}^{N}(V/M)^{-s_{zj}}\sum_{n_z^{(k)}=0}^{n_z}\frac{n_z^{(k)}!}{(n_z^{(k)}-s_{zj})!}P(n_z^{(k)}|n_z). \tag{2.21}$$

Now the quantity:

$$\sum_{n_z^{(k)}=0}^{n_z}\frac{n_z^{(k)}!}{(n_z^{(k)}-s_{zj})!}P(n_z^{(k)}|n_z), \tag{2.22}$$

is by definition the s_{zj}-th factorial moment of the binomial distribution $P(n_z^{(k)}|n_z)$ with success probability $1/M$ and number of trials n_z. This factorial moment is a standard result (see for example [177]) and is given by:

$$\sum_{n_z^{(k)}=0}^{n_z}\frac{n_z^{(k)}!}{(n_z^{(k)}-s_{zj})!}P(n_z^{(k)}|n_z) = \frac{n_z!}{(n_z-s_{zj})!}\left(\frac{1}{M}\right)^{s_{zj}}. \tag{2.23}$$

Substituting the above equation in Eq. (2.21) we obtain:

$$a_j(\vec{n},V) = Vk_j\prod_{z=1}^{N}V^{-s_{zj}}\frac{n_z!}{(n_z-s_{zj})!} = \hat{a}_j(\vec{n},V). \tag{2.24}$$

It follows that the propensities of reactions following mass-action are convergent; this applies to all reaction orders. The convergence of the RDME to the CME in the fast diffusion limit, for reactions up to second-order, has been previously also shown by Gardiner [178] using a completely different method.

2.2.2 Non-convergent propensities

It is common practice to use effective propensities which lump a number of elementary reactions together. One of the most popular of such propensities is the Michaelis-Menten propensity. This can model various processes such as nonlinear degradation of a protein, enzyme catalysis of a protein into a product or the activation of a gene by a protein. Let this protein species be X_i. If the j^{th} reaction is of the Michaelis-Menten type, then it can be described by a term in the deterministic rate equations of the form $f_j(\vec{\phi}) = k_j\phi_i/(K+\phi_i)$. Using Eq. (2.14), one can deduce that a corresponding effective propensity in the CME would be $\hat{a}_j(\vec{n},V) = k_jn_i/(K+n_i/V)$ [179, 180]. The corresponding propensity in the k^{th} subvolume of the RDME would be $\hat{a}_j(\vec{n}^{(k)},V/M) = k_jn_i^{(k)}/(K+Mn_i^{(k)}/V)$ [181].

Substituting the latter propensity of the RDME in Eq. (2.10), we have that in the fast diffusion limit, the RDME converges to a master equation with a propensity for the j^{th} chemical reaction equal to:

$$\begin{aligned} a_j(\vec{n},V) &= Mk_j\sum_{n_i^{(k)}=0}^{n_i}\frac{n_i^{(k)}}{K+Mn_i^{(k)}/V}P(n_i^{(k)}|n_i), \\ &= \frac{k_jV(M-1)^{n_i-1}n_i\ {}_2F_1\left(KV/M+1,1-n_i;KV/M+2;-1/(M-1)\right)}{M^{n_i}(KV/M+1)} \\ &\neq \frac{k_jn_i}{K+n_i/V} = \hat{a}_j(\vec{n},V), \end{aligned} \tag{2.25}$$

where ${}_2F_1(a,b;c;d)$ is a hypergeometric function.

Since $a_j(\vec{n}, V) \neq \hat{a}_j(\vec{n}, V)$, it follows that Michaelis-Menten propensities are non-convergent. However note in the limits of very small or very large $n_i^{(k)}$, $\hat{a}_j(\vec{n}^{(k)}, V/M)$ reduces to $k_j n_i^{(k)}/K$ and $k_j V/M$ respectively; these are special cases of mass-action kinetics Eq. (2.19) and hence in these limits, the Michaelis-Menten propensity can be considered convergent. The largest deviations from mass-action occur when $n_i^{(k)}/V$ is roughly equal to the constant K (the Michaelis-Menten constant); this is the case where the non-convergence of the Michaelis-Menten propensity becomes most apparent.

A generalisation of the Michaelis-Menten propensity, which is sometimes used, is given by the Hill propensity. For the CME this is given by:

$$\hat{a}_j(\vec{n}, V) = \frac{V k_j (n_i)^\theta}{(VK)^\theta + (n_i)^\theta}, \tag{2.26}$$

for some i. The Hill coefficient θ is an integer greater or equal to 1. The corresponding propensity in subvolume k of the RDME is:

$$\hat{a}_j(\vec{n}^{(k)}, V/M) = \frac{(V/M) k_j (n_i^{(k)})^\theta}{(VK/M)^\theta + (n_i^{(k)})^\theta}. \tag{2.27}$$

For general θ it is not possible to evaluate Eq. (2.10) analytically. However, if we can find a set of parameters for which a_j and $\hat{a}_j$ do not agree, then we can be certain that they are not the same function. Choose, for instance, $k_1 = K = V = 1$, $M = n_i = 2$. For these parameters, $\hat{a}_j = 2^\theta/(1 + 2^\theta)$. On the other hand:

$$a_j = \frac{1}{2}\left(\frac{1}{2} + \frac{1}{(1/2)^\theta + 1} + \frac{1}{2}\frac{2^\theta}{(1/2)^\theta + 2^\theta}\right). \tag{2.28}$$

There are no real values of θ for which $\hat{a}_j = a_j$, and therefore it follows that Hill-type propensities are non-convergent.

2.3 Simple convergent and non-convergent example systems

To illustrate the results of this chapter, we briefly apply them to some simple example systems in this section. For simplicity we will use systems consisting of only one species.

2.3.1 A convergent example

A simple convergent example is given by the open dimerisation reaction:

$$\emptyset \to X, \; X + X \to \emptyset. \tag{2.29}$$

The propensity functions of the CME are:

$$\hat{a}_1(n, V) = k_1 V, \; \hat{a}_2(n, V) = \frac{k_2}{V} n(n-1), \tag{2.30}$$

where n is the number of X molecules. The corresponding propensity functions in subvolume k of the RDME are obtained by replacing n by $n^{(k)}$ and V by V/M. These propensity functions can be non-dimensionalised by dividing by $k_1 V$. Then we will have dimensionless propensities:

$$\hat{a}_1 = 1, \; \hat{a}_2 = Kn(n-1), \tag{2.31}$$

where $K = k_2/k_1 V^2$ is a dimensionless parameter. In the RDME description, the diffusion rate parameter k_D will be replaced by a dimensionless parameter $k_D^0 = k_D/k_1 V$, and the RDME

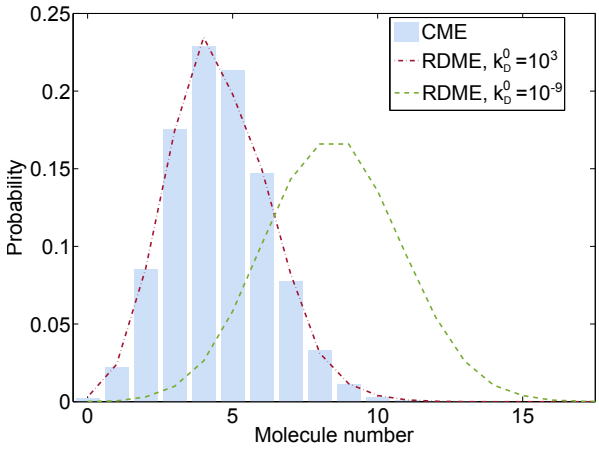

Figure 2.1: Steady state solution of the CME for system (2.29) (blue histogram) compared with the steady-state solutions of the global molecule numbers calculated using the RDME for very slow diffusion (green dashed line) and for very fast diffusion (red dash-dotted line), all obtained with the SSA. Note that the RDME converges to the CME in the limit of fast diffusion, as predicted by our theory. The parameter values are $K = 0.03$, $M = 10$. Note that k_D^0 is varied through k_D whilst all other parameters are constant.

propensities in subvolume k will be:

$$a_1 = \frac{1}{M},\ a_2 = KMn^{(k)}(n^{(k)} - 1), \tag{2.32}$$

Since both propensities are of the mass-action type, they are convergent. Note that the convergence here is obtained in the limit of large k_D at constant values of the volume and of the rate constants, i.e., the limit that k_D^0 tends to infinity at constant K. In Fig. 2.1 we show that the the steady-state distribution of global molecule numbers (sum of molecule number over all subvolumes) calculated using the RDME with very slow diffusion ($k_D^0 = 10^{-9}$) disagrees with the CME while the same computed with very fast diffusion ($k_D^0 = 10^3$) agrees exactly with the CME. The plots are obtained using the stochastic simulation algorithm (SSA) for both the CME [49] and RDME [75]. For the RDME, the simulation consisted of 10 subvolumes connected in a line with reflecting boundaries. The agreement of the CME and RDME in the limit of fast diffusion is in agreement with the theoretical result that both propensities are convergent. Note that the change in the mode of the distribution occurs because the bimolecular reaction happens more frequently when diffusion is fast, thereby reducing the overall molecule number.

2.3.2 A non-convergent example

A simple non-convergent example is given by a protein production and nonlinear protein degradation system:

$$\emptyset \to X,\ X \to \emptyset. \tag{2.33}$$

The propensity functions in the CME are:

$$\hat{a}_1(n, V) = k_1 V,\ \hat{a}_2(n, V) = \frac{k_2 n}{K + n/V}. \tag{2.34}$$

The corresponding propensity functions in subvolume k of the RDME are obtained by replacing n by $n^{(k)}$ and V by V/M. These propensity functions can be non-dimensionalised by dividing by $k_1 V$. Then we will have dimensionless propensities:

$$\hat{a}_1 = 1,\ \hat{a}_2 = \frac{K_1 n}{K_2 + n}, \tag{2.35}$$

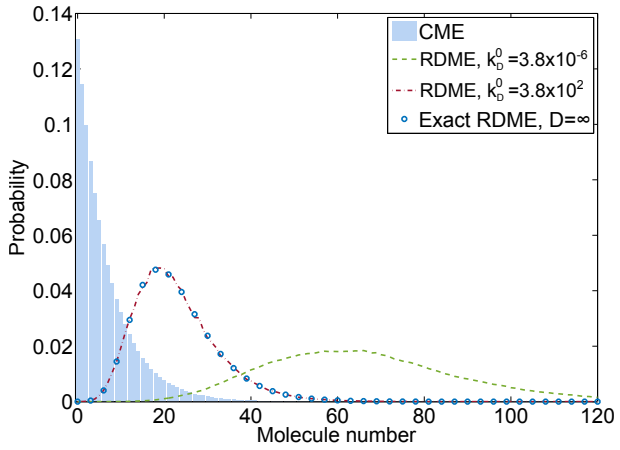

Figure 2.2: Steady state solution of the CME for system (2.33) (blue histogram) compared with the RDME solutions for slow diffusion (green dashed line) and for fast diffusion (red dash-dotted line), all obtained with the SSA, and the exact RDME solution for infinite diffusion given by Eq. (2.38) (blue circles).Parameter values are $K_1 = 1.15$, $M = 10$. The non-dimensional volume is $K_2 = 0.01$. k_D^0 is varied through the diffusion rate k_D.

where $K_1 = \frac{k_2}{k_1}$ and $K_2 = KV$ are dimensionless parameters. In the RDME description, the diffusion rate parameter k_D will be replaced by a dimensionless parameter $k_D^0 = \frac{k_D}{k_1 V}$, and the RDME propensities in subvolume k will be:

$$a_1 = \frac{1}{M},\ a_2 = \frac{K_1 n^{(k)}}{K_2 + M n^{(k)}}, \tag{2.36}$$

The first propensity is convergent but the second is not. Note that the convergence of the first propensity here is obtained in the limit of large k_D at constant values of the volume and of the rate constants, i.e., the limit that k_D^0 tends to infinity at constant K_1 and K_2. It follows that the RDME will not converge to the CME in the fast diffusion limit. In particular, using the method derived in Ref. [24] for general one variable, one step-processes, one can show that the exact steady-state analytical solutions of the CME (Eq. (2.2) with the propensities given by Eq. (2.34)) and of the master equation to which the RDME converges in the fast diffusion limit (Eq. (2.12) with $a_1(n, V) = k_1 V$ and $a_2(n, V)$ given by Eq. (2.25)) are given by:

$$P(0) = C_1,\ P(n) = C_1 \prod_{i=1}^{n} \frac{K_2 + i}{K_1 i}, \tag{2.37}$$

and

$$P(0) = C_2,\ P(n) = C_2 \prod_{i=1}^{n} \frac{M^i (K_2/M + 1)}{K_1 (M-1)^{i-1} i\ {}_2F_1\left(K_2/M + 1, 1 - i; K_2/M + 2; -1/(M-1)\right)}, \tag{2.38}$$

respectively, where C_1 and C_2 are normalisation constants.

In Fig. 2.2 we verify using the SSA that for a small volume ($K_2 = 0.01$) the RDME disagrees with the CME for both very slow and very fast diffusion, i.e., the RDME does not converge to the CME in limit of fast diffusion. Note also that the exact solution of the master equation to which the RDME converges in the fast diffusion limit as given by Eq. (2.38) agrees very well with that obtained using stochastic simulations of the RDME for large diffusion $k_D^0 = 3.8 \times 10^2$; this agreement is an independent verification of our theory.

In Fig. 2.3 we show that for large volumes ($K_2 = 200$) the stochastic simulations agree very well with the exact RDME solution Eq. (2.38) at $k_D^0 = \infty$ and with the exact CME solution Eq. (2.37). In this case the RDME and CME are the Gaussian distribution centred on the solution of the rate equations which is predicted by the LNA. This is in agreement with the

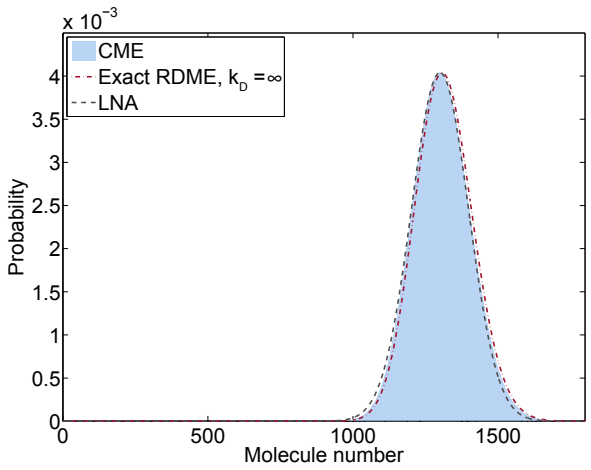

Figure 2.3: Steady state exact solution of the CME given by Eq. (2.37) compared with the steady state exact solution of the RDME for infinite diffusion given by Eq. (2.38) and the LNA for system (2.33). Parameter values are $K_1 = 1.15$, $M = 10$. The non-dimensional volume is $K_2 = 200$ in (b). k_D^0 is varied through the diffusion rate k_D.

results of Section 2.1.4 and shows that the non-convergence problems of the RDME are mostly relevant at small volumes (or equivalently small molecule numbers).

The non-convergence shown in this section makes intuitive sense, since the Michealis-Menten propensity effectively models the enzyme-catalysed degradation of a protein, assuming that the enzyme and protein substrate in each subvolume are in quasi-equilibrium which necessarily requires that the diffusion between neighbouring subvolumes is sufficiently slow. This point is also discussed in in Ref. [181]. Note, however, that our non-convergence results apply to any non-elementary propensity, not just those of the Michaelis-Menten type.

2.4 Summary

In this chapter we have proved a remarkable and counter-intuitive fact, namely that the RDME does not necessarily converge to the CME in the limit of fast diffusion. Conversely, in the limit of *slow* diffusion the RDME decomposes into a set of non-communicating subvolumes with a CME description in each subvolume: the RDME will then be accurate, provided that the subvolume sizes are sufficiently small that they can be assumed to be well-mixed. The RDME with non-elementary reactions can therefore be considered accurate for slow diffusion (and small subvolume sizes) and inaccurate for fast diffusion. We can interpret this as implying that the error of the RDME increases as diffusion rates increase. Intuitively, this occurs because non-elementary systems typically arise from assuming that the fastest timescale is a reaction timescale, an assumption which we violate by increasing the diffusion coefficient.

The consequences of this fact for the RDME as a model are numerous. The class of non-convergent propensities includes Michaelis-Menten-type rates, which are frequently used to model metabolic systems, and Hill-type rates, which describe transcription factor binding. The results in this chapter suggest that the RDME cannot be a consistently accurate spatial model of genetic or metabolic networks, unless they are modelled in complete detail (with all elementary reactions which is often impossible). For the case when the non-elementary reactions are known to effectively model a system of elementary reactions under quasi-equilibrium conditions in well-mixed conditions, the RDME is valid if it can be ascertained that the diffusion is slow enough such that one has chemical quasi-equilibrium in each subvolume.

This chapter could be regarded as an argument against the RDME, however we stress that non-elementary rates make even less sense in BD, where it is utterly unclear how to implement them, or whether it would even be wise to do so. In other words, this chapter does not present a problem with the RDME specifically, but rather a problem with spatial stochastic models in

general. In the next section, we focus on one clear advantage of the RDME over BD: the ability to derive analytical expressions for important statistics.

Chapter 3

Analytical approaches to the reaction-diffusion master equation

The principle advantage of deterministic models (such as the REs or RDEs) over their stochastic counterparts is that they provide quick and easy estimates of mean concentrations. Though these estimates may be systematically incorrect, and though stochastic models provide much more information beyond the mean, the attractiveness of describing chemical kinetics by a single quantity often gives deterministic models the edge.

To counteract this, researchers have attempted to derive simple equations describing the time evolution of the mean of the CME, analogous to the REs [182, 183, 184, 185, 186, 44]. This can be achieved in a number of ways, including moment-closure approximations [182], and the van Kampen expansion [22, 185]. The van Kampen expansion is particularly useful as it is a rigorous perturbative expansion in the inverse square-root of the reaction volume, $V^{-1/2}$, and can therefore be tuned *a priori* to an appropriate level of accuracy for a given system [22].

To zeroth order, the van Kampen expansion of the mean of the CME is simply the REs, which is intuitive since the REs are a large-volume description. To first order, the mean of the CME is described by the effective mesoscopic rate equations (EMREs), which tend to be accurate down to very small numbers of molecules [185].

In this chapter, we show how the EMREs can be derived for the RDME as well as the CME, leading to spatial effective mesoscopic rate equations (sEMRE) [73]. Since the RDME is orders of magnitude more complex than the CME, the sEMRE typically cannot be expressed in simple terms, however we find simple expressions in the case of single-species systems under the assumption of spatial homogeneity. Comparison with $\lambda - \rho$ simulations provides confirmation that our sEMRE is an accurate model.

3.1 Effective mesoscopic rate equations (EMRE)

The REs have already been discussed in great detail, for the specific example $A + B \rightleftharpoons C$ in Eq. (1.2), and in the general case in Eq. (2.13). For our general system of N species $X_1, ..., X_N$, (Eq. (2.1)) they can be expressed neatly as:

$$\frac{d}{dt}\vec{\phi} = S\vec{f}(\vec{\phi}), \tag{3.1}$$

where $\vec{\phi} = (\phi_1, ..., \phi_N)^T$, $S \in \mathbb{R}^{N\times N}$ is a matrix defined by $S_{ij} = r_{ij} - s_{ij}$, and $\vec{f} = (f_1, ..., f_N)^T$. In this section, however, we are interested in estimating the mean of the CME, which will not necessarily agree with the REs. The mean number of molecules of X_i according to the CME is

given by:

$$\langle n_i \rangle = \sum_{n_1=0}^{\infty} ... \sum_{n_N=0}^{\infty} n_i P(\vec{n}, t), \tag{3.2}$$

where $P(\vec{n}, t)$ is the solution of the CME, Eq. (2.2). The van Kampen expansion [22] states that $\vec{n}$ can be written in the form:

$$\vec{n} = V\vec{\phi} + V^{1/2}\vec{\varepsilon}, \tag{3.3}$$

where $\vec{\varepsilon}$ is a vector of error terms. This implies that the CME mean Eq. (3.2) can be written:

$$\langle n_i \rangle = V\phi_i + V^{1/2}\langle \varepsilon_i \rangle, \tag{3.4}$$

so that the question of finding the mean molecule numbers is reformulated in terms of finding the expected errors $\langle \varepsilon_i \rangle$.

It has been shown that $\langle \vec{\varepsilon} \rangle = \vec{0}$ for systems with at most first-order reactions ($\sum_{i=1}^{N} s_{ij} \leq 1 \; \forall j$) [187] and for a subset of reversible systems (including those with bimolecular reactions) in detailed balance [188]. It follows that the RE solution $\vec{\phi}$ is exactly equal to the mean concentrations $\langle \vec{n} \rangle / V$ for these systems. For other systems, $\langle \varepsilon_i \rangle \neq \vec{0}$ and so estimating the expected value is essential to computing accurate mean concentrations.

The first order approximation to $\langle \vec{\varepsilon} \rangle$ is given by the EMREs (originally derived in Ref. [185]). The time-evolution equation for $\langle \vec{\varepsilon} \rangle$ is:

$$\frac{d}{dt}\langle \vec{\varepsilon} \rangle = J\langle \vec{\varepsilon} \rangle + V^{-1/2}\vec{\Delta}, \tag{3.5}$$

where $J = S\frac{\partial \vec{f}(\vec{\phi})}{\partial \vec{\phi}}$ is the Jacobian of the REs, and $\vec{\Delta} \in \mathbb{R}^N$ is a vector whose i^{th} element is defined as:

$$\Delta_i = \frac{1}{2}\left(\sum_{j,k=1}^{N} \frac{\partial J_{ij}}{\partial \phi_k} \langle \varepsilon_j \varepsilon_k \rangle - \sum_{j=1}^{N} \phi_j \frac{\partial J_{ij}}{\partial \phi_j} \right). \tag{3.6}$$

The covariance $\langle \varepsilon_j \varepsilon_k \rangle$ can be computed as the $(j,k)^{\text{th}}$ element of the matrix $C \in \mathbb{R}^{N \times N}$ which solves the Lyapunov equation:

$$\frac{d}{dt}C = JC + CJ^T + D, \tag{3.7}$$

where $D = S \; \text{diag}\left(\vec{f}(\vec{\phi})\right) S^T$ is the diffusion matrix. Note that the covariance of fluctuations in molecule numbers of two species X_i and X_j is $V\langle \varepsilon_i \varepsilon_j \rangle$. Hence the estimate of the mean concentration using the EMRE takes into account, via the vector $\vec{\Delta}$, the coupling between the mean and the covariance of fluctuations. Note that the vector $\vec{\Delta}$ is only non-zero if the Hessian of the rate equations is non-zero and hence a necessary (but not sufficient) condition for $\vec{\varepsilon}$ to be non-zero is that the system is composed of at least one reaction with a nonlinear reaction law, such as a bimolecular reaction. Also note that Eq. (3.6) is only valid for a system obeying mass-action kinetics; a generalisation to the case where some of the reactions are non-elementary can be found in [189], though since the RDME is not well-defined for such systems (see chapter 2) we will not go into the subject in this thesis.

The EMRE itself is a time-evolution equation for the approximate mean concentrations $\vec{\psi}$, which is defined as $\vec{\psi} = \vec{\phi} + V^{-1/2}\langle \vec{\varepsilon} \rangle$, which when substituted into Eq. (3.5) leads to the defining equation of the EMREs:

$$\frac{d}{dt}\vec{\psi} = \frac{d}{dt}\vec{\phi} + J(\vec{\psi} - \vec{\phi}) + V^{-1}\vec{\Delta}. \tag{3.8}$$

In steady-state, all time derivatives are zero, so we recover the simpler equations for the EMRE:

$$\vec{\psi} = \vec{\phi} - V^{-1}J^{-1}\vec{\Delta}, \tag{3.9}$$

and the steady-state Lyapunov equation,

$$JC + CJ^T + D = 0. \tag{3.10}$$

For a system consisting of only one chemical species X, the EMRE simplifies dramatically. The reaction system can be written as:

$$s_j X \xrightarrow{k_j} r_j X, \tag{3.11}$$

for $j = 1, ..., R$, for stoichiometric coefficients s_j and r_j. The stoichiometrix matrix S will in this case be a stoichiometric vector with entries $S_j = r_j - s_j$, and the mass-action rate vector $\vec{f} \in \mathbb{R}^R$ will have elements defined as $f_j(\phi) = k_j \phi^{s_j}$, where ϕ is now the steady-state deterministic concentration of X.

Because this is a single-species system, the Jacobian and diffusion matrices will simply be real numbers, $J = \alpha$ and $D = \beta$ respectively. These are defined as:

$$\alpha = S\frac{\partial \vec{f}(\phi)}{\partial \phi} = \sum_{j=1}^{R} k_j s_j (r_j - s_j)\phi^{s_j - 1},\ \beta = S\ \mathrm{diag}\left(\vec{f}(\phi)\right) S^T = \sum_{j=1}^{R} k_j (r_j - s_j)^2 \phi^{s_j}. \tag{3.12}$$

Note that stable systems must have $\alpha < 0$, since α is the eigenvalue of the Jacobian, while $\beta > 0$ is guaranteed by its definition. The matrix of covariances, C, is now simply a real number corresponding to $\langle \varepsilon^2 \rangle$ and its value can be found by solving Eq. (3.10) to find $\langle \varepsilon^2 \rangle = -\frac{\beta}{2\alpha}$. Similarly, the vector $\vec{\Delta}$ is now a scalar defined as $\Delta = \frac{1}{2}\frac{\partial \alpha}{\partial \phi}\left(\langle \varepsilon^2 \rangle - \phi\right)$. The single-species EMRE in steady-state conditions is therefore given by inserting these values into Eq. (3.9):

$$\psi = \phi + \left(\frac{\beta}{2\alpha} + \phi\right)\frac{1}{2V\alpha}\frac{\partial \alpha}{\partial \phi}. \tag{3.13}$$

Note that the EMRE solution is given by a sum of the RE solution ϕ and a correction which is inversely proportional to the system size V. This result can be shown to be accurate to order V^{-1}; higher-order corrections can also be calculated using the system-size expansion and have been done [35] but we shall not consider them here.

3.2 The spatial EMRE (sEMRE)

Just as the REs provide a deterministic approximation of the CME, one can write spatial rate equations which are a deterministic approximation of the RDME. These equations have been mentioned already, for the example $A + B \rightleftharpoons C$, in Eq. (1.19), but for our general system they take the form:

$$\frac{d}{dt}\phi_i^{(k)} = \sum_{j=1}^{R}(r_{ij} - s_{ij}) f_j(\vec{\phi}^{(k)}) - |\mathcal{N}(k)| k_D^{(i)} \phi_i^{(k)} + k_D^{(i)} \sum_{k' \in \mathcal{N}(k)} \phi_i^{(k')},\ i = 1, ..., N,\ k = 1, ..., M, \tag{3.14}$$

where the first term denotes reactions, the second denotes diffusion out of subvolume k, and the third denotes diffusion into subvolume k from neighbouring subvolumes. The number of neighbouring subvolumes of subvolume k is $|\mathcal{N}(k)|$, which will typically be 2 times the dimensionality of the space. For the remainder of this section we assume a 2-dimensional space, though the calculation can be done for 1 and 3 dimensions [73]. Our 2-dimensional space will consist of a grid of $\sqrt{M} \times \sqrt{M}$ subvolumes, where M is a square number and each subvolume is connected to exactly 4 neighbours, thus taking place on the surface of a torus (periodic boundaries). This assumption enables us to assume each subvolume to be statistically identical.

We can represent Eq. (3.14) in the more compact form:

$$\frac{d}{dt}\vec{\vec{\phi}} = \tilde{S}\vec{\vec{\phi}}, \tag{3.15}$$

where $\vec{\vec{\phi}} \in \mathbb{R}^{NM}$ is a vector of all M local concentrations of all N species, and $\tilde{S} \in \mathbb{R}^{NM \times M(R+4N)}$

is a stoichiometric matrix obtained by treating each diffusion event as an additional reaction – note that there are NM effective species in total (N species in each of M subvolumes) and $M(R+4N)$ effective reactions (R reactions in each of M subvolumes, and a diffusion in each of 4 directions for each of N species in each of M subvolumes). By rewriting the spatial REs in this way, we can subsequently apply the EMRE method to them, but for analytical tractability we will hereafter assume as system of the form (3.11), i.e. $N = 1$. By analogy with the EMRE approach, we need to first determine the $\tilde{S}$, $\tilde{J}$ and $\tilde{D}$ matrices for the spatial REs before we can obtain the sEMRE. Next we consider in detail the construction of these matrices.

First, we consider what we can say about the Jacobian of the spatial REs of this system, $\tilde{J} \in \mathbb{R}^{M\times M}$. Consider the diagonal element $\tilde{J}_{ii}$, which by definition is:

$$\tilde{J}_{ii} = \sum_{k=1}^{M(R+4)} \tilde{S}_{ik} \frac{\partial \tilde{f}_k(\vec{\tilde{\phi}})}{\partial \tilde{\phi}^{(i)}}. \tag{3.16}$$

Note the lack of subscript because we only consider a single species. For the vast majority of values of k, $\tilde{S}_{ik} = 0$; the only non-zero values are those corresponding to reactions inside subvolume i, or diffusion into and out of subvolume i. The contribution to $\tilde{J}_{ii}$ of the internal reactions has already been calculated: it is simply α as defined in Eq. (3.12) (the symmetry of the system implies that in steady-state conditions $\tilde{\phi}^{(i)} = \phi,\ i = 1, ..., M$, where ϕ is the steady-state RE solution). For diffusion *into* subvolume i, $\tilde{S}_{ik} = 1$ and $\tilde{f}_k(\vec{\tilde{\phi}}) = k_D\tilde{\phi}^{(j)}$, where j is the index of a subvolume neighbouring i. It follows that $\frac{\partial \tilde{f}_k(\vec{\tilde{\phi}})}{\partial \tilde{\phi}^{(i)}} = 0$, so there is no contribution to $\tilde{J}_{ii}$. For diffusion *out of* subvolume i, $\tilde{S}_{ik} = -1$ and $\tilde{f}_k(\vec{\tilde{\phi}}) = k_D\tilde{\phi}^{(i)}$. It follows that $\tilde{S}_{ik}\frac{\partial \tilde{f}_k(\vec{\tilde{\phi}})}{\partial \tilde{\phi}^{(i)}} = -k_D$ is the contribution to $\tilde{J}_{ii}$. Since there are 4 distinct diffusion fluxes out of i (one into each neighbouring subvolume), this contribution is multiplied by 4, so that $\tilde{J}_{ii} = \alpha - 4k_D$. Now consider the element $\tilde{J}_{ij}$ where i and j are neighbouring subvolumes:

$$\tilde{J}_{ij} = \sum_{k=1}^{M(R+4)} \tilde{S}_{ik} \frac{\partial \tilde{f}_k(\vec{\tilde{\phi}})}{\partial \tilde{\phi}^{(j)}}. \tag{3.17}$$

The only non-zero contributions to $\tilde{J}_{ij}$ will correspond to reactions that change the number of molecules of X_i (otherwise $\tilde{S}_{ik} = 0$) and which involve X_j (otherwise $\frac{\partial \tilde{f}_k(\vec{\tilde{\phi}})}{\partial \tilde{\phi}^{(j)}} = 0$), and the only reactions with this property are those describing diffusion between subvolumes i and j. For diffusion from i to j, $\tilde{f}_k(\vec{\tilde{\phi}}) = k_D\tilde{\phi}^{(i)}$, so $\frac{\partial \tilde{f}_k(\vec{\tilde{\phi}})}{\partial \tilde{\phi}^{(j)}} = 0$ and there is no contribution to $\tilde{J}_{ij}$. For diffusion from j to i, $\tilde{S}_{ik} = 1$ and $\tilde{f}_k(\vec{\tilde{\phi}}) = k_D\tilde{\phi}^{(j)}$, so the contribution to $\tilde{J}_{ij}$ is $\tilde{S}_{ik}\frac{\partial \tilde{f}_k(\vec{\tilde{\phi}})}{\partial \tilde{\phi}^{(j)}} = k_D$. These are the only reactions contributing to $\tilde{J}_{ij}$, so, for j neighbouring i, $\tilde{J}_{ij} = k_D$.

Finally, if subvolumes i and j are not neighbours, there are no reactions which involve both X_i and X_j, so the Jacobian elements are zero for these entries. In summary:

$$\tilde{J}_{ij} = \begin{cases} \alpha - 4k_D & \text{if } j = i. \\ k_D & \text{if } j \in \mathcal{N}(i). \\ 0 & \text{otherwise.} \end{cases} \tag{3.18}$$

A similar argument can be used to compute the entries of the diffusion matrix $\tilde{D}$, which is given by:

$$\tilde{D}_{ij} = \begin{cases} \beta + 8k_D\phi & \text{if } j = i. \\ -2k_D\phi & \text{if } j \in \mathcal{N}(i). \\ 0 & \text{otherwise.} \end{cases} \tag{3.19}$$

If the subvolumes are numbered from left to right and top to bottom, the matrices $\tilde{J}$ and $\tilde{D}$

are block-circulant matrices, with the following structure:

$$\tilde{J} = \begin{pmatrix} R_J & k_D I & 0 & ... & 0 & k_D I \\ k_D I & R_J & k_D I & ... & 0 & 0 \\ 0 & k_D I & R_J & ... & 0 & 0 \\ \vdots & \vdots & \vdots & \vdots & \vdots & \vdots \\ 0 & 0 & ... & k_D I & R_J & k_D I \\ k_D I & 0 & ... & 0 & k_D I & R_J \end{pmatrix}, \tag{3.20}$$

$$\tilde{D} = \begin{pmatrix} R_D & -2k_D\phi I & 0 & ... & 0 & -2k_D\phi I \\ -2k_D\phi I & R_D & -2k_D\phi I & ... & 0 & 0 \\ 0 & -2k_D\phi I & R_D & ... & 0 & 0 \\ \vdots & \vdots & \vdots & \vdots & \vdots & \vdots \\ 0 & 0 & ... & -2k_D\phi I & R_D & -2k_D\phi I \\ -2k_D\phi I & 0 & ... & 0 & -2k_D\phi I & R_D \end{pmatrix}, \tag{3.21}$$

where,

$$R_J = \begin{pmatrix} \alpha - 4k_D & k_D & 0 & ... & 0 & k_D \\ k_D & \alpha - 4k_D & k_D & ... & 0 & 0 \\ 0 & k_D & \alpha - 4k_D & ... & 0 & 0 \\ \vdots & \vdots & \vdots & \vdots & \vdots & \vdots \\ 0 & 0 & ... & k_D & \alpha - 4k_D & k_D \\ k_D & 0 & ... & 0 & k_D & \alpha - 4k_D \end{pmatrix}, \tag{3.22}$$

$$R_D = \begin{pmatrix} \beta + 8k_D\phi & -2k_D\phi & 0 & ... & 0 & -2k_D\phi \\ -2k_D\phi & \beta + 8k_D\phi & -2k_D\phi & ... & 0 & 0 \\ 0 & -2k_D\phi & \beta + 8k_D\phi & ... & 0 & 0 \\ \vdots & \vdots & \vdots & \vdots & \vdots & \vdots \\ 0 & 0 & ... & -2k_D\phi & \beta + 8k_D\phi & -2k_D\phi \\ -2k_D\phi & 0 & ... & 0 & -2k_D\phi & \beta + 8k_D\phi \end{pmatrix}, \tag{3.23}$$

and $I \in \mathbb{R}^{\sqrt{M}\times\sqrt{M}}$ is the identity matrix.

By analogy with the EMRE Eq. (3.9), from $\tilde{J}$ and $\tilde{D}$ determined above, it is possible to derive the sEMRE:

$$\vec{\tilde{\psi}} = \vec{\tilde{\phi}} - \frac{M}{V}\tilde{J}^{-1}\vec{\tilde{\Delta}}. \tag{3.24}$$

The factor $\frac{M}{V}$ appears because each species now exists in a subvolume of size $\frac{V}{M}$. The i^{th} entry of $\vec{\tilde{\Delta}}$ is defined as in Eq. (3.6) (with tildes on all symbols, and N replaced by M since the latter is the number of effective species), but since the only entries of $\tilde{J}$ which have any ϕ-dependence are the diagonal entries, this can be simplified to $\tilde{\Delta}_i = \frac{1}{2}\frac{\partial\alpha}{\partial\phi}\left(\langle\tilde{\varepsilon}_i^2\rangle - \phi\right)$. By the condition of spatial symmetry, all the $\langle\tilde{\varepsilon}_i^2\rangle$ must be the same, say, $\langle\tilde{\varepsilon}^2\rangle$, which implies that the vector $\vec{\tilde{\Delta}}$ can be simplified to $\vec{\Delta} = \frac{1}{2}\frac{\partial\alpha}{\partial\phi}\left(\langle\tilde{\varepsilon}^2\rangle - \phi\right)\mathbf{1}$, where $\mathbf{1} \in \mathbb{R}^M$ is a column vector of 1s.

The sEMRE is then given by $\vec{\tilde{\psi}} = \phi\mathbf{1} - \frac{M}{2V}\frac{\partial\alpha}{\partial\phi}\left(\langle\tilde{\varepsilon}^2\rangle - \phi\right)\tilde{J}^{-1}\mathbf{1}$. Notice now that the vector $\mathbf{1}$ is an eigenvector of $\tilde{J}$ with eigenvalue α. It follows that $\mathbf{1}$ is also an eigenvector of $\tilde{J}^{-1}$ with eigenvalue $\frac{1}{\alpha}$, and we can therefore simplify $\tilde{J}^{-1}\mathbf{1}$ to $\frac{1}{\alpha}\mathbf{1}$. The sEMRE then becomes a vector with every entry the same, so we write the scalar $\tilde{\psi}$ as:

$$\tilde{\psi} = \phi - \frac{M}{2V\alpha}\frac{\partial\alpha}{\partial\phi}\left(\langle\tilde{\varepsilon}^2\rangle - \phi\right). \tag{3.25}$$

It remains therefore only to find the value of the quantity $\langle\tilde{\varepsilon}^2\rangle$. This is given by the first entry of the matrix $\tilde{C}$ which is defined by the Lyapunov equation given in Eq. (3.10) (with tildes). We notice that by the symmetries of the system, both $\tilde{J}$ and $\tilde{C}$ must be symmetric, circulant matrices [190], which implies that $\tilde{J}\tilde{C} = \tilde{C}\tilde{J}^T$, and therefore the Lyapunov equation can be

simplified to $\tilde{C} = -\frac{1}{2}\tilde{J}^{-1}\tilde{D}$.

Since $\tilde{J}$ is block circulant, its inverse is also, and we can write it as:

$$\tilde{J}^{-1} = \begin{pmatrix} B_1 & B_2 & B_3 & ... \\ B_{\sqrt{M}} & B_1 & B_2 & ... \\ B_{\sqrt{M}-1} & B_{\sqrt{M}} & B_1 & ... \\ \vdots & \vdots & \vdots & \ddots \end{pmatrix}. \tag{3.26}$$

Then $\tilde{C}$ will be given by:

$$\tilde{C} = -\frac{1}{2}\left(B_1 R_D + B_2(-2k_D\phi I) + B_N(-2k_D\phi I)\right). \tag{3.27}$$

The defining equations for the relevant B_i are [191]:

$$\begin{aligned} B_1 &= \frac{1}{\sqrt{M}}\sum_{k=1}^{\sqrt{M}}\left(R_J + 2k_D\cos\left(\frac{2\pi k}{\sqrt{M}}\right)I\right)^{-1}, \\ B_2 &= \frac{1}{\sqrt{M}}\sum_{k=1}^{\sqrt{M}} e^{\frac{2\pi i k}{\sqrt{M}}}\left(R_J + 2k_D\cos\left(\frac{2\pi k}{\sqrt{M}}\right)I\right)^{-1}, \\ B_N &= \frac{1}{\sqrt{M}}\sum_{k=1}^{\sqrt{M}} e^{\frac{2\pi i k(\sqrt{M}-1)}{\sqrt{M}}}\left(R_J + 2k_D\cos\left(\frac{2\pi k}{\sqrt{M}}\right)I\right)^{-1}. \end{aligned} \tag{3.28}$$

Since $R_J + 2k_D\cos\left(\frac{2\pi k}{\sqrt{M}}\right)I$ is a circulant matrix, we can write its inverse as:

$$\left(R_J + 2k_D\cos\left(\frac{2\pi k}{\sqrt{M}}\right)I\right)^{-1} = F^{-1}_{\sqrt{M}}\Lambda_k F_{\sqrt{M}}, \tag{3.29}$$

where $\left(F_{\sqrt{M}}\right)_{j,w} = e^{-\frac{2\pi i j w}{\sqrt{M}}}$. Λ_k is diagonal such that:

$$(\Lambda_k)_{j,j} = \frac{1}{\alpha - 4k_D + 2k_D\cos\left(\frac{2\pi k}{\sqrt{M}}\right) + 2k_D\cos\left(\frac{2\pi j}{\sqrt{M}}\right)}. \tag{3.30}$$

Therefore,

$$B_1 = \frac{1}{\sqrt{M}}F^{-1}_{\sqrt{M}}\tilde{\Lambda}_1 F_{\sqrt{M}}, \tag{3.31}$$

where

$$\left(\tilde{\Lambda}_1\right)_{j,j} = \sum_{k=1}^{\sqrt{M}}\frac{1}{\alpha - 4k_D + 2k_D\cos\left(\frac{2\pi k}{\sqrt{M}}\right) + 2k_D\cos\left(\frac{2\pi j}{\sqrt{M}}\right)}. \tag{3.32}$$

Similarly, $B_2 = \frac{1}{\sqrt{M}}F^{-1}_{\sqrt{M}}\tilde{\Lambda}_2 F_{\sqrt{M}}$ and $B_{\sqrt{M}} = \frac{1}{\sqrt{M}}F^{-1}_{\sqrt{M}}\tilde{\Lambda}_{\sqrt{M}}F_{\sqrt{M}}$, where

$$\left(\tilde{\Lambda}_2\right)_{j,j} = \sum_{k=1}^{\sqrt{M}}\frac{e^{-\frac{2\pi i k}{\sqrt{M}}}}{\alpha - 4k_D + 2k_D\cos\left(\frac{2\pi k}{\sqrt{M}}\right) + 2k_D\cos\left(\frac{2\pi j}{\sqrt{M}}\right)}, \tag{3.33}$$

and

$$\left(\tilde{\Lambda}_{\sqrt{M}}\right)_{j,j} = \sum_{k=1}^{\sqrt{M}}\frac{e^{-\frac{2\pi i k(\sqrt{M}-1)}{\sqrt{M}}}}{\alpha - 4k_D + 2k_D\cos\left(\frac{2\pi k}{\sqrt{M}}\right) + 2k_D\cos\left(\frac{2\pi j}{\sqrt{M}}\right)}. \tag{3.34}$$

$F_{\sqrt{M}}$ has the structure:

$$F_{\sqrt{M}} = \begin{pmatrix} 1 & 1 & 1 & 1 & ... \\ 1 & e^{\frac{-2\pi i}{\sqrt{M}}} & e^{\frac{-4\pi i}{\sqrt{M}}} & e^{\frac{-6\pi i}{\sqrt{M}}} & ... \\ 1 & e^{\frac{-4\pi i}{\sqrt{M}}} & e^{\frac{-8\pi i}{\sqrt{M}}} & e^{\frac{-12\pi i}{\sqrt{M}}} & ... \\ 1 & e^{\frac{-6\pi i}{\sqrt{M}}} & e^{\frac{-12\pi i}{\sqrt{M}}} & e^{\frac{-18\pi i}{\sqrt{M}}} & ... \\ \vdots & \vdots & \vdots & \vdots & \ddots \end{pmatrix}. \tag{3.35}$$

So the contributions to $\langle\tilde{\varepsilon}^2\rangle$, which is the first entry of the matrix $\tilde{C}$, will be obtained by substituting Eq. (3.28) into Eq. (3.27). The first contribution will be proportional to:

$$\begin{pmatrix} 1 & 0 & ... & 0 \end{pmatrix} B_1 R_D \begin{pmatrix} 1 \\ 0 \\ \vdots \\ 0 \end{pmatrix}, \tag{3.36}$$

$$= \begin{pmatrix} 1 & 0 & ... & 0 \end{pmatrix} F^{-1}_{\sqrt{M}} \tilde{\Lambda}_1 F_{\sqrt{M}} \begin{pmatrix} \beta + 8k_D\phi \\ -2k_D\phi \\ 0 \\ \vdots \\ 0 \\ -2k_D\phi \end{pmatrix},$$

$$= \begin{pmatrix} 1 & 1 & ... & 1 \end{pmatrix} \tilde{\Lambda}_1 \begin{pmatrix} \beta + 8k_D\phi - 4k_D\phi \\ \beta + 8k_D\phi - 4k_D\phi\cos\left(\frac{2\pi}{\sqrt{M}}\right) \\ \beta + 8k_D\phi - 4k_D\phi\cos\left(\frac{4\pi}{\sqrt{M}}\right) \\ \vdots \\ \beta + 8k_D\phi - 4k_D\phi\cos\left(\frac{2\pi(\sqrt{M}-1)}{\sqrt{M}}\right) \end{pmatrix},$$

$$= \frac{1}{M}\sum_{j=1}^{\sqrt{M}} \left(\beta + 8k_D\phi - 4k_D\phi\cos\left(\frac{2\pi(j-1)}{\sqrt{M}}\right)\right) \sum_{k=1}^{\sqrt{M}} \frac{1}{\alpha - 4k_D + 2k_D\cos\left(\frac{2\pi k}{\sqrt{M}}\right) + 2k_D\cos\left(\frac{2\pi j}{\sqrt{M}}\right)}.$$

The second contribution will be proportional to:

$$\begin{pmatrix} 1 & 0 & ... & 0 \end{pmatrix} B_2(-2k_D\phi I) \begin{pmatrix} 1 \\ 0 \\ \vdots \\ 0 \end{pmatrix}, \tag{3.37}$$

$$= \begin{pmatrix} 1 & 1 & ... & 1 \end{pmatrix} \tilde{\Lambda}_2 F_{\sqrt{M}} \begin{pmatrix} -2k_D\phi \\ 0 \\ \vdots \\ 0 \end{pmatrix},$$

$$= -\frac{2k_D\phi}{M}\sum_{j=1}^{\sqrt{M}}\sum_{k=1}^{\sqrt{M}} \frac{e^{-\frac{2\pi ik}{\sqrt{M}}}}{\alpha - 4k_D + 2k_D\cos\left(\frac{2\pi k}{\sqrt{M}}\right) + 2k_D\cos\left(\frac{2\pi j}{\sqrt{M}}\right)}.$$

Similarly, the third contribution will be proportional to:

$$-\frac{2k_D\phi}{M}\sum_{j=1}^{\sqrt{M}}\sum_{k=1}^{\sqrt{M}} \frac{e^{-\frac{2\pi ik(\sqrt{M}-1)}{\sqrt{M}}}}{\alpha - 4k_D + 2k_D\cos\left(\frac{2\pi k}{\sqrt{M}}\right) + 2k_D\cos\left(\frac{2\pi j}{\sqrt{M}}\right)}. \tag{3.38}$$

We can combine the second and third contribution into:

$$-\frac{2k_D\phi}{M}\sum_{j=1}^{\sqrt{M}}\sum_{k=1}^{\sqrt{M}}\frac{2\cos\left(\frac{2\pi k}{\sqrt{M}}\right)}{\alpha-4k_D+2k_D\cos\left(\frac{2\pi k}{\sqrt{M}}\right)+2k_D\cos\left(\frac{2\pi j}{\sqrt{M}}\right)}. \tag{3.39}$$

The final result is that:

$$\langle\tilde{\varepsilon}^2\rangle=-\frac{1}{2M}\sum_{j=0}^{\sqrt{M}-1}\sum_{k=0}^{\sqrt{M}-1}\frac{\beta+8k_D\phi-4k_D\phi\cos\left(\frac{2\pi j}{\sqrt{M}}\right)-4k_D\phi\cos\left(\frac{2\pi k}{\sqrt{M}}\right)}{\alpha-4k_D+2k_D\cos\left(\frac{2\pi k}{\sqrt{M}}\right)+2k_D\cos\left(\frac{2\pi j}{\sqrt{M}}\right)}. \tag{3.40}$$

Therefore, combining Eq. (3.40) with Eq. (3.25), we can explicitly write a formula for $\tilde{\psi}$:

$$\tilde{\psi}=\phi+\frac{2\alpha\phi+\beta}{4V\alpha}\frac{\partial\alpha}{\partial\phi}\sum_{j=0}^{\sqrt{M}-1}\sum_{k=0}^{\sqrt{M}-1}\frac{1}{\alpha-4k_D\left(1-\frac{1}{2}\cos\left(\frac{2\pi j}{\sqrt{M}}\right)-\frac{1}{2}\cos\left(\frac{2\pi k}{\sqrt{M}}\right)\right)}. \tag{3.41}$$

Eq. (3.41) can be greatly simplified when $M\gg 1$. The sum can be separated into two parts:

$$\psi=\phi+\frac{2\alpha\phi+\beta}{4V\alpha^2}\frac{\partial\alpha}{\partial\phi}+\frac{2\alpha\phi+\beta}{4V\alpha}\frac{\partial\alpha}{\partial\phi}\sum_{j=0}^{\sqrt{M}-1}\sum_{k=0^*}^{\sqrt{M}-1}\frac{1}{\alpha-4k_D\left(1-\frac{1}{2}\cos\left(\frac{2\pi j}{\sqrt{M}}\right)-\frac{1}{2}\cos\left(\frac{2\pi k}{\sqrt{M}}\right)\right)}. \tag{3.42}$$

The first part corresponds to the term $j=0,k=0$. The second part covers all the terms other than $j=k=0$ (this is denoted by 0^*). Now we consider what happens in the limit of large M. The double sum can be approximated by an integral:

$$\begin{aligned}\sum_{j=0}^{\sqrt{M}-1}\sum_{k=0^*}^{\sqrt{M}-1}&\frac{1}{\alpha-4k_D\left(1-\frac{1}{2}\cos\left(\frac{2\pi j}{\sqrt{M}}\right)-\frac{1}{2}\cos\left(\frac{2\pi k}{\sqrt{M}}\right)\right)}\\&\approx(M-1)\int_0^1\int_0^1\frac{\mathrm{d}x\ \mathrm{d}y}{\alpha-4k_D\left(1-\frac{1}{2}\cos\left(2\pi x\right)-\frac{1}{2}\cos\left(2\pi y\right)\right)}.\end{aligned} \tag{3.43}$$

This is equal to the expected value of the integrand under the Uniform distribution:

$$\int_0^1\int_0^1\frac{\mathrm{d}x\ \mathrm{d}y}{\alpha-4k_D\left(1-\frac{1}{2}\cos\left(2\pi x\right)-\frac{1}{2}\cos\left(2\pi y\right)\right)}=\mathbb{E}\left[\frac{1}{\alpha-4k_D\left(1-\frac{1}{2}\cos\left(2\pi X\right)-\frac{1}{2}\cos\left(2\pi Y\right)\right)}\right], \tag{3.44}$$

for independent identically distributed Uniform random variables X,Y. By Jensen's inequality, we have:

$$\begin{aligned}\mathbb{E}\left[\frac{1}{\alpha-4k_D\left(1-\frac{1}{2}\cos\left(2\pi X\right)-\frac{1}{2}\cos\left(2\pi Y\right)\right)}\right]&\geq\frac{1}{\alpha-4k_D\mathbb{E}\left[1-\frac{1}{2}\cos\left(2\pi X\right)-\frac{1}{2}\cos\left(2\pi Y\right)\right]}\\&=\frac{1}{\alpha-4k_D}.\end{aligned} \tag{3.45}$$

We therefore have a lower bound for the sEMRE:

$$\tilde{\psi}\geq\phi+\frac{2\alpha\phi+\beta}{4V\alpha^2}\frac{\partial\alpha}{\partial\phi}+\frac{2\alpha\phi+\beta}{4V\alpha}\frac{\partial\alpha}{\partial\phi}\frac{M-1}{\alpha-4k_D}=\phi+\left(\phi+\frac{\beta}{2\alpha}\right)\frac{1}{2V\alpha}\frac{\partial\alpha}{\partial\phi}\left(\frac{M\alpha-4k_D}{\alpha-4k_D}\right). \tag{3.46}$$

This leads to an approximate form for Eq. (3.41):

$$\tilde{\psi}\approx\phi+\left(\phi+\frac{\beta}{2\alpha}\right)\frac{1}{2V\alpha}\frac{\partial\alpha}{\partial\phi}\left(\frac{M\alpha-4k_D}{\alpha-4k_D}\right). \tag{3.47}$$

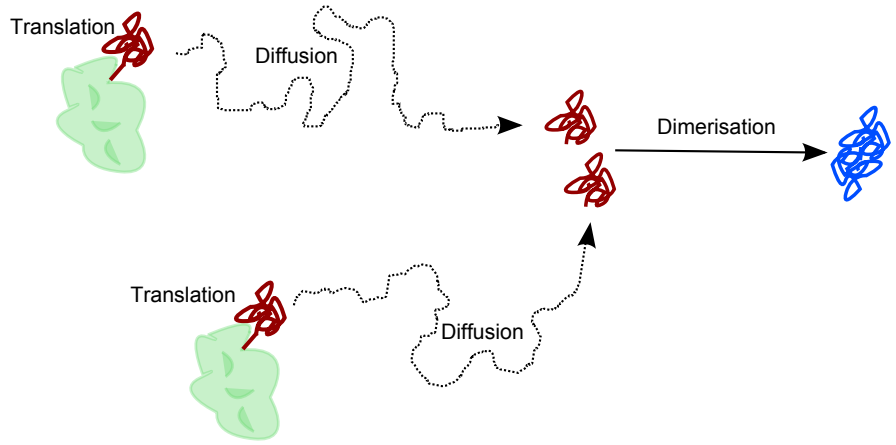

Figure 3.1: Schematic diagram of protein dimerisation model (3.49). Uniformly distributed ribosomes (green) translate proteins (red). These diffuse in the cytosol until a pair combines to form a dimer (blue).

Eq. (3.47) can be written in a particularly informative way to distinguish the contributions from the EMRE and the sEMRE:

$$\tilde{\psi} \approx \underbrace{\phi}_{\text{RE}} + \underbrace{\left(\phi + \frac{\beta}{2\alpha}\right)\frac{1}{2V\alpha}\frac{\partial\alpha}{\partial\phi}}_{\text{EMRE correction}} + \underbrace{\left(\phi + \frac{\beta}{2\alpha}\right)\frac{(M-1)}{2V\alpha}\frac{\partial\alpha}{\partial\phi}\frac{|\alpha|}{|\alpha|+4k_D}}_{\text{sEMRE correction}}. \tag{3.48}$$

Note that the sign of the sEMRE correction is guaranteed to be the same as that of the EMRE correction, since the former is a positive multiple of the latter. Note also that the spatial correction term is proportional to a Michaelis-Menten term, $\frac{|\alpha|}{|\alpha|+4k_D}$, with the absolute values arising from the guaranteed negativity of α. This term monotonically increases from 0 to 1 as the diffusion rate k_D decreases implying that the absolute difference between the stochastic and deterministic solutions $|\tilde{\psi} - \phi|$ increases with decreasing diffusion coefficients. Note also that the difference is proportional to the Hessian of the rate equations $\frac{\partial\alpha}{\partial\phi}$ and hence it is non-zero only if there is at least one bimolecular reaction. Note also that the sEMRE term diminishes to zero in the limit of large k_D: in light of the results in chapter 2, this implies that the distinction between convergent and non-convergent propensities does not exist at the sEMRE level, since even a notionally non-convergent sEMRE will converge.

Hence summarising, our result shows that the steady-state mean concentrations for a spatially-homogeneous one-species system generally depend on the diffusion coefficients. In contrast the spatial deterministic solution ϕ, and the RDEs, have no such dependence. This diffusion dependence is therefore a stochastic effect. In the rest of this chapter, we apply our results to a simple network under the condition of spatial symmetry. We confirm our results by comparison $\lambda - \rho$ simulations.

3.3 Application

In this section we apply the sEMRE to a simple model of protein production and dimerisation in a single cell, shown schematically in Fig. 3.1. Ribosomes (green) translate proteins (red) which diffuse through the cytosol until a pair meets and they dimerise into a product. We do not model the ribosomes explicitly, rather knowing that ribosomes are numerous (in the thousands per cell) and known to be uniformly distributed for some types of cells (for example for E. Coli in the exponential phase, ribosomes are spread uniformly around the cytosol [192]). We therefore roughly model the translation of proteins by ribosomes via a zeroth order reaction

at all points inside a cell. Hence the system in Fig. 3.1 is approximated by the reaction scheme:

$$\emptyset \xrightarrow{k_0} X,\ X + X \xrightarrow{k_1} Y, \tag{3.49}$$

where X is the protein and Y is the dimer.

To test the sEMRE, we perform $\lambda - \rho$ simulations of system (3.49). In order to compute mean concentrations from $\lambda - \rho$, one long simulation is performed (much longer than the time to reach equilibrium), and the mean number of particles is simply the average number over that time. Particles have a diffusion coefficient, D. The area of space is V. The steps of the algorithm are then as follows:

1. Choose a reaction probability per unit time, λ and a time interval Δt. Set time counter $t = 0$. Generate an Exponential$\left(\frac{1}{k_0 V}\right)$ random number τ.

2. Add a Normal random number with zero mean and variance $2D\Delta t$ to each particle coordinate. Add Δt to t.

3. For each pair of intersecting particles (when the distance between the particle centres is less than ρ), generate a uniform random number. If it is less that $\lambda\Delta t$, remove both particles.

4. If $t > \tau$, add a new particle at a uniformly distributed point in space. Generate an Exponential$\left(\frac{1}{k_0 V}\right)$ random number and add it to τ.

5. Repeat steps 2-4 until the desired time has elapsed.

To compare the sEMRE with BD we will need to relate the various parameters used by each of them. This can be done by comparing the two models when diffusion is fast. We expect the sEMRE to emulate the RDME, which (when diffusion is fast) converges to the CME (see chapter 2). Generally, at each BD time step, particle positions are updated by a Normal random number with mean zero and variance $2D\Delta t$; but in the limit of fast diffusion, this Normal distribution will have infinite width. Since our topology has periodic boundary conditions, particles will be uniformly distributed at each time step. Particles collide if they are within ρ of each other. The probability of a collision between two particles in a single time step is therefore the probability that a uniformly distributed point falls within a circle of radius ρ. That is,

$$P(\text{collision}) = \frac{\pi\rho^2}{V}. \tag{3.50}$$

If the number of X molecules is equal to n, there are $n(n-1)/2$ possible pairings of reacting particles. In a given time step Δt, the probability that a given pair collides is $\frac{\pi\rho^2}{V}$, and in BD, the probability that a reaction results in a collision is $\lambda\Delta t$. The probability that a given pair reacts is therefore:

$$P(\text{reaction}) = \frac{\pi\rho^2\lambda\Delta t}{V}. \tag{3.51}$$

Assuming independent collisions, the total *number* of reactions that occur in a given time step is then given by a Binomial$\left(n(n-1)/2, \frac{\pi\rho^2\lambda\Delta t}{V}\right)$ distribution. By definition, the probability of m reactions occuring a Δt is then given by:

$$P(m \text{ reactions}) = \frac{(n(n-1)/2)!}{m!(n(n-1)/2-m)!}\left(\frac{\pi\rho^2\lambda\Delta t}{\Omega}\right)^m\left(1 - \frac{\pi\rho^2\lambda\Delta t}{V}\right)^{n(n-1)/2-m}. \tag{3.52}$$

The probability of 0 reactions is then:

$$P(0 \text{ reactions}) = \left(1 - \frac{\pi\rho^2\lambda\Delta t}{\Omega}\right)^{n(n-1)/2} = 1 - \frac{n(n-1)}{2}\frac{\pi\rho^2\lambda\Delta t}{V} + O((\Delta t)^2), \tag{3.53}$$

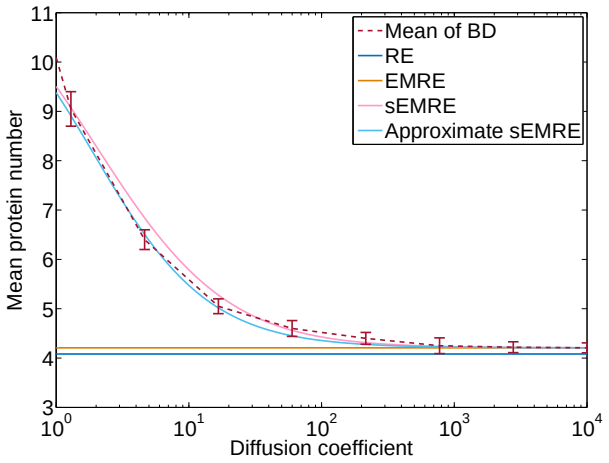

(a)

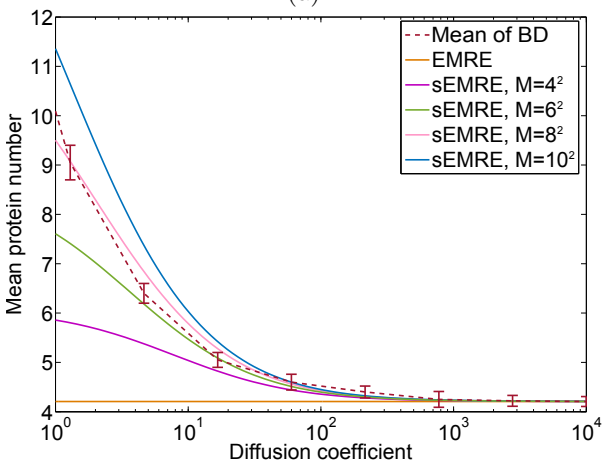

(b)

Figure 3.2: The mean steady-state molecule number of protein X in system (3.49) as a function of the diffusion coefficient D. (a) We compare the result of two dimensional BD simulations in steady-state conditions (dashed red) with the sEMRE, RE and EMRE approximations of the RDME on a two dimensional grid with $M = 8^2$. The RE corresponds to the deterministic spatial approximation of the RDME, the EMRE corresponds to the deterministic approximation of the CME plus a correction to take into account a finite system size V, while the sEMRE corresponds to the EMRE plus a correction to take into account finite diffusion coefficients D. The RE is given by the first term in Eq. (3.58), the EMRE by Eq. (3.58) with $D \to \infty$, the sEMRE by Eq. (3.57) and the approximate sEMRE by Eq. (3.58). (b) Comparison of BD simulations (red) with sEMRE Eq. (3.57) with $M = 4^2$ (purple), $M = 6^2$ (green), $M = 8^2$ (pink) and $M = 10^2$ (blue). Parameter values are $k_0 = 1000$, $k_1 = 30$, $V = 1$, molecule diameter$=\frac{1}{20}$, and $\Delta t = 10^{-5}$. Error bars are the standard deviation of 10 estimates of the mean protein number, each computed from a time average of a BD trajectory of length 10^4 iterations.

and the probability of 1 reaction is:

$$P(1 \text{ reaction}) = (n(n-1)/2)\left(\frac{\pi\rho^2\lambda\Delta t}{V}\right)\left(1-\frac{\pi\rho^2\lambda\Delta t}{V}\right)^{n(n-1)/2-1} \tag{3.54}$$
$$= (n(n-1)/2)\frac{\pi\rho^2\lambda\Delta t}{V} + O((\Delta t)^2).$$

All further terms are $O((\Delta t)^2)$. If Δt is chosen small enough we can ignore terms of $O((\Delta t)^2)$. Although many collisions may occur in a single time step, Δt is chosen small enough so that at most one of these can result in a collision. At the CME level, the reaction $X + X \xrightarrow{k_1} ...$ occurs with a rate $k_1 n(n-1)/V$, which implies that the probability that the reaction occurs in a time step Δt is $P(1 \text{ reaction}) = k_1 n(n-1)\Delta t/V$. Equating this expression with Eq. (3.54), it follows that:

$$(n(n-1)/2)\frac{\pi\rho^2\lambda\Delta t}{V} = \frac{k_1 n(n-1)\Delta t}{V} \implies k_1 = \pi\rho^2\lambda/2. \tag{3.55}$$

The rate of the birth process, k_0, is the same in all models.

The choice of relation between D and k_D is given by Eq. (1.20), corresponding here to $k_D = DM/V$.

The final choice of parameters for comparison is the number of subvolumes M, given that we choose our system size V to be 1 and effective particle diameter to be ρ. There is no obvious choice of subvolume size, except that the subvolume should be larger than a molecule, that is, $M < \rho^{-2}$. Several authors have proposed bounds for a correct choice of M, see Ref. [18] for a summary.

3.3.1 Comparison of BD with sEMRE

Under the RDME, the reaction system (3.49) takes the form:

$$\emptyset \xrightarrow{k_0} X^{(i)}, \quad X^{(i)} + X^{(i)} \xrightarrow{k_1} \emptyset, \quad X^{(i)} \xrightarrow{k_D} X^{(j)}, \quad j \in \mathcal{N}(i), \quad i = 1, ..., M. \tag{3.56}$$

The sEMRE formula given by Eq. (3.41) can be applied specifically to the system (3.49). We find that it gives the formula:

$$\psi = \sqrt{\frac{k_0}{2k_1}} + \frac{\sqrt{2k_0k_1}}{8}\sum_{j=0}^{\sqrt{M}-1}\sum_{k=0}^{\sqrt{M}-1}\frac{1}{V\sqrt{2k_0k_1} + 2DM\left(1-\frac{1}{2}\cos\left(\frac{2\pi j}{\sqrt{M}}\right)-\frac{1}{2}\cos\left(\frac{2\pi k}{\sqrt{M}}\right)\right)}. \tag{3.57}$$

Alternatively we can use the approximate formula given by Eq. (3.47):

$$\psi \approx \sqrt{\frac{k_0}{2k_1}} + \frac{M}{8V}\frac{V\sqrt{2k_0k_1}+2D}{V\sqrt{2k_0k_1}+2DM}. \tag{3.58}$$

In Fig. 3.2(a) we compare the steady-state mean concentrations obtained from BD simulations with the sEMRE formula for $M = 8^2$. The sEMRE agrees well over the whole range of diffusion coefficients, and the approximate formula is also an excellent approximation. The RE and EMRE cease to be good estimates at roughly $D = 100$. In Fig. 3.2(b) we show that, for small enough diffusion coefficients, the choice of M is fundamental to the accuracy of the sEMRE. When $D < 10$ only the sEMRE with $M = 8^2$ gives an accurate estimate of the mean values of BD, however the sEMRE for any M gives good estimates for $D > 10$. This is in agreement with the fact that the RDME agrees with BD only for intermediate subvolume sizes (not too big and not too small); detailed discussions of this fact can be found in Refs. [104, 18]. Note that the dependence of the accuracy of sEMRE with the choice of M stems from the RDME which sEMRE approximates. However this is not of much concern because for all M, sEMRE captures the correct qualitative behaviour (the monotonic increase of the steady-state mean concentrations with decreasing diffusion coefficient) that we observe from BD simulations.

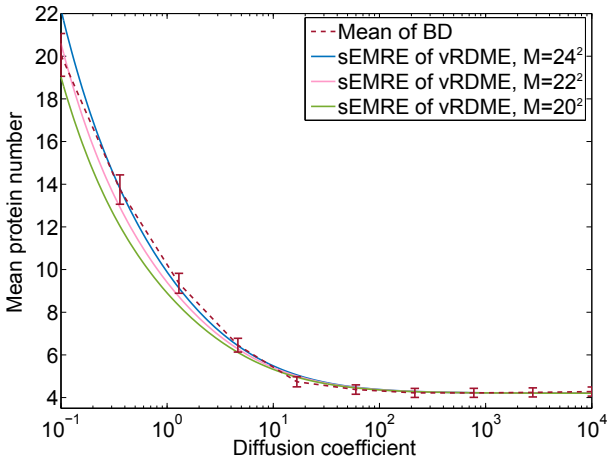

Figure 3.3: The sEMRE of the vRDME system defined in Eq. (3.64) as a function of diffusion coefficient D. The natural choice of M is the total area of space divided by the area of one (circular) particle, in this case $M = 22^2$ (pink line) which passes through every error bar of the BD simulations (red line). Small changes in the choice of M (blue and green lines) do not significantly affect the predictions of the sEMRE. Parameter values are $k_0 = 1000$, $k_1 = 30$, $V = 1$, molecule diameter$=\frac{1}{20}$, and $\Delta t = 10^{-5}$. The parameters $\tilde{k}_0$ and $\tilde{k}_1$ are chosen so that the vRDME and RDME agree in the limit of fast diffusion.

3.3.2 sEMRE of the volume-excluded RDME

The sEMRE is derived for the standard RDME, but can equally be applied to alternative RDMEs. One example is the recently-introduced volume-excluded RDME (vRDME) [34]. The vRDME is a crude model of molecular crowding (as discussed in chapter 1) which is known to agree well with BD, and which assumes that each particle occupies a fixed, non-zero volume, and thereby places an upper bound on the number of particles in the system. This is done by shrinking the subvolume size to be approximately equal to the size of a single particle. subvolumes can then either be empty, or else contain exactly one particle. Bimolecular reactions take place between neighbouring subvolumes, and a particle can diffuse only if a neighbouring subvolume is empty. This is achieved by a introducing an "empty space particle", a dummy species which occupies a subvolume if it is empty. For the dimerisation example, the vRDME replaces the reaction system given by (3.56), with the following:

$$E^{(i)} \xrightarrow{\tilde{k}_0} X^{(i)},\ X^{(i)} + X^{(j)} \xrightarrow{\tilde{k}_1} E^{(i)} + E^{(j)},\ X^{(i)} + E^{(j)} \underset{\tilde{k}_D}{\overset{\tilde{k}_D}{\rightleftharpoons}} E^{(i)} + X^{(j)},\ i = 1, ..., M,\ j \in \mathcal{N}(i), \tag{3.59}$$

where $E^{(i)}$ represents an empty space particle in subvolume i. Note that reaction rates are given as $\tilde{k}_j$, since they will in general take a different numerical value to the k_j used in the RDME.

The sEMRE for the vRDME is derived as follows. We can write down the rate equation for $X^{(i)}$ in the system (3.59):

$$\begin{aligned}\frac{d\tilde{\phi}^{(i)}}{dt} =& \tilde{k}_0\left(\frac{M}{V} - \tilde{\phi}^{(i)}\right) - \sum_{j\in\mathcal{N}(i)} \frac{\tilde{k}_1}{4}\tilde{\phi}^{(i)}\tilde{\phi}^{(j)} \\ &+ \sum_{j\in\mathcal{N}(i)} \tilde{k}_D\left(\frac{M}{V} - \tilde{\phi}^{(i)}\right)\tilde{\phi}^{(j)} - \sum_{j\in\mathcal{N}(i)} \tilde{k}_D\tilde{\phi}^{(i)}\left(\frac{M}{V} - \tilde{\phi}^{(j)}\right),\end{aligned} \tag{3.60}$$

where the first term corresponds to the birth reaction, the second term to the four possible dimerisations (each with a different neighbouring subvolume), and the third and fourth to diffusions into and out of subvolume i respectively. Note that $\left(M/V - \tilde{\phi}^{(i)}\right)$ corresponds to the concentration of empty space in subvolume i, $E^{(i)}$. This is since each subvolume can contain

either E or X, and hence there exists a conservation law in each subvolume. Also note that the factor of $\tilde{k}_1/4$ is due to the fact that the dimerisation can occur between $X^{(i)}$ and four distinct neighbours; by dividing by 4, we ensure that the total dimerisation rate for a given $X^{(i)}$ is $\tilde{k}_1$. By the spatial symmetry of the system, all the $\tilde{\phi}^{(i)}$ are equal, say, ϕ. Since the diffusion terms in Eq. (3.60) cancel under this assumption, ϕ is simply the solution of a quadratic:

$$\phi = \frac{\sqrt{\tilde{k}_0^2 + 4\tilde{k}_1\tilde{k}_0\frac{M}{V}} - \tilde{k}_0}{2\tilde{k}_1}. \tag{3.61}$$

We can then write down the entries for the Jacobian matrix $\tilde{J}$ and diffusion matrix $\tilde{D}$, analogously to the method used for the original sEMRE. For the Jacobian, we have:

$$\tilde{J}_{ij} = \begin{cases} -\tilde{k}_0 - \tilde{k}_1\phi - 4k_D\frac{M}{V} & \text{if } j = i. \\ -\frac{\tilde{k}_1}{4}\phi + k_D\frac{M}{V} & \text{if } j \in \mathcal{N}(i). \\ 0 & \text{otherwise.} \end{cases} \tag{3.62}$$

For the diffusion matrix, we have:

$$\tilde{D}_{ij} = \begin{cases} \tilde{k}_0\left(\frac{M}{V} - \phi\right) + \tilde{k}_1\phi^2 + 8k_D\left(\frac{M}{V} - \phi\right)\phi & \text{if } j = i. \\ \frac{\tilde{k}_1}{4}\phi^2 - 2k_D\left(\frac{M}{V} - \phi\right)\phi & \text{if } j \in \mathcal{N}(i). \\ 0 & \text{otherwise.} \end{cases} \tag{3.63}$$

The method of computing the sEMRE of the vRDME is now identical to the sEMRE of the RDME, albeit with different values of $\tilde{J}$ and $\tilde{D}$. Following the same method, we obtain the analytical expression for the sEMRE:

$$\tilde{\psi} = \phi - \frac{\tilde{k}_1}{2V\left(\tilde{k}_0 + 2\tilde{k}_1\phi\right)}\sum_{j=0}^{\sqrt{M}-1}\sum_{k=0}^{\sqrt{M}-1}\frac{e^{2\pi ij/\sqrt{M}}\left(D_d + 2D_n\left(\cos\left(\frac{2\pi j}{\sqrt{M}}\right) + \cos\left(\frac{2\pi k}{\sqrt{M}}\right)\right)\right)}{J_d + 2J_n\left(\cos\left(\frac{2\pi j}{\sqrt{M}}\right) + \cos\left(\frac{2\pi k}{\sqrt{M}}\right)\right)}, \tag{3.64}$$

where D_d and D_n are the diagonal and neighbouring elements of $\tilde{D}$ respectively, and similarly for J_d and J_n. In other words, $J_d = -\tilde{k}_0 - \tilde{k}_1\phi - 4k_DM/V$, $J_n = -(\tilde{k}_1/4)\phi + k_DM/V$, $D_d = \tilde{k}_0\left(M/V - \phi\right) + \tilde{k}_1\phi^2 + 8k_D\left(M/V - \phi\right)\phi$, $D_n = (\tilde{k}_1/4)\phi^2 - 2k_D\left(M/V - \phi\right)\phi$.

The relationship between the parameters $\tilde{k}_j$ of the vRDME and the parameters k_j of BD and the RDME requires careful attention. A detailed discussion can be found in Ref. [34]. Here, we choose parameters such that the vRDME and BD generally agree when diffusion is fast. To do this, we compare the RE of the vRDME with the RE of the CME (or equivalently the RDME) which we know is the fast-diffusion limit of BD. The RE are convenient, since neither of them depend on the diffusion rate $\tilde{k}_D$ or k_D. It follows that we do not need to worry about rescaling this parameter, therefore we set $\tilde{k}_D = k_D$. The steady-state RE solution of the CME is given by $\phi^r = \sqrt{k_0/(2k_1)}$, while the RE solution of the vRDME is ϕ^V given by Eq. (3.61). We therefore need to choose values of $\tilde{k}_0$ and $\tilde{k}_1$ which allow the concentrations to agree. In this paper, we have chosen:

$$\tilde{k}_0 = k_0, \quad \tilde{k}_1 = 2k_1\left(\frac{M}{V} - \sqrt{\frac{k_0}{2k_1}}\right). \tag{3.65}$$

A significant advantage of the vRDME over the conventional RDME is that the choice of M is automatic in the former case: we simply choose an integer M such that $1/M$ is approximately the volume fraction occupied by a single (circular) particle. The benefits of this can be seen in Fig. 3.3, where we plot the sEMRE in Eq. (3.64) against BD simulations. The particle diameter used in BD is $1/20$, which suggests choosing $M \approx 22^2$, and indeed the sEMRE for this M passes through every error bar down to $D = 10^{-1}$, which is an order of magnitude lower than that plotted in Fig. 3.2. We also show the sEMRE with $M = 20^2$ and $M = 24^2$, which both give good approximations to the BD simulations, demonstrating that M only needs to be approximately correct to give accurate results.

Note that the BD simulations for this example are slightly different, since we are trying to model volume exclusion. We use a version of the Cichocki-Hinsen algorithm, which is closely based on the Doi model (see chapter 5 for a detailed discussion). The only difference between this BD and the algorithm described earlier is in point 3 of the algorithm. In this case we would add "If the Uniform random number is greater than $p\Delta t$, subtract Δt from t and return to 2."

3.4 Summary

In this chapter we have derived an analytical expression for the mean concentrations in the RDME, the sEMRE. This concentration is generally different from that predicted by the REs, EMREs, or the RDEs, and is therefore caused by a combined stochastic and spatial effect. The work in this chapter highlights a clear advantage of the RDME over BD: the ability to derive analytical approximations. By comparing the sEMRE with BD simulations, we have been able to analytically quantify a real effect, something we would not have been able to do with BD alone.

We also demonstrated that using a crude model of crowding, the vRDME, enables us to lose the principle problem of the RDME: how to choose M. In the vRDME, M is automatically given to us by the size of molecules. Other creative methods of fixing the problem of M include treating each subvolume as an actual compartment of the cell (e.g. nucleus, cytosol) [193] or as a single cell in a tissue [194], the latter of which is the subject of the next chapter.

Chapter 4

The reaction-diffusion master equation as a tissue model

Tissues are typically comprised of genetically identical cells which are physically joined together and act collectively. In order to do this effectively, cells in tissues must communicate with other cells in the tissue. Several mechanisms of cell-cell communication exist: long-range endocrine signalling enables cells to communicate with other cells which are relatively far away, short-range paracrine signalling connects nearby cells, and direct communication via diffusion or active-transport allows neighbouring cells to communicate [195].

Direct communication can occur through small watertight passages such as gap junctions in animals, and plasmodesmata in plants. In plant cells, molecules up to and including proteins are known to move through plasmodesmata by pure diffusion [196, 197], while those as large as mRNA are actively transported [198]. In animal cells, peptides diffuse through gap junctions [199], while larger molecules have been shown to be transported across cytoplasmic bridges [200] or tunnelling nanotubes [201]. In essence, a single cell in a tissue is partially dependent on its neighbour cells, but also partially independent of them. This partial-dependence makes tissue modelling awkward: a tissue is not well-mixed, so the CME or REs cannot be used to model it; but a single cell is not a closed system, and so again the CME or REs are not appropriate. In this chapter, we suggest the RDME as a natural model to describe tissue systems. Each subvolume of the RDME corresponds to a single cell in the tissue, and hopping between neighbouring subvolumes models communication between neighbour cells.

This description leads to surprising and counterintuitive analytical predictions about noise control in tissues: depending on the statistics of the biochemical network, transport of molecules between neighbour cells can either increase or decrease the single-cell variability, and equivalently the heterogeneity of the tissue. The work in this chapter suggests that cells may actively modify the rate of transport between neighbours in order to control noise [194]. We note that several other computational tissue models exist in the literature, such as Refs. [202, 203]. The framework in this chapter differs from these in that it covers stochastic biochemistry down to the single-molecule level, rather than relatively macroscopic phenomena such as cell adhesion and tumour growth.

4.1 Illustratory examples

Modelling approaches to genetic networks such as the CME assume that the cell is an isolated volume with no molecules entering or leaving the system from outside (Fig. 4.1 (a)). Tissues of cells violate this assumption: each cell is connected to a number of neighbour cells (Fig. 4.1 (b)), and molecules involved in the genetic network can be transported from cell to cell. The differences between a population of identical independent cells and a tissue of identical connected cells can be seen with stochastic simulations of a simple genetic network.

In Fig. 4.1 (c) we plot three independent realisations of the SSA for the well-known two-stage

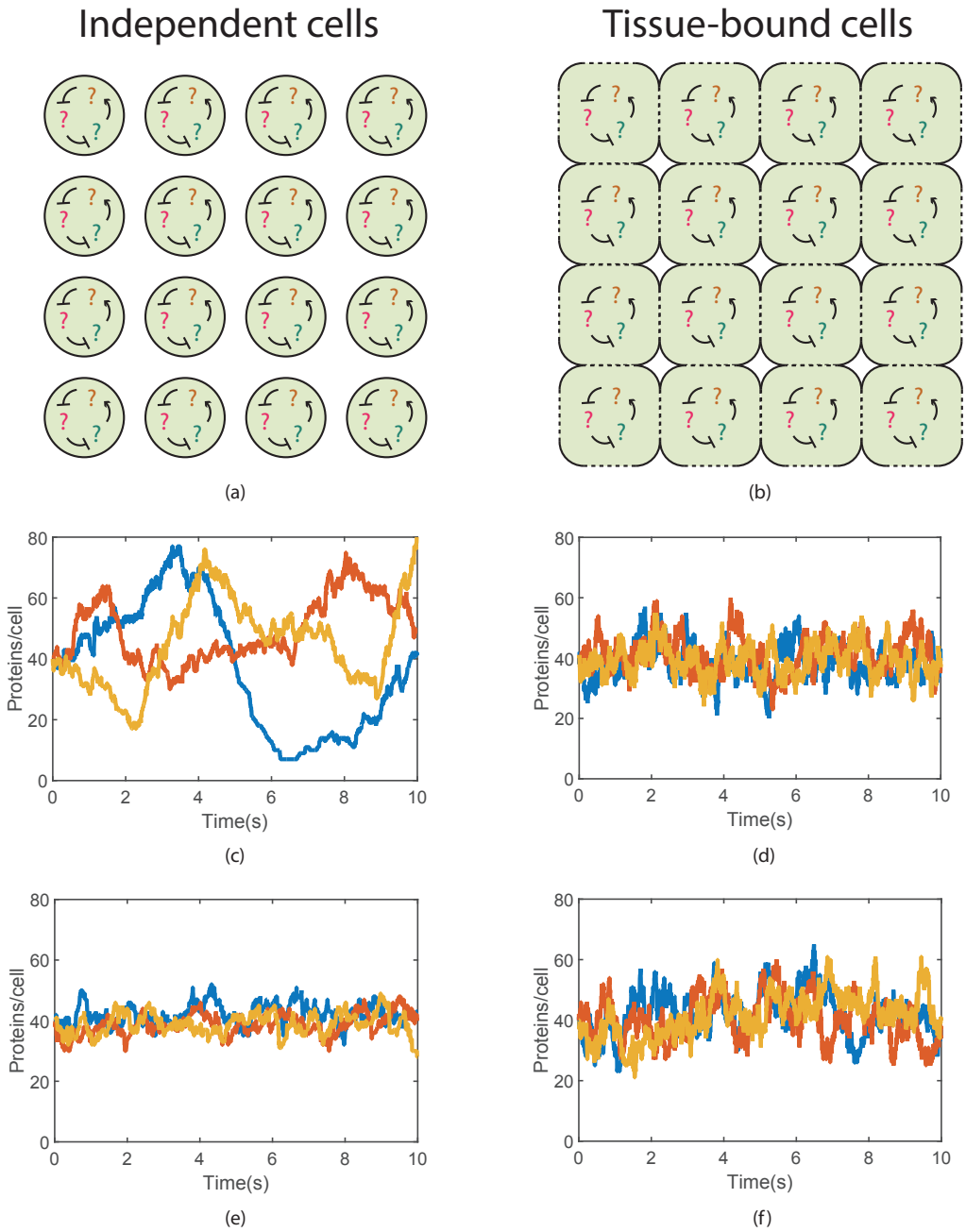

Figure 4.1: Differences between a population of isolated cells and a tissue of cells. (a) A population of isolated cells: each cell contains an identical genetic network. (b) A tissue of cells: each cell contains an identical genetic network and some molecules can be transported between neighbouring cells (dotted lines). (c) Typical single-cell protein trajectories of system (4.1) in isolated cells. (d) Typical single-cell protein trajectories of system (4.1) in a tissue of connected cells: noise is clearly reduced compared to (c). (e) Typical single-cell protein trajectories of system (4.3) in isolated cells. (f) Typical single-cell protein trajectories of syfstem (4.3) in a tissue of connected cells: noise is clearly increased compared to (e). Parameter values are $v_0 = 4,\ d_0 = 1,\ v_1 = 10,\ d_1 = 1,\ k_t = 10,\ M = 100,\ V_C = 1$ for system (4.1) and $k_1 = 32,\ k_2 = 0.01,\ t = 10,\ M = 100,\ V_C = 1$ for system (4.3).

gene expression network [31]:

$$\emptyset \underset{d_0}{\overset{v_0}{\rightleftharpoons}} M,\ M \xrightarrow{v_1} M + P,\ P \xrightarrow{d_1} \emptyset, \tag{4.1}$$

in which a molecule of mRNA (M) is transcribed with rate v_0 and decays with rate d_0. The mRNA can translate a protein (P) with rate v_1 which in turn decays with rate d_1. The trajectories in Fig. 4.1 (c) correspond to the number of protein molecules in three independent cells.

To model a tissue, we imagine a grid of M cells (Fig. 4.1 (b)) with the genetic network (4.1) inside each cell. In addition, we couple neighbouring pairs of cells by allowing the protein P to be transported between them with a rate k_t. To model this, we think of protein transport from cell i to cell j as analogous to diffusion between subvolumes i and j in the RDME. Specifically, we can write the system in cell i as:

$$\emptyset \underset{d_0}{\overset{v_0}{\rightleftharpoons}} M_i,\ M_i \xrightarrow{v_1} M_i + P_i,\ P_i \xrightarrow{d_1} \emptyset,\ P_i \underset{k_t}{\overset{k_t}{\rightleftharpoons}} P_j, \tag{4.2}$$

where M_i and P_i denote the mRNA and protein respectively in cell i, and the reaction $P_i \underset{k_t}{\overset{k_t}{\rightleftharpoons}} P_j$ denotes the transport of protein from cell i to cell j if i and j are neighbouring cells. We note that this model of transport implies exponentially distributed waiting times between successive transport events, an assumption that has previously been used when modelling active transport in tissues [204, 73], and of course in modelling reaction-diffusion systems (chapters 1-3). The main results of this chapter do not depend on the exponential assumption since we only analyse the fast limit of transport, though it is convenient for simulations at finite transport rates. Naturally, this model also imples exponentially distributed reaction times, as discussed in detail in Chapter 1.

We simulated system (4.2) with a version of the SSA [75] with $M = 100$ cells, giving 100 trajectories of protein number, one for each cell. Three typical trajectories are plotted in Fig. 4.1 (d). Notably, the tissue trajectories in Fig. 4.1 (d) are considerably less variable (more homogeneous) than the isolated cell trajectories in Fig. 4.1 (c).

This apparent increase in homogeneity is perhaps unsurprising, and may be thought of as the obvious consequence of increasing coupling. However, remarkably, coupling can also *reduce* the homogeneity in a tissue. For example, a simple system representing the synthesis of a protein P, and its consequent dimerisation into a homodimer D, is defined by the reactions:

$$\emptyset \xrightarrow{k_1} P,\ P + P \xrightarrow{k_2} D. \tag{4.3}$$

In a tissue, this system involves the transport of P between neighbouring cells i and j, with the reactions:

$$\emptyset \xrightarrow{k_1} P_i,\ P_i + P_i \xrightarrow{k_2} D_i,\ P_i \underset{k_t}{\overset{k_t}{\rightleftharpoons}} P_j. \tag{4.4}$$

We simulated system (4.3) both without and with transport using the same version of the SSA, and three typical single-cell trajectories of the protein P are plotted in Fig. 4.1 (e) & (f) respectively. The independent cell trajectories are relatively homogeneous, while the tissue-bound cell trajectories are substantially more variable (more heterogeneous).

An intuitive explanation can be made for these initially surprising observations. The transport of molecules between cells has two distinct effects on the single-cell variability: (1) by moving molecules into and out of cells, it allows for greater cell-cell variation; (2) by smoothing out concentration gradients between neighbouring cells, it homogenises concentrations across the tissue.

The effect of transport on single-cell variability is determined by the trade-off between effects (1) and (2). In Fig. 4.1 (c), the cells have large fluctuations in molecule number which will be reduced by effect (2), but new fluctuations will be induced by effect (1). In Fig. 4.1 (d) new fluctuations have been added, but these are not large enough to offset the reduction in the original fluctuations, and so, overall, homogeneity is increased by transport. Meanwhile, for system (4.3), effect (2) is much less significant because the single-cell variability in Fig. 4.1 (e)

is already small, so effect (1) dominates and there is an overall increase in heterogeneity in Fig. 4.1 (f).

4.2 Theory

To make this intuition mathematically precise, we consider a generalised system of N species $X_1, ..., X_N$ and any number of reactions, a tissue with volume V_T, and a cell of volume V_C. Further, we let n_i be the number of molecules of X_i in the tissue, while m_i is the number of molecules of X_i in the cell. Note that because each cell contains the same genetic network, the variance of fluctuations in a single cell, $\langle m_i^2 \rangle - \langle m_i \rangle^2$, is a non-normalised measure of the single-cell variability. For a given species X_i, we define our measure of single-cell variability, L, to be:

$$L = \frac{V_T \left(\langle m_i^2 \rangle - \langle m_i \rangle^2 \right)}{V_C \left(\langle n_i^2 \rangle - \langle n_i \rangle^2 \right)}, \tag{4.5}$$

i.e., the ratio of the variance of fluctuations in a single cell to the variance of fluctuations in the entire tissue, scaled by volume. The reason for this definition becomes clear when we consider the limiting case of weak cell-cell coupling (i.e. isolated cells).

Let $P(\vec{n}; V_T)$ be the probability that there are $\vec{n} = (n_1, ..., n_N)$ molecules in the entire tissue. Now, let $\vec{m} = (m_1, ..., m_N)$ be the number of molecules in the single cell, and let the corresponding probability distribution be $Q(\vec{m}; V_C)$.

If transport is slow, the system in each cell is independent of the rest of the population, and so, by the Bienaymé formula [19], the sum of the variances in each cell is equal to the variance in the tissue. The variance in a single cell is then given by:

$$\langle m_i^2 \rangle - \langle m_i \rangle^2 = \left[\langle n_i^2 \rangle - \langle n_i \rangle^2 \right] / M = (V_C / V_T) \left[\langle n_i^2 \rangle - \langle n_i \rangle^2 \right]. \tag{4.6}$$

Furthermore since all cells are statistically identical the mean concentration in each cell is the same and equal to that of tissue, $\langle m_i \rangle / V_C = \langle n_i \rangle / V_T$. It follows immediately from these considerations that $L = 1$.

That is, if $L = 1$, then the cell-to-cell variability is at the level we would expect if the cells were completely independent of each other. This can be considered as a neutral state, neither particularly heterogeneous, nor especially homogeneous.

If $L < 1$, then the single-cell variability is lower than we would expect from the Bienaymé formula, given the tissue-level variance. It follows that the cells are more homogeneous than decoupled cells. On the other hand, if $L > 1$, then the cell-to-cell variability is higher than we would expect from the Bienaymé formula, given the tissue-level variance. It follows that the cells are more heterogeneous than decoupled cells. L is therefore a non-dimensional statistical measure of single-cell variability (or equivalently, population heterogeneity).

With this in mind, we next consider what happens to a tissue of cells with cell-cell coupling. At zero coupling, we will naturally have $L = 1$. As the coupling strength increases, L will change, but the magnitude of the change will depend on a number of system-specific factors including the topology of the tissue (which cells are coupled to which), the structure of the genetic network, and the rates of the reactions involved. To bypass these issues, we consider the special case of infinitely fast cell-cell transport, and we reason that the behaviour at finite transport rates will lie between the zero-coupling and infinite-coupling cases.

For the fast transport limit we can relate the local solution Q to the global solution P using the theorem of total probability:

$$Q(\vec{m}; V_C) = \sum_{\vec{n}=0}^{\infty} Pr(\vec{m}|\vec{n}; V_C, V_T) P(\vec{n}; V_T), \tag{4.7}$$

where the notation $\sum_{\vec{n}=0}^{\infty}(\cdot)$ is shorthand for $\sum_{n_1=0}^{\infty} ... \sum_{n_N=0}^{\infty}(\cdot)$, and $Pr(\vec{m}|\vec{n}; V_C, V_T)$ is the probability of finding $\vec{m}$ molecules in V_C *given* that there are $\vec{n}$ molecules in V_T.

As discussed for the RDME in chapter 2, the limit of fast transport implies that molecules move into and out of the the cell much more frequently than they are involved in reactions. The molecules are uniformly distributed in V_T under these conditions, so that the probability

that a randomly chosen molecule is in V_C is simply $\frac{V_C}{V_T}$. It follows from combinatorics that the probability of finding m_i molecules of species X_i in V_C given that there are n_i in V_T is $(n_i!/(m_i!(n_i-m_i)!)(V_C/V_T)^{m_i}(1-V_C/V_T)^{n_i-m_i}$, that is, a Binomial distribution. It follows that $Pr(\vec{m}|\vec{n};V_C,V_T)$ is the product of the mass functions of N Binomial$(n_i, V_C/V_T)$ distributions for each species X_i. An expression for the single-cell distribution Q in terms of the global distribution P can then be written:

$$Q(\vec{m};V_C) = \sum_{\vec{n}=0}^{\infty} P(\vec{n};V_T) \prod_{i=1}^{N} \left[\binom{n_i}{m_i} \left(\frac{V_C}{V_T}\right)^{m_i} \left(1-\frac{V_C}{V_T}\right)^{n_i-m_i} \mathbf{1}_{\vec{m}\leq\vec{n}} \right]. \tag{4.8}$$

The indicator function $\mathbf{1}_{\vec{m}\leq\vec{n}}$ prevents the expression from evaluating the impossible probabilities of finding more molecules in V_C than in V_T, and therefore permits us to sum from zero to infinity without worry. Since this equation gives the single-cell distribution Q, we can use it to evaluate the single-cell second moment which is given by $\langle m_i^2\rangle = \sum_{\vec{m}=0}^{\infty} m_i^2 Q(\vec{m},V_C)$. Swapping the summations over $\vec{n}$ and $\vec{m}$, and absorbing the indicator function into the latter summations, gives:

$$\langle m_i^2\rangle = \sum_{\vec{n}=0}^{\infty} P(\vec{n};V_T) \left[\sum_{m_1=0}^{n_1} \ldots \sum_{m_M=0}^{n_M} m_i^2 \prod_{k=1}^{N} \binom{n_k}{m_k} \left(\frac{V_C}{V_T}\right)^{m_k} \left(1-\frac{V_C}{V_T}\right)^{n_k-m_k} \right]. \tag{4.9}$$

The local second moment is therefore the expected value of the quantity in square brackets under the global distribution P. The quantity in square brackets, however, is merely the expected value of m_i^2 under the M independent Binomial$(n_i, V_C/V_T)$ distributions, and is therefore equal to $n_i\left(\frac{V_C}{V_T}\right)\left(1-\frac{V_C}{V_T}\right) + n_i^2\frac{V_C^2}{V_T}$. It follows that the second moment is given by:

$$\langle m_i^2\rangle - \langle m_i\rangle^2 = \frac{V_C}{V_T}\langle n_i\rangle + \frac{V_C^2}{V_T^2}\left(\langle n_i^2\rangle - \langle n_i\rangle - \langle n_i\rangle^2\right). \tag{4.10}$$

Combining Eqs. (4.5) and (4.10), and defining the Fano factor (FF) as the ratio of tissue-level variance to the mean, $FF = \frac{\langle n_i^2\rangle - \langle n_i\rangle^2}{\langle n_i\rangle}$, we find that the single-cell variability at infinite coupling is given by:

$$L = \frac{V_C}{V_T} + \frac{1-\frac{V_C}{V_T}}{FF}. \tag{4.11}$$

We note now that FF is a standard statistical measure of the size of fluctuations. Probability distributions with $FF = 1$ are said to have *Poissonian fluctations*, while $FF < 1$ corresponds to *sub-Poissonian* and $FF > 1$ to *super-Poissonian*. Our earlier intuition suggested that systems with large fluctuations would tend to see a reduction in cell-to-cell variability as coupling strength increases. Now we see that this is indeed the case: combining $FF > 1$ with Eq. (4.11), we find that $L < 1$ at infinite coupling strength, suggesting that coupling tends to decrease single-cell variability for super-Poissonian systems. Alternatively, choosing $FF < 1$ we find that $L > 1$ at infinite coupling strength, implying that coupling will increase single-cell variability for sub-Poissonian systems.

For system (4.1), the Fano factor can be computed exactly since the moment equations for the corresponding CME are closed [42]. In particular, we have that $FF = 1 + \frac{v_1}{d_0+d_1} > 1$, implying that increasing the transport rate will reduce the single-cell variability, as shown in Fig. 4.1 (c-d).

For system (4.3), the presence of a bimolecular reaction prevents the moment equations from closing, and so the moments are instead obtained from the steady-state distribution of molecule numbers. The mean and variance are given in Ref. [108], but we will not state them here since they are complicated expressions. Instead we note that $FF < 1$ for all parameter values, suggesting that the single-cell variability will increase as cell-cell transport increases. See the next section for more details of these calculations.

For these examples the qualitative changes in single-cell variability are independent of parameter values, though this would not be the case for systems with Fano factors which can vary from sub-Poissonian to super-Poissonian. We note that these results are independent of the spatial structure of the tissue: they apply equally to neighbour-neighbour and long-range

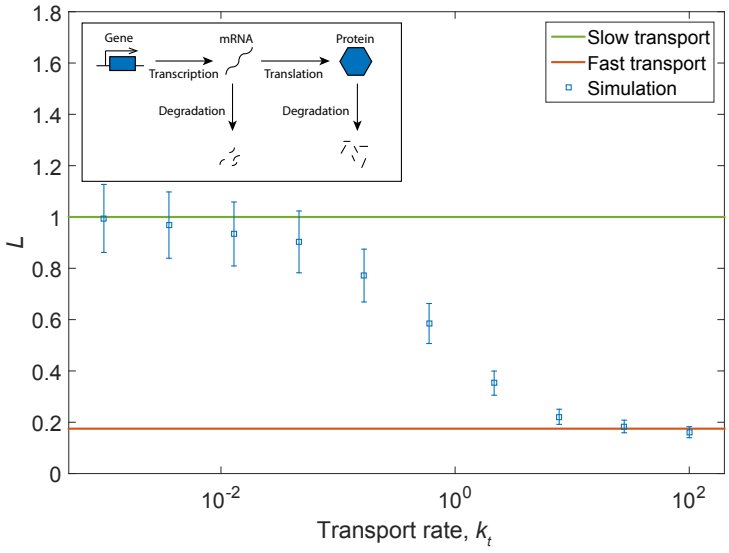

Figure 4.2: L as a function of protein transport rate for the two-stage gene expression system (4.1). Theoretical values for the fast transport limit (red), and slow transport limit (green) are shown as solid lines. Simulation data is shown for the average single-cell variability (blue squares) for a variety of protein transport rates. Parameter values are $v_0 = 3,\ d_0 = 1,\ v_1 = 10;\ d_1 = 1,\ V_C = 1,\ V_T = 100$. Inset: schematic diagram of system (4.1).

interactions, and indeed any kind of coupling provided no cells in the tissue are disconnected from the population. We also stress that these results apply equally to systems out of equilibrium, including oscillatory systems and systems far from steady-state, since no assumptions have been made on the type of biochemical network inside each cell.

We note here that a similar prediction for the dependence of local noise on diffusion relative to Fano factor was made in Ref. [205], for an approximate model of a particular gene system. According to our model, the local noise is only guaranteed to be Fano factor-dependent if the statistics at the whole-tissue level are diffusion-independent, a requirement which is contradicted by our work in chapter 3, where diffusion was shown to affect statistics at the global level. As a result, only a ratio of local to global statistics (such as L) has a clear dependence on diffusion and Fano factor.

4.3 Verification of theory using stochastic simulations

Our theory predicts that the single-cell variability L should move from 1 to the value given in Eq. (4.11) as cell-cell transport increases. In this section we test the accuracy of this prediction on data from detailed stochastic simulations using a version of the SSA [75] that is well-suited to simulating tissues.

First, we again consider the two-stage gene expression system (4.1) as shown in Fig. 4.1 (c-d) and Fig. 4.2 inset. Since the moments of the CME are closed for this system [42] we can find exact expressions for the tissue-level mean, $V_T v_0 v_1/(d_0 d_1)$, and the tissue-level variance, $(V_T v_0 v_1/(d_0 d_1))\,(1 + v_1/(d_0 + d_1))$. It follows that $FF = 1 + v_1/(d_0 + d_1)$, and so Eq (4.11) implies that L will decrease from 1 to $(d_0 + d_1 + v_1 V_C/V_T)/(d_0 + d_1 + v_1)$ as transport increases.

As a second example we consider the protein synthesis and dimerisation system (4.3) as shown in Fig. 4.1 (e-f) and Fig. 4.3 inset. The mean and variance are given in Ref. [108], and they imply that $FF = 3/4 - \phi I_1'(4\phi)/I_1(4\phi) + \phi/(1/(4\phi) + I_1'(4\phi)/I_1(4\phi))$, where $\phi = V_T\sqrt{k_1/(2k_2)}$ and $I_1(x)$ is the modified Bessel function of the first kind [206] and $I_1'(x)$ is its derivative. Numerical analysis confirms that $FF < 1$ for all values of ϕ, suggesting that L will

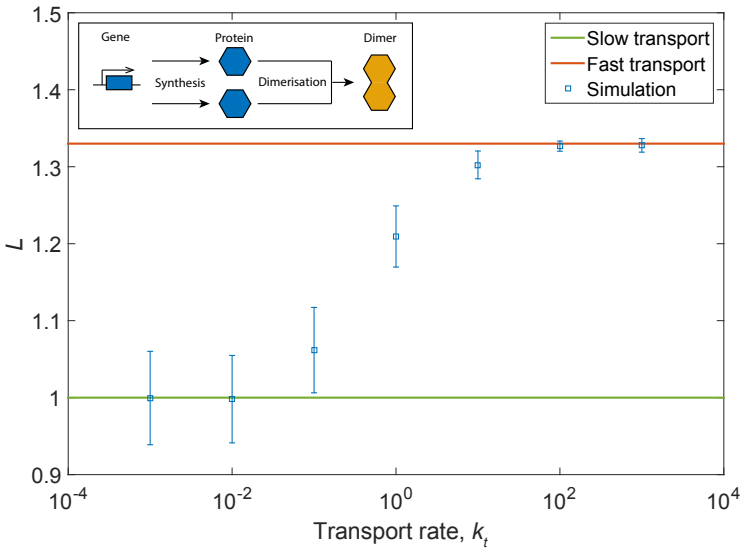

Figure 4.3: L as a function of protein transport rate for the dimerisation system (4.3). Theoretical values for the fast transport limit (red) and slow transport limit (green) are shown as solid lines. Simulation data is shown for the average single-cell variability L (blue squares) for a variety of protein transport rates. Parameter values are $k_1 = 32,\ k_2 = 0.01,\ V_C = 1,\ V_T = 100$. Inset: schematic diagram of system (4.3).

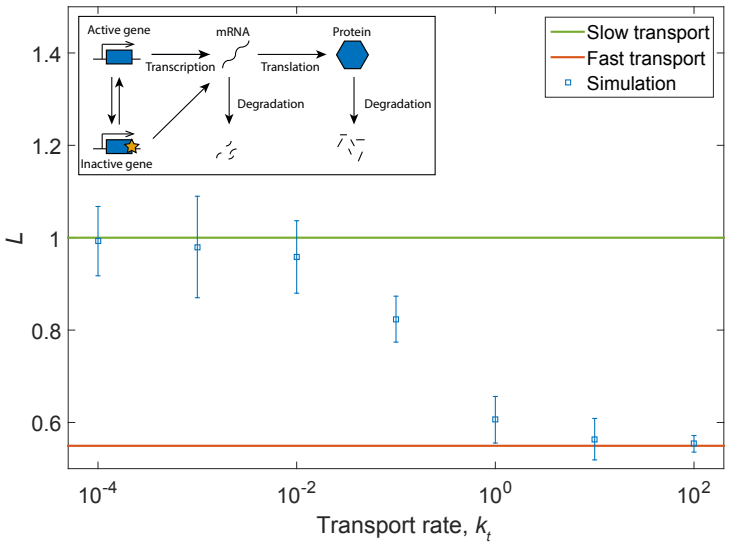

Figure 4.4: L as a function of protein transport rate for the three-stage gene expression system (4.12). Theoretical values for the fast transport limit (red), and slow transport limit (green) are shown as solid lines. Simulation data is shown for the average single-cell variability (blue squares) for a variety of protein transport rates. Parameter values are $k_{\text{on}} = 0.1,\ k_{\text{off}} = 0.1,\ v_0^{\text{on}} = 3,\ v_0^{\text{off}} = 1,\ d_0 = 1,\ v_1 = 1,\ d_1 = 1,\ V_C = 1,\ V_T = 25$. Inset: schematic diagram of system (4.12).

increase from 1 as cell-cell transport increases.

For our third example we consider the bimodal three-stage gene expression network studied in Refs. [31, 207] (Fig. 4.4 inset):

$$G_{\rm on} \underset{k_{\rm on}}{\overset{k_{\rm off}}{\rightleftharpoons}} G_{\rm off},\ G_{\rm on} \xrightarrow{v_0^{\rm on}} G_{\rm on} + M,\ G_{\rm off} \xrightarrow{v_0^{\rm off}} G_{\rm off} + M,$$
$$M \xrightarrow{d_0} \emptyset,\ M \xrightarrow{v_1} M + P,\ P \xrightarrow{d_1} \emptyset, \tag{4.12}$$

in which a gene can be in an active state ($G_{\rm on}$) or an inactive state ($G_{\rm off}$). The active gene transcribes mRNA (M) with a rate $v_0^{\rm on}$, while the inactive gene transcribes mRNA with a rate $v_0^{\rm off}$. The protein is translated as in the earlier system (4.1). We again calculate the mean and variance of fluctuations for the protein P from the moment equations, as for the previous examples, and we find that the Fano factor is larger than 1 so Eq. (4.11) again implies that L will decrease as cell transport increases.

In summary, in Figs. 4.2, 4.3 and 4.4 we compare the analytical expressions for fast transport, Eq. (4.11), with the simulation data for systems (4.1), (4.3) and (4.12) respectively. It is clear that in every case our theoretical predictions are correct. For each example the single-cell variability, L, from simulations (blue squares) moves from the slow limit, 1, (green line) to the predicted fast-transport limit (red line). As predicted by the Fano factor criterion, for systems (4.1) and (4.12) L decreases with transport rate, while L increases for system (4.3).

4.4 Application to experimental data

Testing our predictions on simulations is useful, because by varying the rate of transport we can confirm that increasing it leads to the predicted change in single-cell variability, but with experimental data the transport rate is both fixed and completely unknown. However, we know that L lies between 1 and the value given by Eq. (4.11), and that the parameters of Eq. (4.11) are either tissue-level quantities (FF), or easily calculable (V_T and V_C). It follows that we can use tissue-level timecourse data to estimate L, without any knowledge of the underlying genetic network. In general, the corresponding single-cell data would not be available, however we specifically choose examples with both tissue-level and single-cell data so as to check that our estimates are correct.

We first apply our method to fluorescence data of GFP concentration in two distinct rat pituitary tissues [208] in which cells communicate both via paracrine signalling and active transport across gap junctions. The fluorescence data is available at the single-cell level, so the tissue-level data is obtained simply by summing up the single-cell fluorescence. We apply our method to this tissue-level data, and subsequently check its accuracy using single cells.

The first tissue is taken from a day 18.5 embryonic rat (E18.5), where cell-cell junctions are rare and their related proteins (E-, N-cadherin and β-catenin) and paracrine signalling proteins are expressed at a low level; while the second tissue is taken from a day 1.5 post-natal rat (P1.5) where junctions are considerably more common, and there is a high level of expression of related proteins [208]. The authors of Ref. [208] note that the P1.5 tissue, while clearly more mature than the E18.5 tissue, has not yet reached the level of connectivity of the adult tissue for which the number of gap junctions is likely to be even higher. With this in mind, we expect L in the E18.5 cells to be noticeably closer to 1 than the P1.5 cells, but the P1.5 cells should not be too close to (4.11) since they still are not fully mature.

In Fig. 4.5 (a) and (b) we plot the fast and slow transport limits (green and red lines), and L averaged over each cell (blue squares) and bars representing one standard deviation above the mean (blue bars) for the E18.5 and P1.5 tissues respectively. As expected, L remains between the two in both cases, but is noticeably closer to 1 in Fig. 4.5 (a) than in (b).

The above dataset is further confirmation of our theory, but both it and the simulated systems are either in equilibrium or approaching it. Since this is frequently not the case in reality, we now apply our method to two oscillating datasets, one which we expect to have fast transport and one with slow transport. We stress that our method should apply to oscillatory systems since we have made no assumptions about the underlying genetic networks – only that the same genetic networks should be present in each cell, with the same reaction rates.

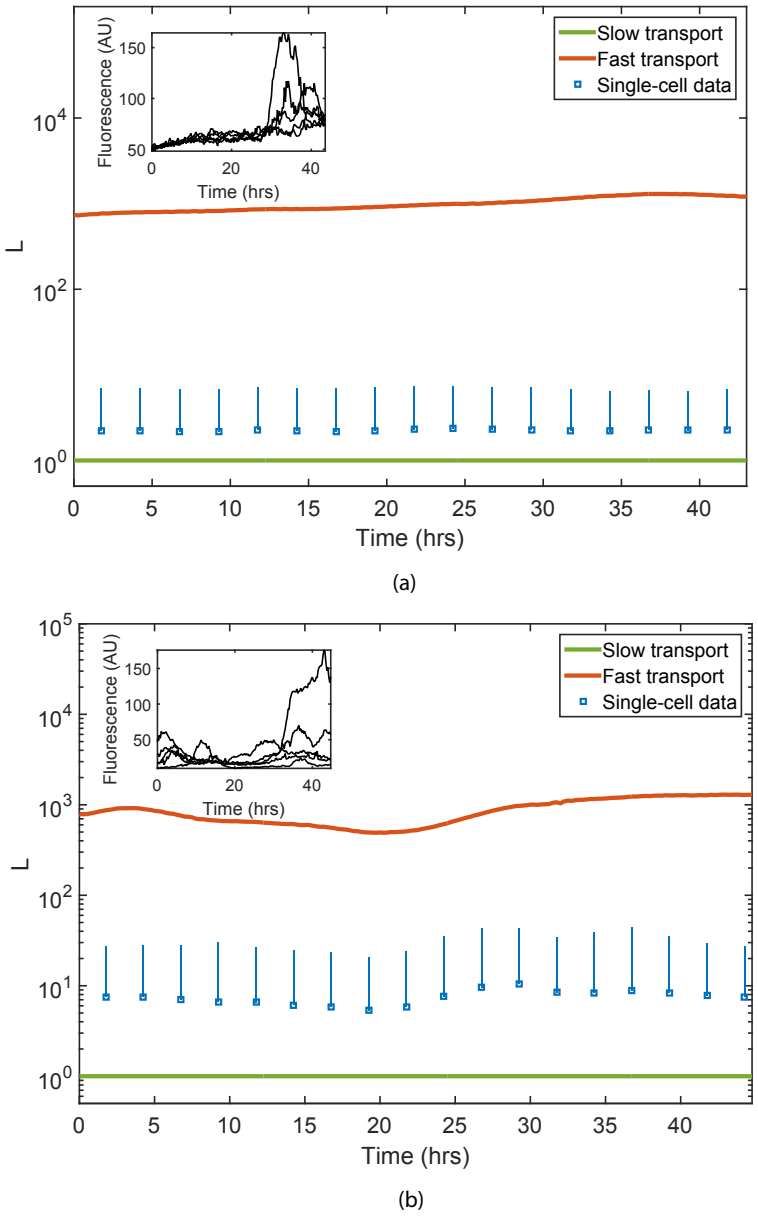

Figure 4.5: Comparison of fast (red) and slow (green) transport limits with single-cell data (blue squares: mean; blue bars: 1 standard deviation above mean) for (a) a tissue of 117 E18.5 rat pituitary cells, (b) a tissue of 114 P1.5 rat pituitary cells. Insets: typical single-cell trajectories from the raw data. Data is taken from Ref. [208].

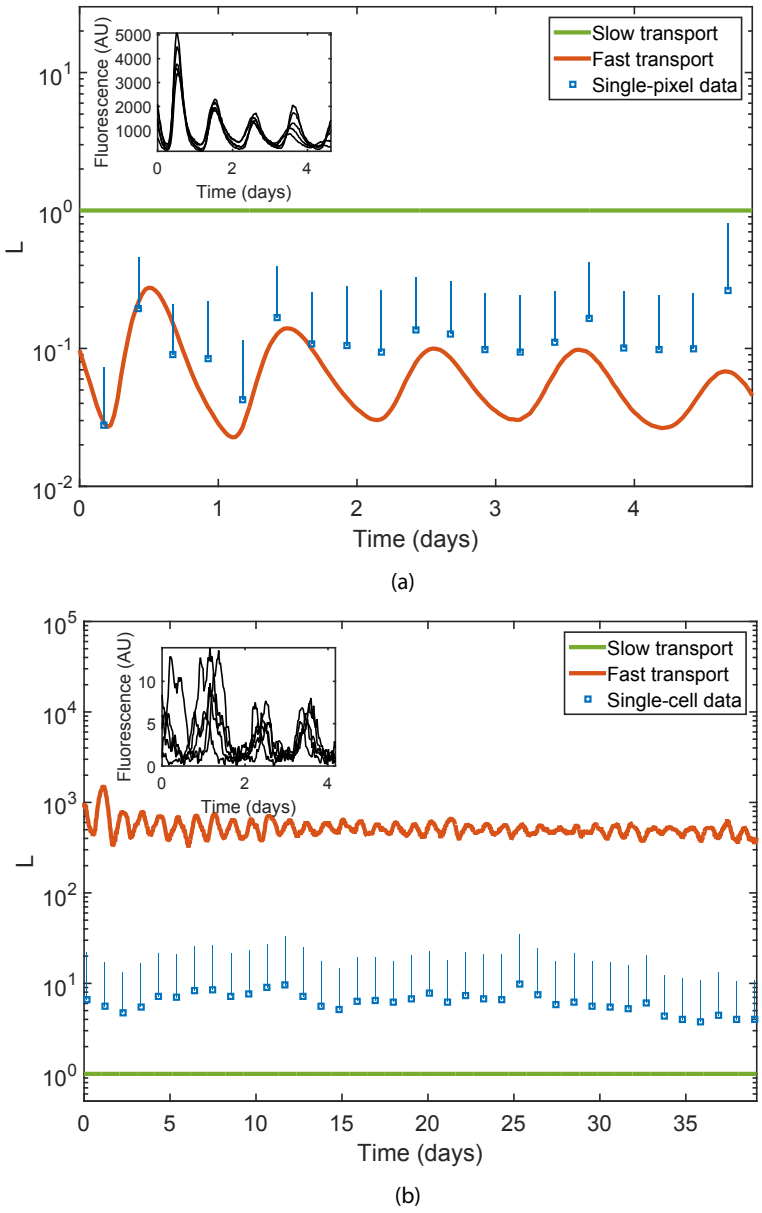

Figure 4.6: Comparison of fast (red) and slow (green) transport limits with single-pixel data (blue squares: mean; blue bars: 1 standard deviation above mean) for (a) a single leaf of *Arabidopsis thaliana*, (b) a population of 30 mouse fibroblast cells. Insets: typical single-cell trajectories from the raw data. Data is taken from (a) Ref. [209], (b) Ref. [210].

The second dataset corresponds to luminescence data of an oscillating protein concentration in a single leaf of *Arabidopsis thaliana* [209]. The luminescence data is available in image form, in which each pixel is close to single-cell resolution, so we can apply our method to the whole-leaf protein trajectory and subsequently check its accuracy with the single-pixel data.

In Fig. 4.6 (a) we plot the slow and fast transport limits (green and red lines respectively) over time, and also L averaged over each pixel of the leaf image (blue squares) and bars representing one standard deviation above the mean (blue bars). Since proteins are frequently transferred between cells in a plant tissue, we might expect L to remain between the two limits but close to the fast limit, and such proves to be the case.

The third dataset consists of luminescence data of an oscillating protein concentration in a small population of mouse fibroblast cells [210]. The cells were imaged on the same plate for a period of over a month, and were sufficiently far apart that single-cell resolution is easily possible. The cells therefore do not exactly form a tissue (though we might expect some very low-level exchange of material) so we expect L to be close to 1.

In Fig. 4.6 (b) we plot the limits (green and red lines), and L averaged over each cell (blue squares) and bars representing one standard deviation above the mean (blue bars). As expected, L remains between the two, but is significantly closer to 1 than to the fast limit.

4.5 Summary

In this chapter, we have treated the RDME as a model of a tissue, thus providing a natural definition of M: the number of cells in the tissue. This model allowed us to make counterintuitive predictions about multicellular biology, namely that single-cell variability can either increase or decrease depending on the rate of direct cell-cell transport. This claim is not purely theoretical: we confirmed its validity with three different experimental datasets from plants and animals.

The work in this chapter highlights the value of mathematical models like the RDME in real biological discovery. Beyond merely explaining phenomena already known to experimentalists, modelling can illuminate new behaviours in advance of their observation in the laboratory. In chapter 6 we will see another example of modelling predicting new biochemical behaviour, but first in the next chapter we focus on fast algorithms for BD.

Chapter 5

Accelerated Brownian dynamics using implicit crowder molecules

In chapter 1 we discussed how BD was obtained by systematically simplifying Newtonian molecular dynamics, and adding in reactive behaviour. One of the necessary simplifications was the removal of the force term in Eq. (1.28), using the argument the intermolecular forces are negligible if concentrations are dilute. As already mentioned, the diluteness assumption typically breaks down inside cells [139, 140], which is the environment to which we would like to apply our models. As a result, BD models which incorporate the force term (thereby emulating the crowded cytoplasmic conditions) are a necessary tool for simulating biochemical networks.

Though crowding was only recognised as an important biological effect relatively recently, algorithms to accurately study the behaviour of hard sphere colloids (uniform suspensions of insoluble particles) was a popular problem in chemical physics long before the biochemical implications of volume exclusion were fully appreciated [211, 212, 213]. One such algorithm was proposed by Cichocki and Hinsen [160]. The idea behind the Cichocki-Hinsen algorithm is simple to state: only one particle is moved at a time, and if the attempted move results in a collision the particle is simply placed back in its previous position, thereby crudely modelling a steric repulsion. Despite its relative simplicity, the Cichocki-Hinsen algorithm has been proved to converge to the Smoluchowski equation in the limit of short simulation time-steps [160]. Furthermore, it has been shown to agree perfectly with far more detailed algorithms which incorporate particle velocity and momentum [214]. It is therefore commonly used to simulate Brownian diffusion of hard spheres in the study of both physical chemistry [215, 216, 217] and cell biology [218, 219, 220]. However because of its fine-grained detail each simulation is computationally expensive, and many independent simulations are required to get good statistical samples.

In this chapter, we propose a modification to the Cichocki-Hinsen algorithm for reaction-diffusion systems. Our simplification arises from distinguishing between reactive particles (which may either be point particles or have a finite volume) and hard sphere crowders. Assuming that the crowder particles are uniformly distributed, we rigorously derive the probability that a reactive particle will collide with a crowder in a single time step, and use this to write a modified Cichocki-Hinsen algorithm which does not explicitly simulate crowders: we call this the *crowder-free* algorithm. We show that the crowder-free algorithm results in a dramatic speed increase over the original Cichocki-Hinsen algorithm of up to three orders of magnitude. Perhaps more surprisingly, the output data of the two algorithms is near-indistinguishable in terms of short-time diffusion coefficients, long-time diffusion coefficients and reaction dynamics for each example that we test.

5.1 Point particles in a crowded environment

We first describe the Cichocki-Hinsen algorithm as applied to a system of reactive point particles in a sea of inert spherical crowders of radius R. The boundaries of the reaction volume can be of any type (periodic, reflective etc) as long as the number of crowder particles remains

constant in time (i.e. no absorbing boundaries). Since the original Cichocki-Hinsen algorithm was written for purely diffusive systems, we have added some steps for reactive systems using the $\lambda - \rho$ model.

If reaction j is a bimolecular reaction, it is assigned a reaction distance ρ_j. Bimolecular reaction j occurs with a rate λ_j when two reactive particles of the relevant type come within a distance ρ_j of each other. Particles created by bimolecular reactions are typically placed midway between the two parent particles (this is the method we employ in our examples), though different placement may be appropriate for different examples. Unbinding reactions are assigned a rate λ_j and an unbinding distance σ_j. These reactions occur with rate λ_j and normally the daughter particles are placed diametrically opposite each other on a sphere of diameter σ_j centered around the parent particle, at a uniformly distributed angle (this again is the method we employ in our examples). Other standards exist for unbinding reactions (including those with more than two daughter particles) and choice of which to implement is up to the user. Other monomolecular and zero-order reactions are simply assigned a rate λ_j. Note that reaction distances and unbinding distances are not physical radii, and do not exclude any volume.

Cichocki-Hinsen algorithm with reactive point particles

1. Uniformly distribute the reactive particles and the crowders in the volume, such that no crowders are intersecting each other and no reactive particles lie inside a crowder. Let N be the total number of particles (reactive and crowders), and randomly assign each particle a unique index $1, ..., N$.

2. For each $i = 1, ..., N$, propose a new position for particle i at a random Normal$(0, \sqrt{2D_i\Delta t})$ displacement in each spatial dimension, where D_i is the diffusion coefficient of particle i and Δt is the simulation time step. If this new position causes an intersection between any particles (reactive and crowder), place particle i back in its original position. If not, place particle i in the new position.

3. For each reactive particle involved in a bimolecular reaction j, check if any reactive particles of the appropriate types lie inside a sphere of radius ρ_j around the particle. For each appropriate reactive particle inside this sphere, propose a reaction with probability $\lambda_j\Delta t$. If successful, check if any daughter particles would intersect a crowder. If so, skip the reaction; if not, allow the reaction to proceed.

4. For each reactive particle of a type involved in a unimolecular reaction j, propose a reaction with probability $\lambda_j\Delta t$. If successful, check if any daughter particles would intersect a crowder. If so, skip the reaction; if not, allow the reaction to proceed.

5. For each zero-order reaction, propose a reaction with probability $\lambda_j\Delta t$. If successful, check if any of the new particles would intersect a crowder. If so, skip the reaction; if not, allow the reaction to proceed.

6. Advance time by Δt. Let N be the new total number of particles and randomly reassign each particle a unique index $1, ..., N$. Return to (2) and repeat until a target time has elapsed.

The overwhelmingly time-consuming step of this algorithm is step (2), in which potential particle overlaps must be checked N times. The reaction steps (3)-(5) also involve potential overlaps, but as Δt should typically be taken small enough that at most one reaction could plausibly happen per time step, these should not be particularly time-consuming. Our aim in the next subsection is therefore to reduce the time taken by step (2). Note that step (1) can also be particularly time-consuming: although our simplification does not particularly aim to fix that problem, it happens that by increasing the speed of step (2) we also dramatically shorten step (1).

5.1.1 Derivation

We first make two observations which form the basis of our method of reducing the time taken by the Cichocki-Hinsen algorithm. Firstly, the crowders are inert and contribute little

to the actual reactive behaviour of the system; their only function is to occasionally prevent a reactive particle from moving or reaction from happening. Secondly, the crowders are uniformly distributed in space: this implies that each proposed reactive particle movement has roughly the same chance of being impeded by a crowder.

One common method of modelling diffusion in a crowded environment, based on the crowder uniformity assumption, is to simply replace the diffusion coefficient D with $D(1-\phi)$, where ϕ is the proportion of the total volume occupied by crowders [93]. The idea is that if a particle attempts to move to a new location, there is a $1-\phi$ probability of that location not being occupied by a crowder. This is a valid assumption if the random particle displacement at a time step $\delta x \gg R$, that is, if the particle moves by a distance much greater than the crowder size, such that its new location can be roughly considered a uniform random variable. However, it makes little sense to permit $\delta x \gg R$, because that would allow particles to pass through crowders with a single jump.

On the other hand, permitting $\delta x \ll R$ makes physical sense, because the tiny perturbations which make up Brownian motion are much smaller than any particle radius. Furthermore, this is precisely the limit in which Cichocki and Hinsen proved their algorithm to be exact [160]. In that limit, however, we cannot use the $1-\phi$ assumption. To understand why not, consider that the particle is already in a permitted location: this implies that with probability 1 there is a small sphere with radius $\varepsilon > 0$ around the particle which does not intersect any crowders. This local effect implies that the particle's new position cannot be treated as uniformly distributed: if δx is small enough ($\delta x < \varepsilon$), the particle's new position is guaranteed to not intersect any crowders. In summary, if we require that $\delta x \ll R$, then the probability that the particle's new position is illegal (intersects a crowder) is not given by $1-\phi$ but by some function of δx. We now attempt to derive that function.

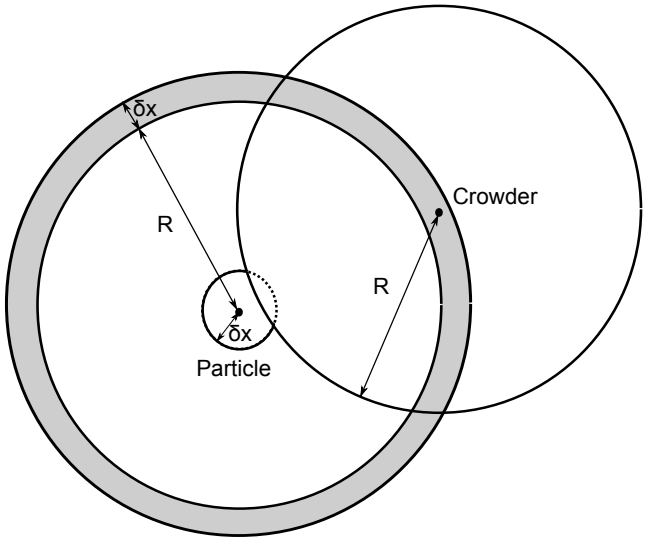

Figure 5.1: Diagram of a point particle attempting to move near a crowder of radius R. The particle attempts to displace itself a distance δx, such that its future position is on the surface of sphere of radius δx around its current position. There may be crowders with their centres in the spherical shell of radius $R+\delta x$ (grey region), which could prevent the particle displacement. The proposed position will be illegal if it is on the dotted segment of the sphere of radius δx.

Consider what happens when a point-particle proposes to move by a displacement δx. This is illustrated in Fig. 5.1. The particle's proposed new position will be on the surface of a sphere of radius δx around its current position. There will be no crowders with their centres in a sphere of radius R around the particle (otherwise the point particle could not be where it is currently), however there is a non-zero probability that there are crowders with their centres inside the spherical shell between the sphere of radius $R+\delta x$ and the sphere of radius R (the grey region in Fig. 5.1). If there are crowders in this region, then there is some probability that the point particle's proposed new position is illegal: this is precisely the probability that

the proposed position intersects the crowder (the dotted line segment in Fig. 5.1).

Now, suppose that there are N_C crowders of radius R inside a volume V. Assuming a uniform crowder distribution, the probability that a given crowder could collide with the point particle in a single time-step is simply the ratio of the volume of the grey region to the total volume:

$$p = \frac{\frac{4}{3}\pi(R+\delta x)^3 - \frac{4}{3}\pi R^3}{V} = \frac{4\pi R^2 \delta x}{V} + o\left(\frac{\delta x}{R}\right). \tag{5.1}$$

The probability of finding n crowders in the grey region is then given by the Binomial distribution:

$$P(n \text{ crowders}) = \frac{N_C!}{n!(N_C-n)!} p^n (1-p)^{N_C-n}. \tag{5.2}$$

Of course, Eq. (5.2) is only valid for small n, because there is a physical limit to how many crowders can fit in the relevant region. However, this is of little concern, since we are only concerned with the probabilities up to $o(\delta x/R)$, which turns out to correspond only to $n = 0$ and $n = 1$.

$$P(0 \text{ crowders}) = 1 - \frac{4\pi N_C R^2 \delta x}{V} + o\left(\frac{\delta x}{R}\right), \tag{5.3}$$

$$P(1 \text{ crowder}) = \frac{4\pi N_C R^2 \delta x}{V} + o\left(\frac{\delta x}{R}\right). \tag{5.4}$$

We now consider the probability that the proposed new point particle position intersects the crowder. This is given by the surface area of the spherical cap of the sphere of radius δx which lies inside the sphere of radius R around the crowder (represented in two dimensions by the dotted line segment in Fig. 5.1) divided by the total surface area of the sphere of radius δx. This is given by:

$$P(\text{intersect}) = \frac{2\pi \delta x \frac{(R-\delta x+d)(R+\delta x-d)}{2d}}{4\pi \delta x^2}, \tag{5.5}$$

where d is the separation between the centres of the point particle and the crowder [206]. The expected value of d admits no straightforward solution, so we use the approximation $R + \frac{\delta x}{2}$ which is accurate to $o(\delta x/R)$. Inserting this into Eq. (5.5) gives:

$$P(\text{intersect}) = \frac{1}{4} - \frac{3\delta x}{16R} + o\left(\frac{\delta x}{R}\right). \tag{5.6}$$

Combining Eq. (5.4) with Eq. (5.6) gives the probability that the proposed move is illegal:

$$P(\text{illegal}) = \frac{4\pi N_C R^2 \delta x}{V}\left(\frac{1}{4} - \frac{3\delta x}{16R}\right) = \frac{\pi N_C R^2 \delta x}{V} + o\left(\frac{\delta x}{R}\right). \tag{5.7}$$

Writing this in terms of the proportion of occupied volume, $\phi = \frac{\frac{4}{3}\pi N_C R^3}{V}$, leads to the simplified expression:

$$P(\text{illegal}) = \frac{3\phi \delta x}{4R} + o\left(\frac{\delta x}{R}\right). \tag{5.8}$$

We can therefore write a much faster version of Cichocki-Hinsen algorithm which *does not include any crowders*. Only point particles need to be modelled explicitly in our algorithm, while the effect of crowders is incorporated by denying a point particle's proposed movement with probability $P(\text{illegal})$. For obvious reasons, we call this a *crowder-free* algorithm. This idea is shown in Fig. 5.2. The left panel shows the Cichocki-Hinsen algorithm with crowders (red) and point particles (blue, purple). The points are not allowed to intersect the crowders, but the reaction radii are. The right panel shows the crowder-free algorithm, which looks identical to Cichocki-Hinsen without crowders. It is clear that the crowder-free algorithm will be easier to simulate.

Since none of the remaining particles in the crowder-free algorithm occupy any volume, we can move all particles simultaneously. The algorithm therefore essentially reduces to the classical Doi algorithm, with an extra clause for preventing particle movement. Some minor

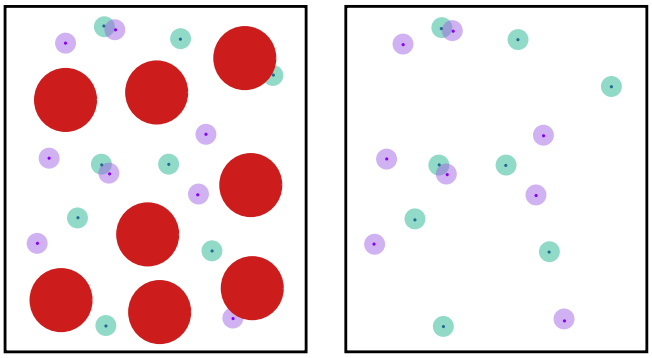

Figure 5.2: Cartoons of the Cichocki-Hinsen algorithm (left) and the crowder-free algorithm (right) for reactive point particles. The point particles (blue, purple) may have a reaction radius (translucent circle) which does not exclude any volume and is therefore permitted to intersect crowders (red) or other particles. The centres of the point particles (solid dots) are not permitted to intersect crowders.

changes must also be made to the reaction parts of the algorithm (steps (3)-(5)), which originally prevented a reaction if a newly created particle would intersect a crowder. Since we no longer explicitly model crowders, we must modify this step. If the reaction is either bimolecular or unbinding, the new particle will be placed at a small displacement σ from a previous particle location. (In the case of bimolecular reactions, the new particle will typically be a short distance from the location of both parent particles: the shorter of these two distances should be considered σ for the purposes of the ensuing considerations.) If $\sigma/R \ll 1$, then we can simply modify the diffusion formula to become $P(\text{illegal}) = 3\phi\sigma/(4R)$. Can we assume that $\sigma/R \ll 1$? In some cases, such as monomolecular conversion reaction of the type $A \to B$, we will have $\sigma = 0$, and it would be absurd to prevent such reactions due to crowding. However, some reactions may have quite a large unbinding distance, and the diffusion formula may prove to be invalid. At each such reaction, we therefore check if $\sigma/R < 0.1$. If this condition is true, we use the formula $P(\text{illegal}) = 3\phi\sigma/(4R)$, otherwise we use the formula $P(\text{illegal}) = \frac{4}{3}\pi N_C R^3/V$, which is the probability that a uniformly distributed point particle would intersect a crowder. The choice of 0.1 arises from the notion of at least an order of magnitude difference in size between σ and R, since this was the requirement for the validity of Eq. (5.8) when it was originally derived. For zero-order reactions, we always use the formula $P(\text{illegal}) = (4/3)\pi N_C R^3/V$, since particles created by these reactions have no parent particles.

Crowder-free algorithm with reactive point particles

1. Uniformly distribute the reactive particles in the volume.

2. Propose new positions for all particles at a random Normal$(0, \sqrt{2D_i\Delta t})$ displacement in each spatial dimension, where D_i is the diffusion coefficient of particle i and Δt is the simulation time step. Calculate δx, the length of the displacement, for each particle. With probability $\frac{3\phi\delta x}{4R}$ reject the proposed move, otherwise accept it.

3. For each particle of a type involved in a bimolecular reaction j, check if any particles of the appropriate types lie inside a sphere of radius ρ_j around the particle, where ρ_j is the reaction distance for the relevant reaction. For each appropriate particle inside this sphere, propose the reaction with probability $\lambda_j\Delta t$, where λ_j is the corresponding reaction rate. For each daughter particle, calculate σ, the length of the displacement from the nearest parent particle. If $\frac{\sigma}{R} < 0.1$, with probability $\frac{3\phi\sigma}{4R}$ reject the proposed reaction, otherwise accept it. Otherwise if $\frac{\sigma}{R} \geq 0.1$, with probability $\frac{\frac{4}{3}\pi N_C R^3}{V}$ (where N_C is the number of crowders) reject the proposed reaction, otherwise accept it.

4. For each reactive particle of a type involved in a unimolecular reaction, propose a reaction with probability $\lambda_j\Delta t$, where λ_j is the reaction rate. For each daughter particle, calculate

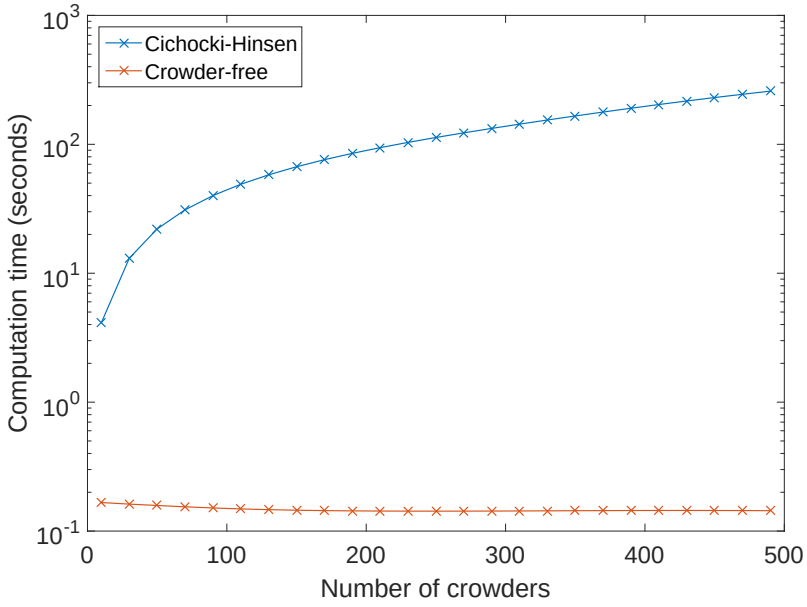

Figure 5.3: Time taken for 100 time steps of both the Cichocki-Hinsen algorithm (blue) and the crowder-free algorithm (red), for a single point particle diffusing in space. With only 10 crowders, the crowder-free algorithm is over 10 times faster. With 500 crowders, the crowder-free algorithm is over 10^3 times faster. Parameter values are $V = 1$, $R = 0.05$, $\Delta t = 10^{-5}$, $D = 0.1$ for the point particle, $D = 0.01$ for the crowders.

σ, the length of the displacement from the parent particle. If $\frac{\sigma}{R} < 0.1$, with probability $\frac{3\phi\sigma}{4R}$ reject the proposed reaction, otherwise accept it. Otherwise if $\frac{\sigma}{R} \geq 0.1$, with probability $\frac{\frac{4}{3}\pi N_C R^3}{V}$ reject the proposed reaction, otherwise accept it.

5. For each zero-order reaction, propose a reaction with probability $\lambda_j \Delta t$, where λ_j is the reaction rate. With probability $\frac{\frac{4}{3}\pi N_C R^3}{V}$ reject the proposed reaction, otherwise accept it.

6. Advance time by Δt. Return to (2) and repeat until a target time has elapsed.

In the next section, we confirm that the crowder-free algorithm is orders of magnitude faster than Cichocki-Hinsen, while retaining its accuracy.

5.1.2 Comparative tests

In our first test of the crowder-free algorithm, we consider a single point particle diffusing in space, surrounded by a uniform distribution of crowders. In this scenario, the crowder-free algorithm should show a dramatic improvement over the original Cichocki-Hinsen algorithm in terms of computation time.

Indeed, as shown in Fig. 5.3, we find that the crowder-free algorithm is at least an order of magnitude faster than the standard algorithm when there are only 10 crowders, this increases to three orders of magnitude when there are 500 crowders. A significant advantage is that the crowder-free algorithm does not scale with number of crowders, making it particularly useful for studying high levels of crowding.

Note that the computation speed for the crowder-free algorithm is slightly *faster* for higher crowding levels. The reason for this is that as the number of crowders increases, the probability that the diffusing particle does not move on a given time step increases. It takes marginally less computational time to not move a particle than it does to move one (since we do not need to update the particle position).

Of course, fast simulation is of little use if the results of the algorithm are inaccurate. In our second test, we therefore use sample paths from both algorithms to compute the effective

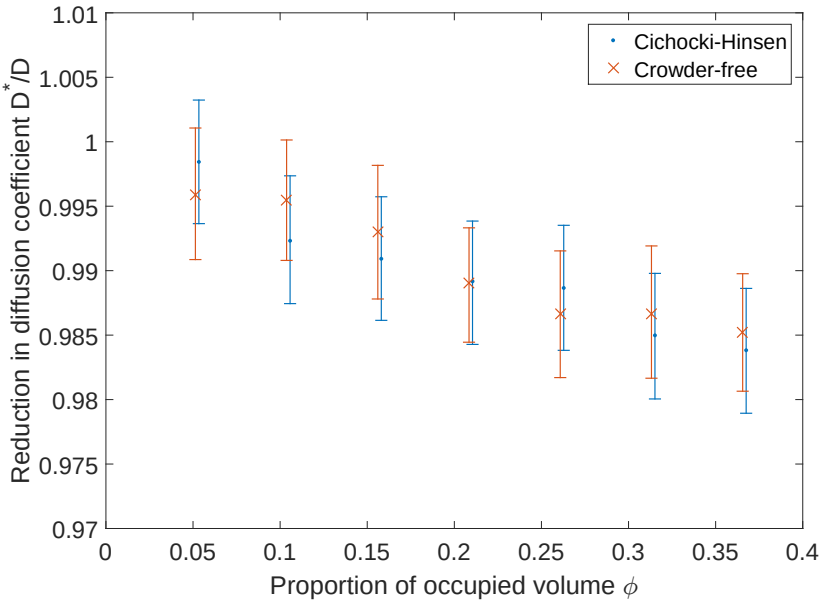

Figure 5.4: Relative reduction in short-time diffusion coefficient for both the Cichocki-Hinsen algorithm (blue) and the crowder-free algorithm (red), for a single point particle diffusing in space, as a function of the proportion of occupied volume ϕ. All data points are an average of 10 simulations, error bars are 1 standard deviation. Parameter values are $V = 1$, $R = 0.05$, $\Delta t = 10^{-5}$, $D = 0.1$ for the point particle, $D = 0.01$ for the crowders.

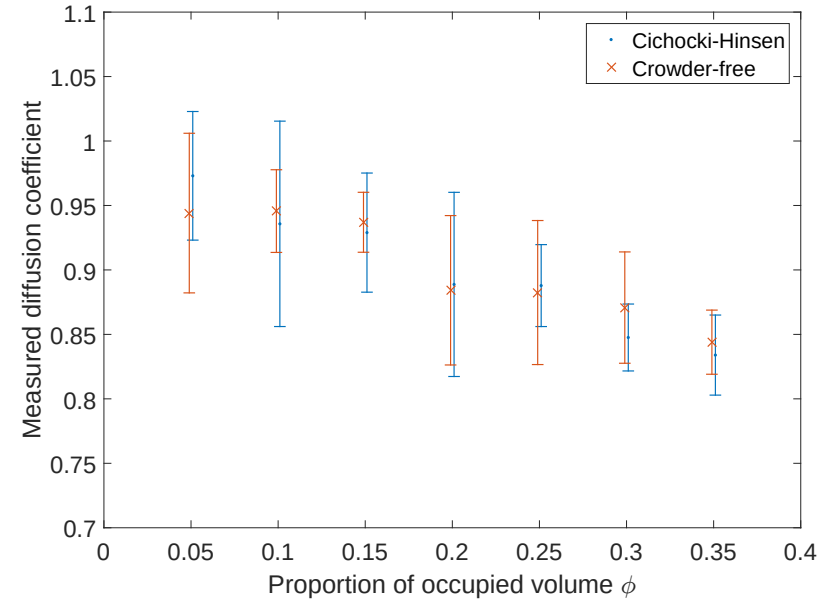

Figure 5.5: Measured long-time diffusion coefficient for both the Cichocki-Hinsen algorithm (blue) and the crowder-free algorithm (red), for a single point particle diffusing in space, as a function of the proportion of occupied volume ϕ. All data points are an average of 3 simulations, error bars are 1 standard deviation. Parameter values are $V = 1$, $R = 0.1$, $\Delta t = 10^{-4}$, $D = 1$ for the point particle, $D = 0.01$ for the crowders. Diffusion coefficients were estimated using the method described in Ref. [221].

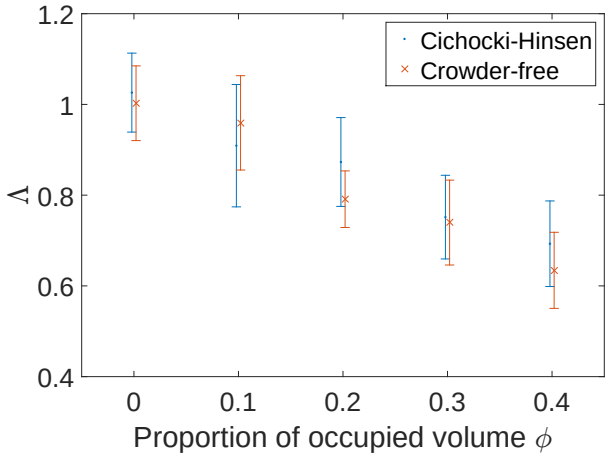

(a)

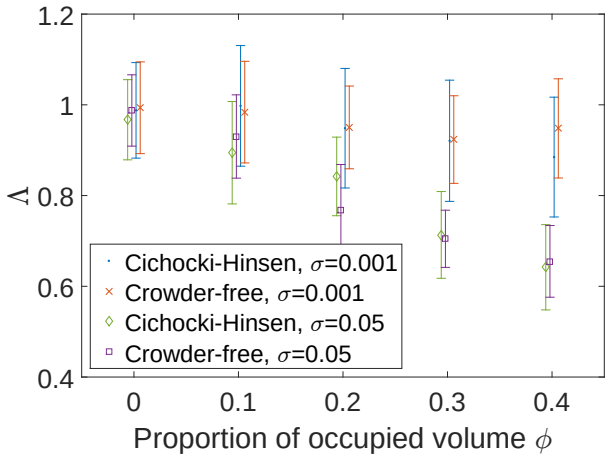

(b)

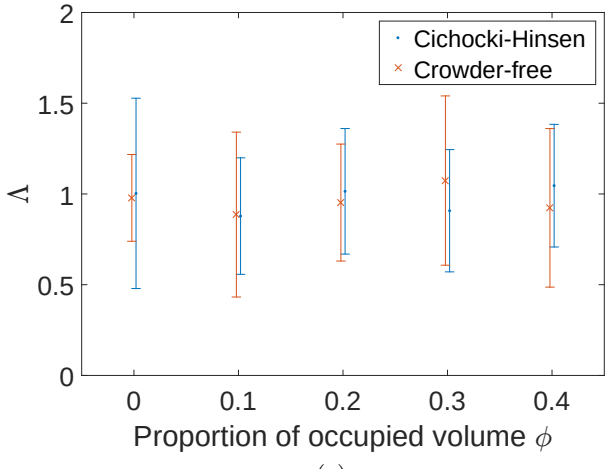

(c)

Figure 5.6: (a) Λ for a zero-order reaction $\emptyset \to X$. (b) Λ for an unbinding (first order) reaction $X \to Y + Z$, for different unbinding distance $\sigma = 0.001$ and $\sigma = 0.05$. (c) Λ for a binding (second order) reaction $X + Y \to Z$. For all plots, $R = 0.05$, $D = 1$, $\Delta t = 10^{-4}$, $V = 1$. All data points are an average of 100 independent simulations, error bars are 1 standard deviation. The quantity Λ is the ratio between the actual frequency of the reaction and the rate specified in the algorithm; thus $\Lambda = 1$ corresponds to crowding having no effect on reaction frequency.

short-time diffusion coefficient D^* of a single point particle in crowded space [151]. This is done by performing a simulation with input diffusion coefficient D, computing the squared displacement of the particle at each time step and taking the mean of that value over the entire simulation. This value is equated to $6D^*\Delta t$ to find an estimate for the effective short-time diffusion coefficient D^*.

The non-dimensional parameter $\frac{D^*}{D}$ is the effective reduction in short-time diffusion coefficient due to crowding. For no crowding, we expect $\frac{D^*}{D} = 1$, and the value should decrease as crowding increases. This is because large jumps are more likely to result in a collision with a crowder than small jumps, so the effective diffusion coefficient appears to be reduced. In Fig. 5.4 we plot $\frac{D^*}{D}$ as a function of the proportion of occupied volume ϕ. As expected, both algorithms show a reduction in the effective short-time diffusion coefficient as crowding increases, and both algorithms give very similar results, with their error bars always intersecting. Each data point is an average of 10 simulations, each simulation ran until the point particle, initially located at $(\frac{1}{2}, \frac{1}{2}, \frac{1}{2})$, left the unit cube with corners at $(0, 0, 0)$ and $(1, 1, 1)$.

It has been shown, however, that short-time diffusion coefficients can differ strongly from long-time diffusion coefficients measured over a whole trajectory [151]. In Fig. 5.5, therefore, we also plot the long-time diffusion coefficients estimated using the unbiased diffusion estimator developed in Ref. [221]. Each point in Fig. 5.5 is the mean of 3 independent simulations of length 10^3 time-steps, and each error bar corresponds to the standard deviation.

We have confirmed that the crowder-free algorithm simulates diffusion as accurately as the original Cichocki-Hinsen algorithm, but we have not tested whether it accurately simulates reactions. In our next test, we check that some basic reactions happen with the same frequency for both algorithms. In Fig. 5.6 we show the results of these tests. In Fig. 5.6 (a) we compare the Cichocki-Hinsen algorithm with the crowder-free algorithm for a zero-order reaction under a variety of crowding levels. The quantity Λ on the y-axis is the ratio between the actual frequency of the reaction and the rate specified in the algorithm, $\Lambda = 1$ therefore corresponds to no effect of crowding. We observe that both algorithms show the same linear reduction in effective rate as crowding increases. In Fig. 5.6 (b) we perform the same comparison for an unbinding reaction of the form $X \to Y + Z$, for two different unbinding distances $\sigma = 0.001$ and $\sigma = 0.05$. The $\sigma = 0.001$ case corresponds to a short distance (as defined in the algorithm) and so we would use Eq. (5.8) in the crowder-free algorithm, wherease $\sigma = 0.05$ corresponds to a large distance, and so we would use ϕ, the volume occupied, in the crowder-free algorithm. For both parameter sets, the crowder-free algorithm agrees well with Cichocki-Hinsen. The unbinding reaction with a larger unbinding distance is naturally more affected by crowding than the reaction with a smaller unbinding distance, since large jumps are more likely to be impeded by a crowder. In Fig. 5.6 (c) we perform the same test for a binding reaction of the form $X + Y \to Z$, again both algorithms agree well, though because these are point-particles there does not appear to be a significant effect of crowding on the binding rate. This differs from the finite-size particle case shown in Fig. 5.11.

To confirm the above test, we finally use both algorithms to compute the equilibrium distribution of the reaction $A + B \rightleftharpoons C$ in the presence of low and high levels of crowding. We expect the typical number of C molecules to be higher for high crowding, because the unbinding reaction will occur less frequently.

For each algorithm, we simulated two long trajectories of a system initially consisting of 30 uniformly distributed A molecules and 30 uniformly distributed B molecules, in a sea of 10 (low crowding) and 700 (high crowding) crowders. The simulation time was much longer than the time for the system to reach equilibrium. In Fig. 5.7 we show the equilibrium distribution for the number of C molecules. The mean number of C molecules shifts from around 6 with low crowding to around 11 with high crowding. The crowder-free algorithm agrees almost perfectly with the Cichocki-Hinsen algorithm for both examples, thus confirming that the crowder-free algorithm accurately imitates the Cichocki-Hinsen algorithm, but with a dramatic reduction in computation time.

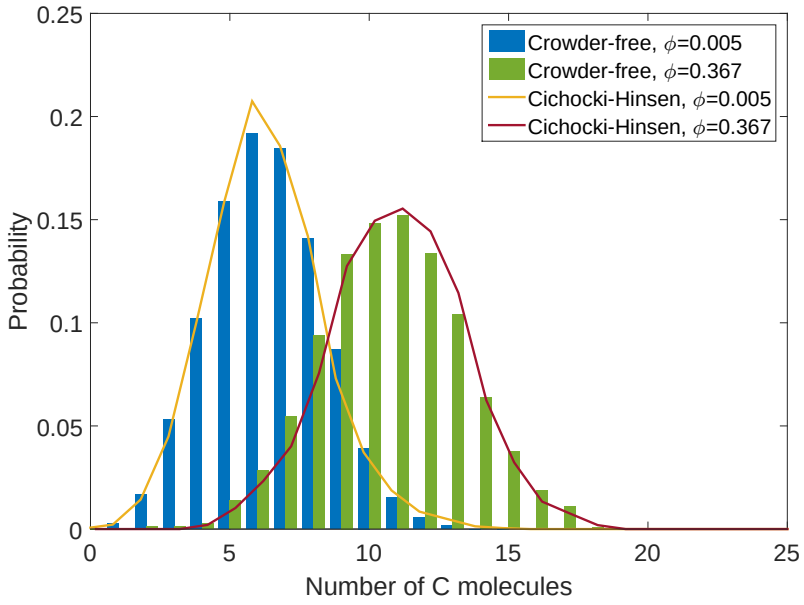

Figure 5.7: Equilibrium distribution of the number of C molecules for $A + B \to C$, $C \to A + B$. Each distribution is a time average over single long trajectory of length 10^5 iterations. Parameter values are $V = 1$, $R = 0.05$, $\Delta t = 10^{-4}$, $D_0 = 0.1$ for the point particle, $D_0 = 0.01$ for the crowders, reaction radius $\rho_1 = 0.025$, forward reaction rate $\lambda_1 = 9 \times 10^3$, backward reaction rate $\lambda_2 = 1$, unbinding distance $\sigma = 0.025$.

5.1.3 A note on more complex systems

The crowder-free algorithm proposed above specifically concerns a uniform distribution of crowders with the same radius, however the results can equally be applied to more complex systems.

For sets of crowders with different radii, say $N_C^{(i)}$ crowders of radius R_i for $i = 1, ..., k$, we can simply use the formula:

$$P(\text{illegal}) = \sum_{i=1}^{k} \frac{N_C^{(i)} \pi R_i^2 \delta x}{V}, \tag{5.9}$$

which will give the probability of a move δx resulting in a collision. Of course, this formula relies on the assumption that $\delta x \ll R_i$ for all $i = 1, ..., k$.

For systems with a non-uniform distribution of crowders of radius R, the algorithm can still be used if the crowder distribution is locally uniform. In that case, we can divide the volume up into k subvolumes V_i with $N_C^{(i)}$ crowders for $i = 1, ..., k$, whre $V_1 + ... + V_k = V$ and $N_C^{(1)} + ... + N_C^{(k)} = N_C$. Then we can apply the formula:

$$P(\text{illegal}) = \frac{N_C^{(i)} \pi R^2 \delta x}{V_i}, \tag{5.10}$$

for a point particle in the i^{th} subvolume. However, this method will only work if the crowder distribution remains roughly constant in time. If the crowders are diffusing fast enough that the overall distribution flattens on the timescale of the simulation, then subvolume i will not always contain $N_C^{(i)}$ crowders. Since we do not know how $N_C^{(i)}$ will change *a priori*, we cannot use the crowder-free algorithm for such examples.

5.2 Finite-size particles in a crowded environment

Studying the behaviour of reactive point particles in the presence of crowders provides useful information about real biochemical systems in which the reactive particles are much smaller than the crowders they encounter. This is an accurate description of, for example, small proteins or amino acids diffusing in the vicinity of ribosomes or large enzymes. However, biochemical particles also encounter crowders with a similar size to themselves. In order to study these examples effectively, we must also be able to simulate reactive particles which occupy a non-zero volume. A version of the Cichocki-Hinsen algorithm for which the reactive particles occupy a non-zero volume is given below. Since reactive particles now have a physical radius, we no longer need to define a reaction distance for bimolecular reactions: particles react with a rate λ_j if they physically intersect. This is known as partial-absorption Smoluchowski binding [170].

Cichocki-Hinsen algorithm with finite-size reactive particles

1. Uniformly distribute the reactive particles and the crowders in the volume, such that no particles (reactive or crowder) are intersecting each other. Let N be the total number of particles, and randomly assign each particle a unique index $1, ..., N$.

2. Uniformly sample an integer i from $1, ..., N$. Propose a new position for particle i at a random Normal$(0, \sqrt{2D_i\Delta t})$ displacement in each spatial dimension, where D_i is the diffusion coefficient of particle i and Δt is the simulation time step. If particle i is a crowder, check if this new position causes an intersection between any particles. If so, place particle i back in its original position, if not, place particle i in the new position. Otherwise if particle i is a reactive particle, check if this new position causes an intersection between i and exactly one other reactive particle and no crowders. If so, and if that particle can react with i, proceed to (3). Otherwise, if the new position causes any other type of intersection, place the particle back in its original position, if not, place the particle in its new position. Proceed to (4).

3. Propose a bimolecular reaction j with probability $\lambda_j\Delta t$, where λ_j is the corresponding reaction rate. If unsuccessful, place particle i back in its previous position and proceed to (4). Otherwise if successful, check if any daughter particles would intersect another particle. If so, skip the reaction, place particle i back in its original position; if not, allow the reaction to proceed.

4. For each reactive particle of a type involved in a unimolecular reaction j, propose a reaction with probability $\lambda_j\Delta t/N$, where λ_j is the reaction rate. If successful, check if any daughter particles would intersect any other particles. If so, skip the reaction; if not, allow the reaction to proceed.

5. For each zero-order reaction j, propose a reaction with probability $\lambda_j\Delta t/N$, where λ_j is the reaction rate. If successful, check if any of the new particles would intersect another particle. If so, skip the reaction; if not, allow the reaction to proceed.

6. Advance time by $\Delta t/N$. Let N be the new total number of particles and randomly reassign each particle a unique index $1, ..., N$. Return to (2) and repeat until a target time has elapsed.

Note that this algorithm is distinct from the Cichocki-Hinsen algorithm in Section 5.1 in several ways, mainly because in this algorithm time is advanced by $\frac{\Delta t}{N}$ at each time step. This is because here step (3) is nested inside step (2). The reason for this is that bimolecular reactions occur in this algorithm when two reactive particles physically intersect. This is an illegal move, and if the particles do not react then they must not be allowed to remain in that position, but rather revert to the previous position, hence bimolecular reactions and diffusion are closely coupled in this algorithm. It follows that N can change during steps (2)-(3), and so it does not make sense to place step (2) inside a for-loop over $i = 1, ..., N$.

Again, step (2) is the overwhelmingly time consuming step for this algorithm, so as before we will attempt to find an expression giving the probability that a given jump causes an intersection

with a crowder. However, we will not be able to get substantial speed gains on the same scale that we obtained with point-particles, because now even a crowder-free algorithm will contain finite-size reactive particles. Our speed increase will arise from removing a subset of the volume-occupying particles (the crowders) rather than all of them, as before. Obviously, our method will work best if there are many more crowders than reactive particles, though it will always be faster than the standard algorithm.

5.2.1 Derivation

To derive an analogous formula to Eq. (5.8) for the finite-volume case, consider a reactive particle with radius $r > 0$ attempting to move a distance δx in a sea of N_C uniformly distributed crowders of radius R. In Section 5.1, we observed that, to first order in $\frac{\delta x}{R}$, the probability of a reactive particle performing an illegal move depends only on its behaviour in the vicinity of a single crowder. However, a particle of radius r moving near a single crowder of radius R is identical to a point-particle moving near a crowder of radius $R + r$: in both cases, the two particle centres are forbidden from being nearer than $R + r$ from each other. It follows that Eq. (5.7) can be easily adapted for use in this section, but with R replaced by $R + r$. In other words, we can simply write:

$$P(\text{illegal}) = \frac{\pi N_C (R+r)^2 \delta x}{V} + o\left(\frac{\delta x}{R+r}\right). \tag{5.11}$$

Observe that we do not need to consider the probability of intersecting reactive particles here. This is because the reactive particles will all be simulated explicitly, so a collision between reactive particles in the crowder-free algorithm will be simulated identically to the original algorithm.

As before, we will also need to moderately adapt the reaction part of our algorithm. Again, if a daughter particle is created a small distance σ from a parent particle, and $\sigma \ll R + r$, then we can use the formula $P(\text{illegal}) = \frac{\pi N_C (R+r)^2 \sigma}{V}$. Note, however, that this is much less likely to occur with finite-size particles, since σ will typically be a similar order of magnitude to r, which is in turn typically a similar order of magnitude to R. We could alternatively use the probability that a uniformly distributed point in space can accomodate a particle of radius r. Users may wish to simulate reactions where it makes more sense to use $P(\text{illegal}) = \frac{\pi N_C (R+r)^2 \sigma}{V}$ as the probability that a new particle is obstructed by a crowder (for instance, an enzyme releasing a much smaller substrate). Since these matters are system-specific, we leave it up to the user to decide which formula is more appropriate. However, for almost all reactions we will use the probability that a uniformly distributed point in space can accomodate a particle of radius r.

This probability is not the simple expression used in Section 5.1, rather it derives from scaled particle theory (SPT). The reason for this is that there are unoccupied points in space which are inaccessible to the particle of radius r. These are the points which do not lie inside a crowder but do lie within a distance $R + r$ from a crowder's centre. SPT has been used to obtain analytical expressions for the effect of crowding on intrinsic noise in two-dimensional systems, and was observed to give very accurate results [222]. In three dimensions, it offers an expression for the probability that a uniformly distributed point in space of volume V can accomodate a particle of radius r, given that the space contains N_C crowders of radius R [138]:

$$\begin{aligned}\log\left[P(\text{legal})\right] = \log(1-\phi) - \frac{Br}{1-\phi} - \frac{4\pi A r^2}{1-\phi} - \frac{B^2 r^2}{2(1-\phi)^2} \\ - \frac{4\pi}{3}\left[\frac{N_C}{V(1-\phi)} + \frac{B^2 C}{3(1-\phi)^3} + \frac{AB}{(1-\phi)^2}\right] r^3,\end{aligned} \tag{5.12}$$

where $A = \frac{N_C R}{V}$, $B = \frac{4\pi N_C R^2}{V}$, and $C = \frac{N_C R^2}{V}$. The crowder-free algorithm for finite-size reactive particles is then as follows:

Crowder-free algorithm with finite-size reactive particles

1. Uniformly distribute the reactive particles in the volume, such that no particles are in-

tersecting each other. Let N be the total number of particles, and randomly assign each particle a unique index $1, ..., N$.

2. Uniformly sample an integer i from $1, ..., N$. Propose a new position for particle i at a random Normal$(0, \sqrt{2D_i\Delta t})$ displacement in each spatial dimension, where D_i is the diffusion coefficient of particle i and Δt is the simulation time step. With probability $\frac{\pi N_C (R+r)^2 \delta x}{V}$, where r is the radius of particle i, put the particle back in its original position. Otherwise, check if this new position causes an intersection between i and exactly one other particle. If so, and if that particle can react with i, proceed to (3). Otherwise, if the new position causes any other type of intersection, place the particle back in its original position, if not, place the particle in its new position. Proceed to (4).

3. Propose a bimolecular reaction j with probability $\lambda_j \Delta t$, where λ_j is the corresponding reaction rate. If unsuccessful, place particle i back in its previous position and proceed to (4). Otherwise if successful, evaluate P(legal) according to Eq. (5.12) for each daughter particle. Let p be the product of each P(legal). With probability $1 - p$, skip the reaction, place particle i back in its original position. Otherwise check if any daughter particles would intersect another particle. If so, skip the reaction, place particle i back in its original position; if not, allow the reaction to proceed.

4. For each reactive particle of a type involved in a unimolecular reaction j, propose a reaction with probability $\lambda_j \Delta t/N$, where λ_j is the reaction rate. If the reaction is of the type $A \to B$ and the radius of B is less than or equal to that of A, allow the reaction to proceed. Otherwise, evaluate P(legal) according to Eq. (5.12) for each daughter particle. Let p be the product of each P(legal). With probability $1-p$, skip the reaction. Otherwise, check if any daughter particles would intersect any other particles. If so, skip the reaction; if not, allow the reaction to proceed.

5. For each zero-order reaction j, propose a reaction with probability $\lambda_j \Delta t/N$, where λ_j is the reaction rate. If successful, evaluate P(legal) according to Eq. (5.12). With probability $1 - P$(legal), skip the reaction. Otherwise check if any of the new particles would intersect another particle. If so, skip the reaction; if not, allow the reaction to proceed.

6. Advance time by $\Delta t/N$. Let N be the new total number of particles and randomly reassign each particle a unique index $1, ..., N$. Return to (2) and repeat until a target time has elapsed.

There is one significant case for which our crowder-free algorithm will not give accurate results, namely if the crowders are stationary and the level of crowding is high. Simulating such systems with Cichocki-Hinsen reveals that reactive particles can get trapped in regions surrounded by stationary crowders, and simply stay there for the entirety of the simulation without reacting or moving significantly. Obviously, these cases cannot be covered by the crowder-free algorithm because all reactive particles (of the same radius) have the same probability of diffusing at any time. We therefore recommend not using the crowder-free algorithm for systems with stationary crowders unless the level of crowding is sufficiently low that no trapping regions could exist. Note that this is not a problem if the reactive particles are point-particles, because they occupy no volume and will always be able to escape from a trapping region eventually.

5.2.2 Comparative tests

In this section we perform similar tests on the crowder-free algorithm for finite-size particles to those we performed in section 5.1.2. We initially test the time taken for both methods to simulate pure diffusion in the presence of an increasing number of crowders. To ensure that the results are different from those in section 5.1.2, we now simulate 50 diffusing "reactive" particles (so-called even though they do not react in this example) in a sea of crowders. Of course, we do not expect to get anywhere near the 1000-fold speed increase that we achieved for the point-particle case: even with no crowders, we have to simulate 50 volume-occupying molecules, constantly ensuring that they do not intersect.

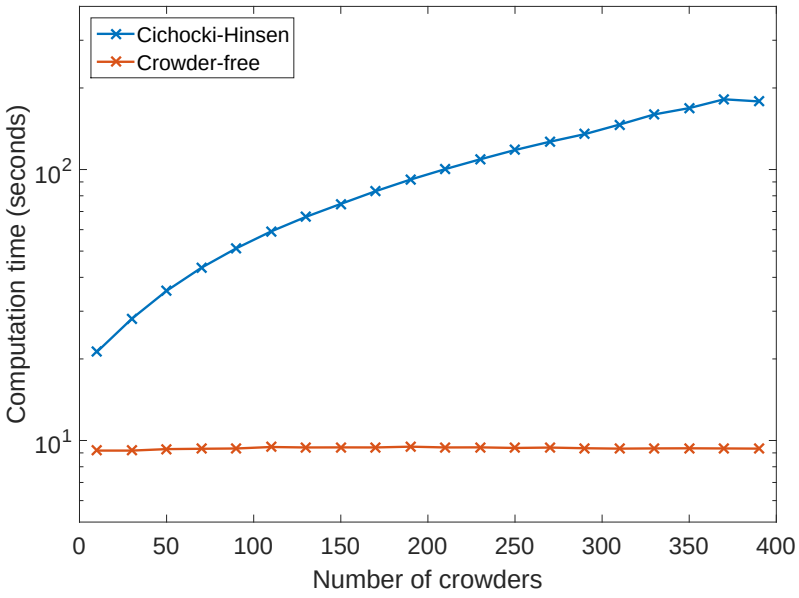

Figure 5.8: Time taken for 100 time steps of both the Cichocki-Hinsen algorithm (blue) and the crowder-free algorithm (red), for 50 finite-size particles diffusing in crowded space. With only 10 crowders, the crowder-free algorithm is more than twice as fast. With 400 crowders, the crowder-free algorithm is over 20 times faster. Parameter values are $V = 1$, $R = 0.05$, $r = 0.02$, $\Delta t = 10^{-5}$, $D = 0.1$ for the point particle, $D = 0.1$ for the crowders.

The results of this test are plotted in Fig. 5.8. With 10 crowders, the crowder-free algorithm takes half the time of the Cichocki-Hinsen algorithm, while with 400 crowders, the crowder-free algorithm has a speed increase of over 20 times. Even for finite-size particles, therefore, the crowder-free algorithm offers a considerable speed increase, and its lack of dependence on crowder number makes it especially useful for studying high levels of crowding. The next test we perform compares estimates of short-time diffusion coefficients from the two algorithms. In both cases, we simulate 20 finite-size particles diffusing in a sea of crowders. Because of this, a single simulation gives 20 different estimates of the diffusion coefficient. In Fig. 5.9 we plot the mean (points) and standard deviation (error bars) of this sample of 20, for a variety of levels of crowding. Since the "reactive" particles themselves occupy a volume, we incorporate this into our calculation of the proportion of occupied volume ϕ. As in Fig. 5.4, the two algorithms agree, with errorbars intersecting for each data point. Note that, compared to Fig. 5.4, the diffusion coefficient is reduced more for the same level of crowding. This confirms the intuitive hypothesis that finite-size particles are more influenced by crowding than point particles.

As in the point-particle case, we also study the long-time diffusion coefficients of finite-sized particles. In Fig. 5.10 we plot the long-time diffusion coefficients estimated using the unbiased diffusion estimator developed in Ref. [221]. We calculated the diffusion coefficient for three different particle sizes, ranging from the same size as the crowders to several orders of magnitude smaller than the crowders. Both algorithms agree well, and we observed that, as we might expect, the diffusion of smaller particles is less affected by crowding than larger particles. Each point in Fig. 5.10 is the mean of 10 independent simulations of length 10^3 time-steps, and each error bar corresponds to the standard deviation.

In our next test, we check that zero, first, and second-order reactions happen with the same frequency for both the Cichocki-Hinsen algorithm and our crowder-free algorithm for a variety of particle sizes. In Fig. 5.11 we show the results of these tests. In Fig. 5.11 (a) we compare the Cichocki-Hinsen algorithm with the crowder-free algorithm for a zero-order reaction under a variety of crowding levels, and for two particle sizes. As before, the quantity Λ on the y-axis is the ratio between the actual frequency of the reaction and the rate specified in the algorithm, $\Lambda = 1$ therefore corresponds to no effect of crowding. We observe that both algorithms show

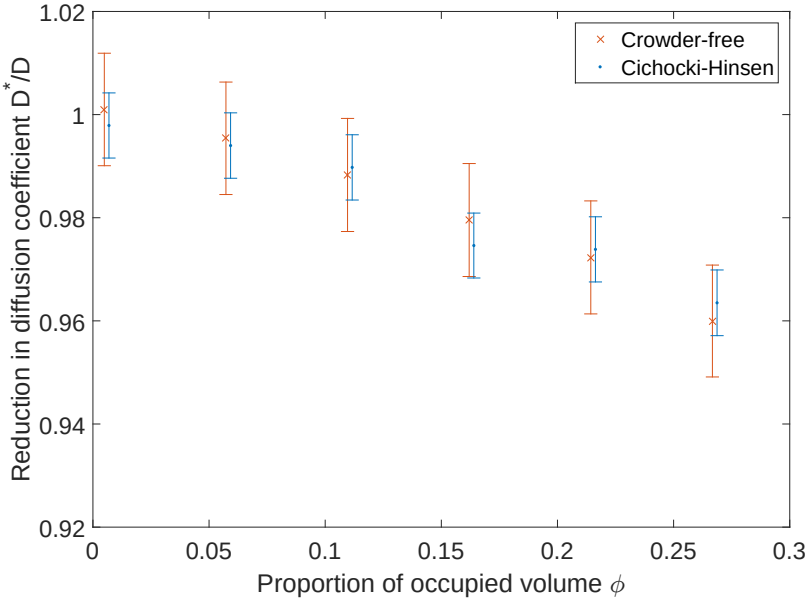

Figure 5.9: Relative reduction in short-time diffusion coefficient for both the Cichocki-Hinsen algorithm (blue) and the crowder-free algorithm (red), for a single finite-sized particle diffusing in space, as a function of the proportion of occupied volume ϕ. All data points are an average of 20 particles from a single simulation, error bars are 1 standard deviation. Parameter values are $V = 1$, $R = 0.05$, $r = 0.02$, $\Delta t = 10^{-5}$, $D = 0.1$ for the point particle, $D = 0.1$ for the crowders.

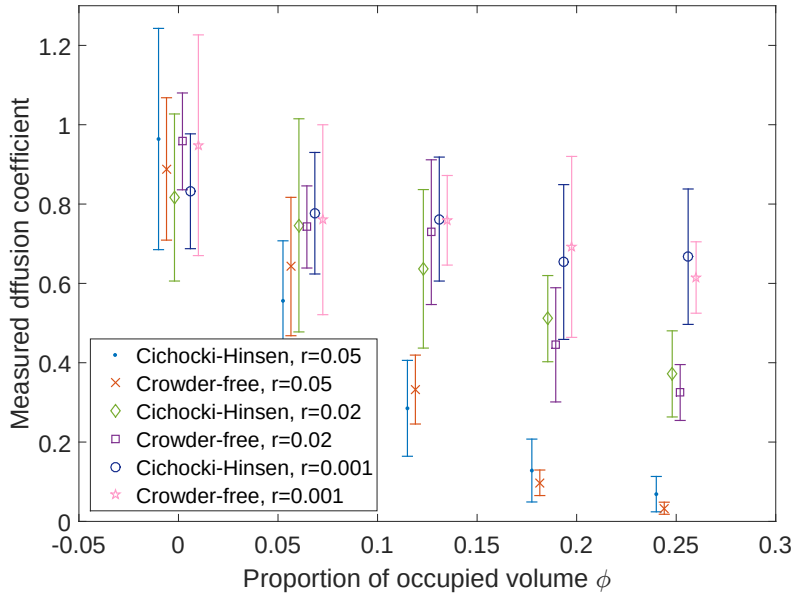

Figure 5.10: Measured long-time diffusion coefficient for both the Cichocki-Hinsen algorithm and the crowder-free algorithm, for a variety of sizes of tracer particles, as a function of the proportion of occupied volume ϕ. All data points are an average of 10 independent simulations, error bars are 1 standard deviation. Parameter values are $V = 1$, $R = 0.05$, $\Delta t = 10^{-3}$, $D = 1$.

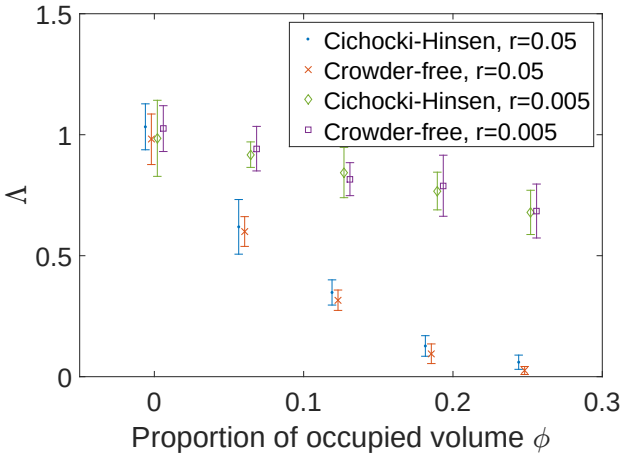

(a)

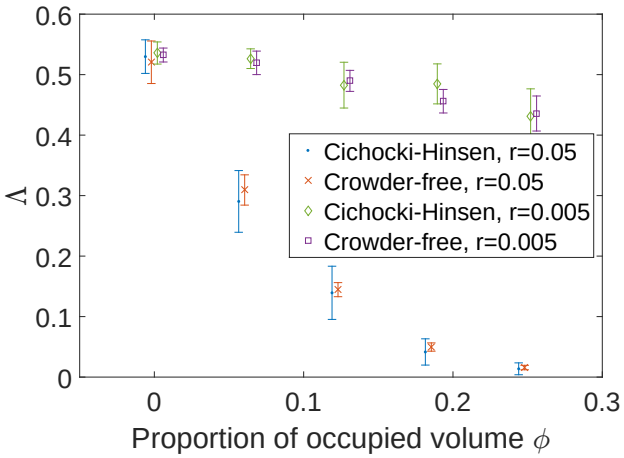

(b)

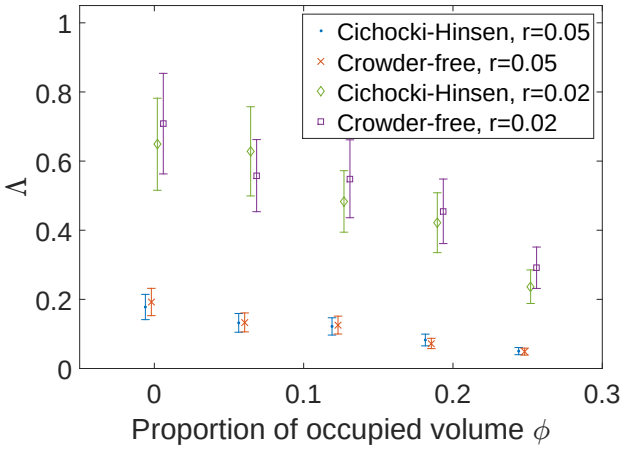

(c)

Figure 5.11: (a) Λ for a zero-order reaction $\emptyset \to X$, for different particle radii $r = 0.05$ and $r = 0.005$. (b) Λ for an unbinding (first-oder) reaction $X \to Y + Z$, for different Y radii $r = 0.05$ and $r = 0.005$. (c) Λ for a binding (second-order) reaction $X + Y \to Z$, for different X and Y radii, $r = 0.05$ and $r = 0.02$. For all plots, $R = 0.05$, $D = 1$, $\Delta t = 10^{-4}$, $V = 1$. All data points are an average of 100 independent simulations, error bars are 1 standard deviation. The quantity Λ is the ratio between the actual frequency of the reaction and the rate specified in the algorithm; thus $\Lambda = 1$ corresponds to crowding having no effect on reaction frequency.

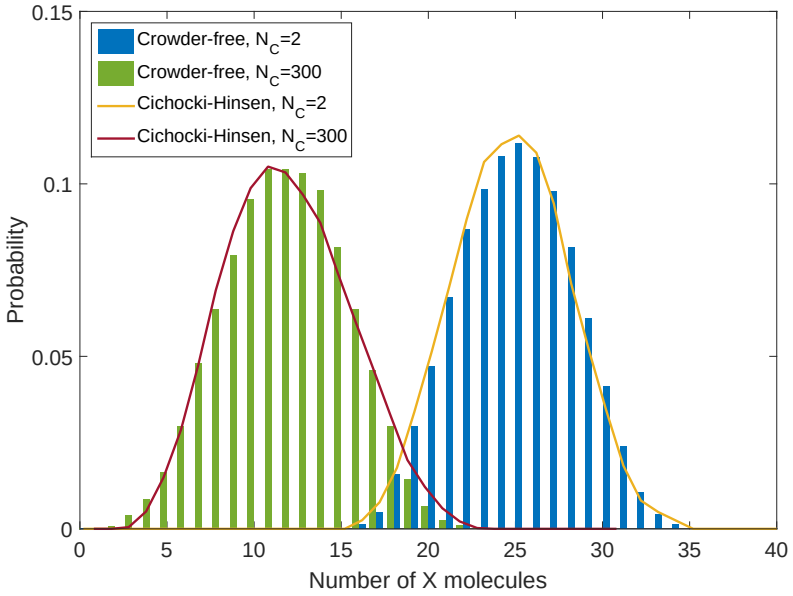

Figure 5.12: Equilibrium distributions of the reaction $\emptyset \to X$, $X + X \to \emptyset$ for both crowder-free algorithm (histograms) and Cichocki-Hinsen algorithm (lines) for low (blue, yellow) and high (green, red) crowding conditions. Each distribution is a time average over single long trajectory of length $10^5 - 10^7$ iterations. The crowder-free algorithm generally requires many fewer iterations than Cichocki-Hinsen, because the total number of particles is lower. Parameter values are $V = 1$, $R = 0.05$, $r = 0.05$, $\Delta t = 3 \times 10^{-5}$, $D = 0.1$ for the point particle, $D = 0.1$ for the crowders. For the zero-order reaction, $\lambda_1 = 2 \times 10^2$, for the bimolecular reaction, $\lambda_2 = 3 \times 10^4$.

the same linear reduction in effective rate as crowding increases, and the rate is reduced more for large particles than for small ones. In Fig. 5.11 (b) we perform the same comparison for an unbinding reaction of the form $X \to Y + Z$, for two different parameter sets. First for X unbinding into equal sized Y and Z with radius 0.05 and unbinding distance 0.1, and second for X unbinding into different sized Y and Z, with radii 0.01 and 0.005 respectively, and unbinding distance 0.015. For both parameter sets, the crowder-free algorithm agrees well with Cichocki-Hinsen. In Fig. 5.11 (c) we perform the same test for a binding reaction of the form $X+Y \to Z$, for two different parameter sets. First for X and Y with radius 0.05, and second for X and Y with radius 0.02. Again both algorithms agree well for both parameter sets, and we note that higher crowding reduces the binding rate, because it takes longer for particles to find each other.

Finally, we compare the algorithms' performance at estimating an equilibrium distribution of a chemical reaction. This time we simulate the reaction $\emptyset \to X$, $X + X \to \emptyset$, in which particles are created at uniformly distributed points in space and react with a fixed rate when they collide. This system has previously been studied spatially as an example of protein synthesis and degradation [73]. We expect that, contrary to the example in Fig. 5.7, crowding will reduce the mean number of X, since the creation of X will be less likely in crowded conditions.

In Fig. 5.12 we plot the equilbrium distribution of the number of X molecules for both algorithms in both low and high crowding conditions. Each distribution is calculated as a time average over a single long trajectory, of between 10^5 and 10^7 iterations. The crowder-free algorithm clearly requires fewer iterations than Cichocki-Hinsen because each iteration of both algorithms advances time by $\frac{\Delta t}{N}$ where N is the total number of particles, and Cichocki-Hinsen generally has many more particles to simulate. As predicted, the mean of the distribution is much lower in the high crowding example than the low crowding example. As with all previous tests, the crowder-free algorithm agrees almost perfectly with the Cichocki-Hinsen algorithm, confirming that our algorithm suffers little apparent loss of accuracy compared to the Cichocki-

Hinsen algorithm, despite its considerable speed increases. Note that the value of ϕ for these examples, because the number of reactive particles fluctuates over time, and therefore so does ϕ.

5.3 Summary

In this chapter, we proposed a modification to the commonly used Cichocki-Hinsen BD algorithm for simulating reaction-diffusion systems in a crowded environment. We call our modified algorithm a *crowder-free* algorithm because we do not simulate crowders explicitly. Instead, we rigorously derive the probability that a small displacement of size δx would result in a collision with a crowder. This implies that, instead of simulating crowders, we can simply reject each attempted particle displacement with precisely that probability. We tested our algorithm in terms of both speed and accuracy, both for cases with reactive point particles and with finite-size reactive particles. The crowder-free algorithm always provides a speed increase over the underlying Cichocki-Hinsen algorithm: this speed increase varied from 2 to over 1000 for the set of examples studied in this paper. Furthermore, the crowder-free algorithm provides data which is near-indistinguishable from the data extracted from the corresponding Cichocki-Hinsen algorithm: this was shown to be true for both diffusive and reactive information. The crowder-free algorithm therefore shows no apparent loss of accuracy compared to the Cichocki-Hinsen algorithm, which, coupled with the clear speed increases, makes it a very attractive algorithm for simulating chemical reactions in a crowded environment.

The work in this chapter goes a significant way to alleviating the cost of simulating biochemistry with realistic conditions. In the next chapter we take this idea further to show how we can apply analytical techniques to BD, to obtain PDEs describing particle motion under crowded conditions.

Chapter 6

Analytical approaches to Brownian dynamics

In chapter 5 we proposed an algorithm for simulating BD in a crowded environment, without the large computational cost typically associated with such simulations. In this chapter we go a step further, and attempt to obtain analytical expressions describing the diffusion of particles in a crowded environment. These expressions take the form of advection-diffusion equations describing the evolution of the probability density function of a particle's position.

At the heart of the method derived in this chapter is the idea that crowders may not be uniformly distributed in space. The uniformity assumption (which we employed in chapter 5) is common and useful for deriving equations and algorithms, but may not be strictly true in biology. Even in prokaryotes, where the cell interior is completely membrane free, distinct subcellular compartments exist. Firstly, there is a clear demarcation between the cytoplasm and the nucleoid owing to a significant difference in the concentration of macromolecules [223, 224]. Secondly, macromolecules are actively transported to opposite ends of the cell in preparation for cell division, leading to a bimodal crowder distribution [225, 226]. Thirdly, phase separation is known to occur in the cytoplasm owing to hydrophobic and elecrostatic interactions between different macromolecular species, leading to distinct regions of high and low crowder density [227]. These effects imply that the cell interior consists of a highly non-uniform distribution of crowders which is maintained over long timescales.

The work in this chapter demonstrates that heterogeneous crowding leads to highly irregular behaviour for diffusing particles, including multimodal and assymetric probability distributions for their spatial positions. We suggest that heterogeneous crowding could be one of the methods cells use to organise their constituent molecules. We note that heterogeneous crowding is already a feature of some spatial simulation algorithms [228], but our interest is in the analytical treatment of heterogeneous crowding.

6.1 Diffusion equations with macromolecular crowding

Mathematical models of macromolecular crowding tend to assume that macromolecules are homogeneously (uniformly) distributed throughout the cell, but in reality the local concentration of macromolecules can vary widely on a subcellular length-scale (see above). The consequences of this discrepancy are demonstrated in Fig. 6.1. The top cartoon shows a typical trajectory of a small Brownian particle (red) in a homogeneous distribution of macromolecules (blue) at a moderate level of crowding. The trajectory, starting in the centre of the volume (red circle), is essentially Brownian, although frequent collisions with macromolecules will tend to reduce the small particle's diffusion coefficient. The bottom cartoon shows a typical trajectory of a small Brownian particle (red) in a heterogeneous distribution of macromolecules (blue), with alternating regions of high and low crowding. In this case the small particle, again starting from the centre (red circle), is directed preferentially towards a region of low crowding, and - since it is then trapped between regions of high crowding - it will tend to remain there much longer than is predicted by a standard diffusion equation. Although both cases in Fig. 6.1 have

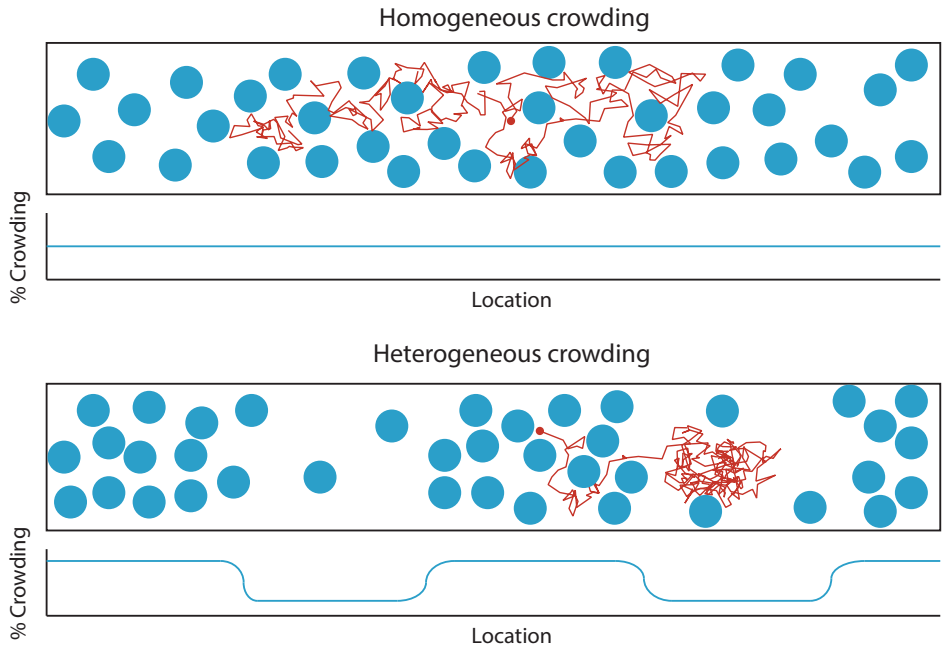

Figure 6.1: Cartoons showing the difference between homogeneous and heterogeneous crowding. TOP: a uniform distribution of large particles (blue) corresponds to homogeneous crowding. A small particle (red) will tend to exhibit Brownian diffusion, with a reduced diffusion coefficient. BOTTOM: a non-uniform distribution of large particles (blue) corresponds to heterogeneous crowding. A small particle (red) will tend to be directed towards less-crowded regions.

the same overall level of crowding, the behaviour of a small particle varies greatly between the two. In this section, we therefore attempt to derive a diffusion equation for the small particle which can capture the irregular motion induced by heterogeneous macromolecular crowding.

We consider the three dimensional space $(-\infty, \infty) \times [0, L] \times [0, L]$ with reflective boundaries, in which particles can diffuse in all dimensions, but we are only interested in the first dimension. We consider two species of spherical particles, X_1 and X_2, with radii r_1 and r_2 respectively and intrinsic diffusion coefficients D_1 and D_2 respectively. Let θ_i^j be the concentration of X_i particles in the region $[jh, (j+1)h) \times [0, L] \times [0, L]$, for some grid-spacing $h > 0$ and integer j, and let p_i^j be the probability that a random point in $[jh, (j+1)h) \times [0, L] \times [0, L]$ can accomodate a single particle of species X_i. Then, as discussed in chapter 1, we can approximately model diffusion of particles as a hopping between neighbouring grid points, and this approximation will tend to be better for smaller grid-spacings h. A particle of X_i can hop from $[jh, (j+1)h) \times [0, L] \times [0, L]$ to $[(j+1)h, (j+2)h) \times [0, L] \times [0, L]$ with rate $\frac{D_i}{h^2} p_i^{j+1}$. Incorporating p_i^j into the hopping rate accounts for the probability that a particle is blocked by crowders. Taking a mean-field approach to this description (analogously to Eq. (1.17)) leads to a spatially-discrete diffusion equation for the concentration of X_i:

$$\frac{\partial \theta_i^j}{\partial t} = \frac{D_i}{h^2} \left[p_i^j (\theta_i^{j-1} + \theta_i^{j+1}) - (p_i^{j-1} + p_i^{j+1}) \theta_i^j \right]. \tag{6.1}$$

Similar mean-field equations have been derived for equal-sized particles, such as in Refs. [93, 150]. The equations for θ_1^j and θ_2^j are not independent, but are rather coupled via the quantity p_i^j which is naturally a function of both θ_1^j and θ_2^j. The quantity p_i^j is the probability that a random point in $[jh, (j+1)h) \times [0, L] \times [0, L]$ can accommodate a particle of X_i, which, as discussed in chapter 5 (specifically Eq. (5.12)), is approximately given by scaled particle theory

(SPT) [138, 139]:

$$p_i^j = (1-\phi_j)\exp\left[-\frac{r_i}{1-\phi_j}\left(B_j + \left(4\pi A_j + \frac{B_j^2}{2(1-\phi_j)}\right)r_i + \frac{4\pi r_i^2}{3}\left(d_j + \frac{B_j^3}{12\pi(1-\phi_j)^2 + \frac{A_j B_j}{1-\phi_j}}\right)\right)\right], \tag{6.2}$$

where $d_j = \sum_i \theta_i^j$, $A_j = \sum_i r_i\theta_i^j$, $B_j = \sum_i 4\pi r_i^2\theta_i^j$, and $\phi_j = \sum_i \frac{4}{3}\pi r_i^3\theta_i^j$. Note that we are using the SPT formula for p_i^j rather than the more usual $1-\phi_j = 1-\sum_i \frac{4}{3}\pi r_i^3\theta_i^j$ [150]. This is because we require p_i^j to be the probability that a random point is surrounded by a sufficiently large empty region to at least accomodate a whole particle of radius r_i. This probability is given by SPT, whereas $1-\phi_j$ is merely the probability that a random point can accomodate a point-particle, and is therefore an overestimate of the required quantity. For more information, see Ref. [95].

Defining $\theta_i(x) = \theta_i^{j=\lfloor x/h \rfloor}$ and $p_i(\theta_1(x), \theta_2(x)) = p_i^{j=\lfloor x/h \rfloor}$, and taking the limit $h \to 0$, we use Eq. (6.1) to obtain continuous PDEs for the concentrations θ_i:

$$\frac{\partial \theta_i}{\partial t} = D_i\left[p_i\frac{\partial^2}{\partial x^2}\theta_i - \theta_i\frac{\partial^2}{\partial x^2}p_i\right]. \tag{6.3}$$

Again the PDEs for θ_1 and θ_2 are coupled via the functions p_i. We now consider the case where $\theta_2(x,t) \ll \theta_1(x,t)$ for all x and t. It follows that $p_i(\theta_1,\theta_2) \approx p_i(\theta_1,0)$. Intuitively, this means that the X_2 concentration is so low that it does not affect the diffusion of any particles, but the X_1 concentration affects the diffusion of both species. We therefore simply write $p_i(\theta_1)$. It follows that the diffusion equation for X_1 is completely self-contained, while the diffusion equation for X_2 depends on X_1. We can write the two equations as:

$$\frac{\partial \theta_1}{\partial t} = \frac{\partial}{\partial x}\left[D_1\left(p_1 - \theta_1\frac{\partial p_1}{\partial \theta_1}\right)\frac{\partial}{\partial x}\theta_1\right], \tag{6.4}$$

$$\frac{\partial \theta_2}{\partial t} = \frac{\partial}{\partial x}\left[D_2 p_2\frac{\partial}{\partial x}\theta_2\right] - \frac{\partial}{\partial x}\left[D_2\theta_2\frac{\partial p_2}{\partial \theta_1}\frac{\partial \theta_1}{\partial x}\right]. \tag{6.5}$$

In other words, X_1 obeys a nonlinear diffusion equation with diffusion coefficient $D_1\left(p_1 - \theta_1\frac{\partial p_1}{\partial \theta_1}\right)$, while X_2 obeys a nonlinear advection-diffusion equation with diffusion coefficient $D_2 p_2$ and velocity $D_2\frac{\partial p_2}{\partial \theta_1}\frac{\partial \theta_1}{\partial x}$ in the positive x direction. For more details on deriving nonlinear PDEs from lattice models, see Refs. [229, 95]. Note that identical advection-diffusion equations have been derived in the context of chemotaxis [230, 231], though naturally the form of p_i in that context will be quite different, and not based on SPT.

We now further consider the case where $r_2 \ll r_1$. Combining this with the earlier assumption that $\theta_2(x,t) \ll \theta_1(x,t)$, it follows that we are now considering a single small particle of type X_2 diffusing amongst several large particles of type X_1. Let $\varepsilon = \frac{r_2}{r_1}$. Perturbatively expanding Eq. (6.2) in small ε gives the following:

$$p_2(\theta_1) = 1 - (1+3\varepsilon)\frac{4}{3}\pi r_1^3\theta_1 + o(\varepsilon^2). \tag{6.6}$$

Furthermore, from the Stokes-Einstein relation, we have that $\frac{D_1}{D_2} = \varepsilon$. It follows that the timescale on which θ_1 changes is much slower than that of θ_2. We can therefore make a quasi-stationarity assumption about θ_1 on the timescale of θ_2: we say $\theta_1 = \theta_1(x)$. Note that this stationarity is consistent with our earlier biological observations that heterogeneous crowder distributions are maintained over long timescales. Finally, letting $\phi(x) = \frac{4}{3}\pi r_1^3\theta_1(x)$ be the proportion of volume occupied by X_1 at x, and writing $\theta(x,t) = \theta_2(x,t)$ and $D = D_2$, we have

a linear advection-diffusion equation for X_2:

$$\frac{\partial \theta}{\partial t} = \frac{\partial}{\partial x}\left[D(1-(1+3\varepsilon)\phi)\frac{\partial \theta}{\partial x}\right] + \frac{\partial}{\partial x}\left[D(1+3\varepsilon)\frac{\partial \phi}{\partial x}\theta\right]. \tag{6.7}$$

We therefore have a rigorously derived advection-diffusion equation for the concentration of small molecules diffusing in a completely generic crowder distribution $\phi(x)$. This PDE shows that particle motion is affected in two distinct ways. (i) The particle's local diffusion coefficient is rescaled by a factor of $1-(1+3\varepsilon)\phi(x)$, where ε is the ratio of small to large particle radii and $\phi(x)$ is the local proportion of volume occupied by crowders. This recovers the classical $1-\phi$ scaling in the case of point-particle diffusion ($\varepsilon = 0$). (ii) The particle moves with a velocity $-D(1+3\varepsilon)\frac{\partial \phi}{\partial x}$ in the positive x direction, that is, a velocity directed towards less crowded regions and proportional to the gradient of the crowder distribution. If ϕ is constant (i.e. a uniform crowder density), this velocity becomes zero, and the particle will obey a standard diffusion equation (albeit with a reduced diffusion coefficient). Particle motion will generally be governed by the interplay between effects (i) and (ii), since particles will tend to move towards more dilute regions of space but will tend to move faster in those regions.

6.2 Applications

Using Eq. (6.7), we can investigate the motion of small molecules in a variety of crowder distributions. Of particular interest are the mean and variance (mean squared displacement) of θ as function of time. In particular, whether the variance is superlinear or sublinear, which would correspond to super- and subdiffusion respectively (see chapter 1).

The mean and variance of θ cannot be obtained directly from Eq. (6.7), so instead we write the solution of the advection-diffusion equation as a Taylor series in time:

$$\theta(x,t) = \sum_{i=0}^{\infty} \theta^{(i)}(x)\frac{t^i}{i!}, \tag{6.8}$$

where $\theta^{(i)}(x) = \frac{\partial^i \theta}{\partial t^i}|_{t=0}$. The time derivatives can be immediately obtained from Eq. (6.7) by thinking of the right-hand side as a differential operator acting on θ:

$$\theta^{(i)} = \left[D\left((1+3\varepsilon)\phi'' + (1-(1+3\varepsilon)\phi)\frac{\partial^2}{\partial x^2}\right)\right]^i \delta(x), \tag{6.9}$$

where we have assumed $\theta(x,0) = \delta(x)$, and ϕ'' denotes the second derivative of $\phi(x)$. Each $\theta^{(i)}$ is then a sum of products of derivatives of $\phi(x)$ and $\delta(x)$.

The n^{th} moment of θ is defined as:

$$\mu^{(n)}(t) = \int_{-\infty}^{\infty} x^n \theta(x,t)dx = \sum_{i=0}^{\infty}\frac{t^i}{i!}\int_{-\infty}^{\infty} x^n \theta^{(i)}(x)dx, \tag{6.10}$$

so that the variance is given by $\mu^{(2)}(t) - (\mu^{(1)}(t))^2$. At very short times, the t term of the variance will dominate, so the particle motion will be diffusive. We can then investigate the transition to subsequent anomalous diffusion at short times by looking at the t^2 term of the variance. If the coefficient of this term is positive, then the variance will be initially superlinear, and so the motion will be initially superdiffusive. Similarly, if the t^2 term is negative, the motion will be initially subdiffusive. A zero coefficient for the t^2 term denotes normal diffusion.

By squaring the expression for $\mu^{(1)}(t)$, and observing that $\int_{-\infty}^{\infty} x\delta(x)dx = 0$, we find the coefficient of the t^2 term in the expansion of the variance:

$$\gamma = \frac{1}{2}\int_{-\infty}^{\infty} x^2\theta^{(2)}(x)dx - \left[\int_{-\infty}^{\infty} x\theta^{(1)}(x)dx\right]^2. \tag{6.11}$$

The initial anomalous diffusion follows immediately:

$$\begin{aligned} \gamma < 0 \quad &\Longrightarrow \quad \text{subdiffusion} \\ \gamma = 0 \quad &\Longrightarrow \quad \text{normal diffusion} \\ \gamma > 0 \quad &\Longrightarrow \quad \text{superdiffusion} \end{aligned} \tag{6.12}$$

We now apply the advection-diffusion equation to a variety of physically-plausible heterogeneous crowder distributions. Since our PDE is (i) derived from a lattice description, (ii) uses a mean-field assumption, and (iii) uses the approximate SPT theory, it is not clear how accurate its predictions will be. We therefore also compare our PDE with hard-sphere BD simulations using the Cichocki-Hinsen algorithm [160], which suffer from none of these limitations (see chapter 5).

First, we study a Gaussian crowder distribution $\phi(x) = ke^{-x^2}$, where k is the maximum volume occupied. (Note that k must be less than 0.74, the densest sphere packing). This could represent a local distribution of ribosomes, which are known to assemble near individual strands of mRNA [232, 233]. The symmetry of this example implies that the mean of θ is zero for all times, but the variance may vary. Using this ϕ in Eq. (6.11) gives $\gamma = 10D^2k(1+3\varepsilon)(1-k(1+3\varepsilon))$. Since $k < 0.74$ and ε is "small", say $\varepsilon \leq 0.1$, it follows that $k(1+3\varepsilon) < 1$, and hence $\gamma > 0$. Therefore a small particle in a Gaussian crowder distribution will transition from diffusive to superdiffusive motion at short times. In Fig. 6.2 we confirm this with BD simulations. In the inset, we plot MSD against time, and it is clear that our analytical theory is correct initially, and our PDE is correct for all times shown. In the main figure we plot a snapshot of the distribution at a fixed time, where the PDE and BD both exhibit bimodal behaviour, clearly distinct from normal diffusion. The bimodal distribution arises because the small particle is directed (by the advection term in Eq. (6.7)) down one or other of the slopes of the Gaussian distribution.

Next, we study a bimodal Gaussian crowder distribution $\phi(x) = kx^2e^{1-x^2}$, where again k is the maximum volume occupied. This could represent the bimodal distribution of macromolecules characteristic of cells undergoing division [225, 226]. The symmetry of this example again implies that the mean of θ is zero for all times, but the variance may vary. Using this ϕ in Eq. (6.11) gives $\gamma = -10D^2ek(1+3\varepsilon) < 0$. Therefore a small particle in a bimodal Gaussian crowder distribution will transition from diffusive to subdiffusive motion at short times. In Fig. 6.3 we confirm this with BD simulations. In the plot of MSD against time (inset), we observe that the particle motion transitions from diffusive to subdiffusive at short times, as predicted, but later becomes superdiffusive. In the main figure we plot a snapshot of the distribution at a fixed time ($t = 10$), where the PDE and BD both exhibit trimodal behaviour, clearly distinct from normal diffusion. A number of effects give rise to this irregular behaviour: the small particle is initially trapped (by the advection term in Eq. (6.7)) between the two peaks of the bimodal crowder distribution - hence subdiffusion - but eventually it will move past one of these peaks and be directed (by the advection term) down the outer slope - hence superdiffusion. At $t = 10$, for the parameter set chosen, there is a significant chance that the particle is still trapped in the central region, but also a significant chance that the particle has moved past one or other of the peaks, hence the trimodal behaviour.

Finally, we study a step-like crowder distribution $\phi = \frac{k}{\pi}\left(\arctan(s(x+w)) + \frac{\pi}{2}\right)$, where again k is the maximum volume occupied, s is a measure of the sharpness of the step, and w is the distance between the step and the initial particle. This could represent a phase boundary such as the point where nucleoid meets cytosol. This example is asymmetric, so we expect the mean particle position to change with time, as well as the particle variance. We find that, at short times, the mean particle position is given by $\mu^{(1)}(t) = -\frac{2Dks(1+3\varepsilon)}{\pi(1+s^2w^2)}t + o(t^2)$, so that the particle performs directed motion towards the left (less crowded half) of the space. We also find that $\gamma = \frac{2}{\pi^2}D^2k^2s^2(1+3\varepsilon)^2 > 0$, so the motion will initially transition from diffusive to superdiffusive. In Fig. 6.4 we confirm the change in mean position with BD simulations (inset). It is clear that our analytical theory is qualitatively correct, and our PDE is correct for all times shown. In the main figure we plot a snapshot of the distribution at a fixed time, where the PDE and BD both exhibit non-Gaussian asymmetric behaviour, clearly distinct from normal diffusion. The steep slope of the crowder distribution causes the particle to be directed to the

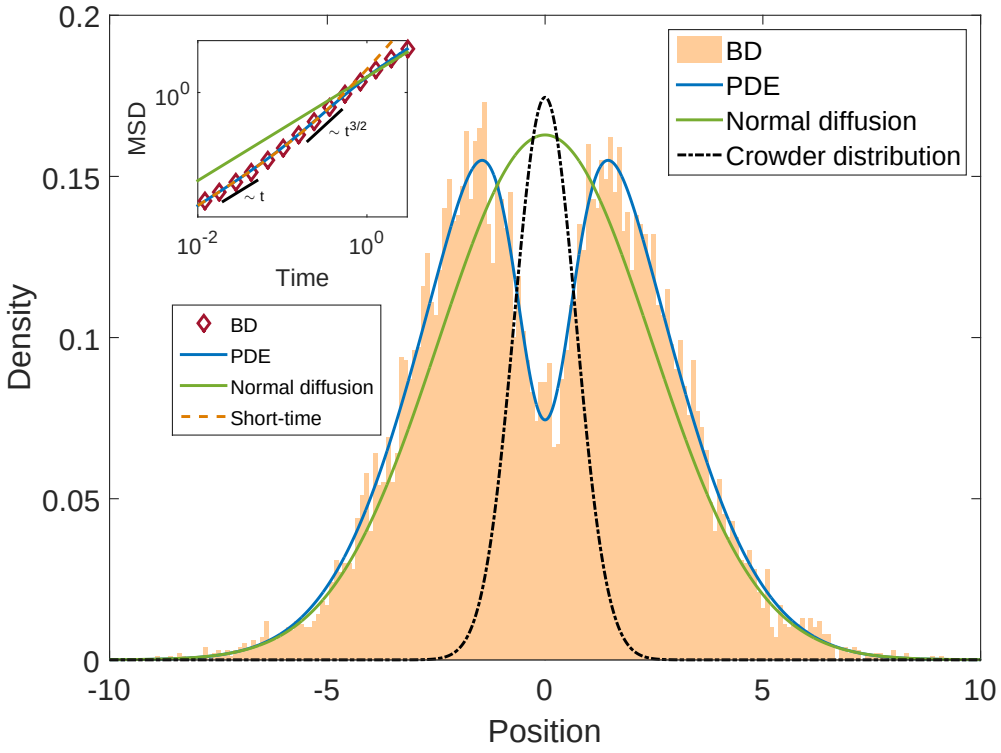

Figure 6.2: Inset: Mean-squared displacement against time for a small particle diffusing in a Gaussian distribution of crowders $\phi(x) = ke^{-x^2}$. Main: Probability density of small particle location for the same system at time $t = 3$. Crowder distribution not to scale. Parameter values: $k = 0.52$, $\varepsilon = 0.1$, $D = 1$, $L = 1$, $\Delta t = 10^{-5}$. BD averaged over 10^5 simulations.

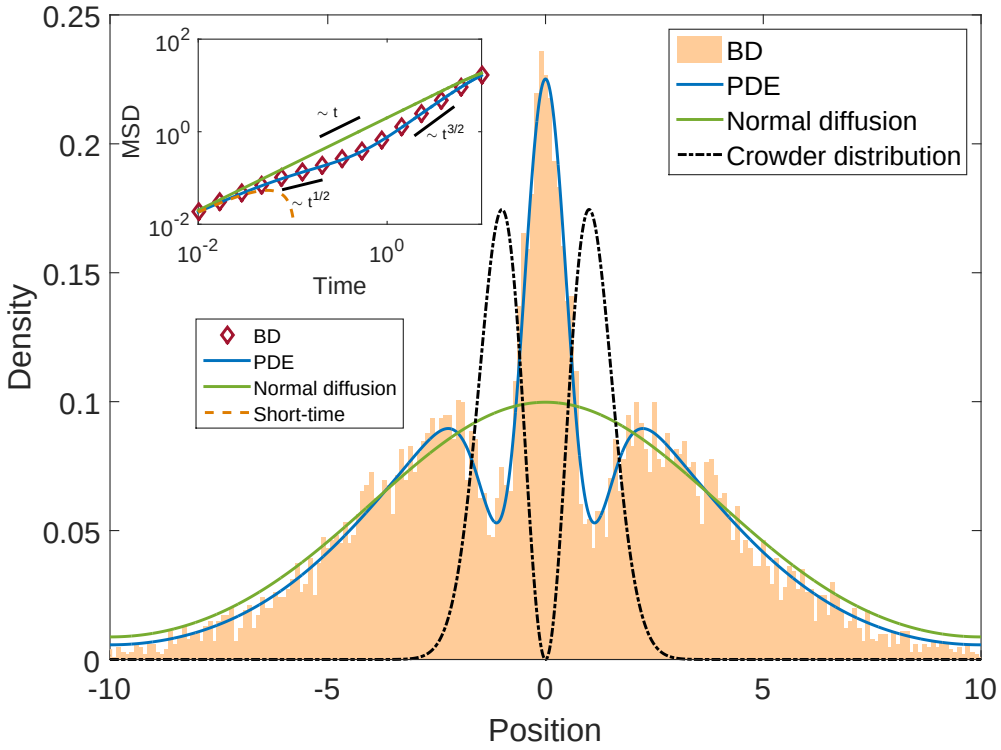

Figure 6.3: Inset: Mean-squared displacement against time for a small particle diffusing in a bimodal Gaussian distribution of crowders $\phi(x) = kx^2e^{1-x^2}$. Main: Probability density of small particle location for the same system at time $t = 10$. Crowder distribution not to scale. Parameter values: $k = 0.52$, $\varepsilon = 0.1$, $D = 1$, $L = 1$, $\Delta t = 10^{-5}$. BD averaged over 10^5 simulations.

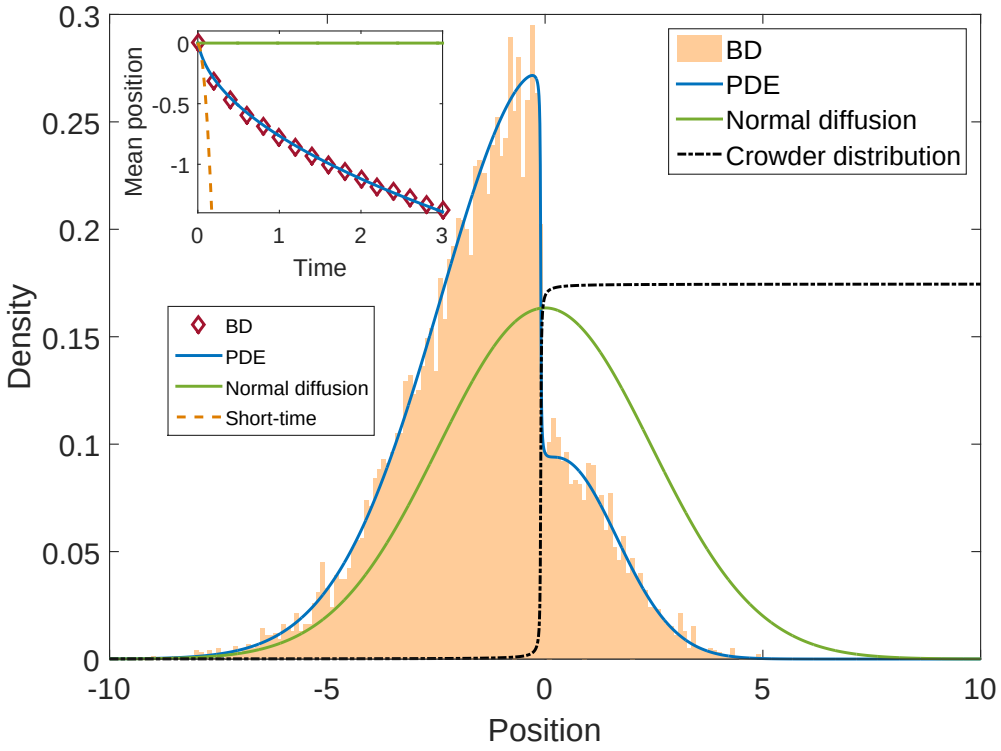

Figure 6.4: Inset: Mean particle position against time for a small particle diffusing in a step-like distribution of crowders $\phi(x) = \frac{k}{\pi}\left(\arctan(s(x+w)) + \frac{\pi}{2}\right)$. Main: Probability density of small particle location for the same system at time $t = 3$. Crowder distribution not to scale. Parameter values: $s = 100,\ w = 0.1,\ k = 0.52, \varepsilon = 0.1, D = 1, L = 1, \Delta t = 10^{-5}$. BD averaged over 10^5 simulations.

left (by the advection term in Eq. (6.7)) with high speed: this causes the particle to outrun normal diffusion in the negative half of the space. There is a small chance that the particle will diffuse into the right half of the space, but the diffusion coefficient here is significantly reduced so that normal diffusion is considerably faster.

6.3 Summary

In this chapter, we derived an analytical PDE to describe the motion of a small particle in the presence of a heterogeneous distribution of crowder molecules, a realistic scenario for cellular biochemistry. We found that diffusion coefficients are reduced in the presence of crowders, in a manner which depends on both the density of crowders and the size of the diffusing particle. Furthermore, particles experience a net velocity directed towards more dilute regions of space.

The work in this chapter shows, on the one hand, that analytical expressions can be derived which match excellently with BD, and show perfect agreement with simulations even in highly non-linear situations. On the other hand, as with the work in chapter 4, the chapter demonstrates that modelling can predict real biological effects (the directed motion of small molecules) before they are demonstrated in the laboratory, thus providing valuable directions for future biological research.

Chapter 7

Discussion

In this thesis, we have studied in detail the two most popular models of spatial stochastic chemical kinetics: the reaction-diffusion master equation (RDME) and Brownian dynamics (BD). These models can be used to simulate real biochemical systems, such as genetic or metabolic networks. However, open questions remain about the validty of these models, and when it is appropriate to use them.

In chapter 1, we showed how the two models are derived. The RDME is obtained by starting at the simplest model possible in chemical kinetics (the REs) and systematically adding in stochasticity and diffusion. In contrast, BD is obtained by starting from a highly complex MD model and systematically simplifying out negligible effects. Owing to their utterly different derivations, we do not typically expect the RDME and BD to agree, yet they are both attempts to model the same kinds of processes. Owing to its origin in a more physical MD model, we might typically expect BD to be the "better" model. However, over the course of the subsequent chapters, we found that the reality is not so simple.

In chapter 2, we found that the RDME can be considered an accurate model of chemical kinetics, but only if the reactions are of the elementary form. Non-elementary reactions (such as those with Hill or Michaelis-Menten rates) lead to internal contradictions, where the RDME predicts different behaviour from the CME even when diffusion is infinitely fast. This fact could be construed as an argument against the RDME and in favour of BD. However, BD has no method of implementing non-elementary reaction kinetics (although methods of implementing elementary reactions of any order have been developed [234]), and so the work in chapter 2 merely highlights a significant problem for spatial modelling in general. To model spatial systems correctly, all relevant species and reactions must be explicitly incorporated.

In chapter 3, we approached the RDME from an analytical perspective. We applied the EMRE method (originally intended to obtain approximations to the mean of the CME) to the RDME, obtaining relatively simple expressions for mean spatial concentrations in the case of single-species systems. This chapter highlighted a clear advantage of the RDME over BD: the RDME has an analytical form to which any method which applies to the CME can equally be applied. Thus we found that mean concentrations depend on diffusion coefficients in a non-trivial manner, a phenomenon not predicted by the deterministic RDEs but demonstrated to be true using BD simulations. Without the RDME, this behaviour could not have been analytically quantified. Nonetheless, we were still faced with the most pressing problem of the RDME: choosing M, the number of subvolumes.

In chapter 4, we proposed an application of the RDME which eliminates the problem of M. In this application, the RDME is treated as a model of a tissue, and each subvolume represents a cell in that tissue. Using this model, we predicted that the rate of transport between neighbour cells could seriously impact on the single-cell variability, and thus the heterogeneity of the tissue. We found that systems with intrinsically sub-Poissonian fluctuations tend to induce greater heterogeneity in tissues when transport rates increase, contrasted with greater homogeneity for super-Poissonian systems. These predictions were confirmed with real experimental data from animal and plant tissues, highlighting again the value of the RDME as a model for making real, testable predictions.

In chapter 5 we moved to studying BD in detail. A significant problem of BD is the issue of

crowding, since BD typically uses point-particles which exclude no volume, but biomolecules can be very large and in high concentrations. Yet incorporating crowding in BD simulations is time consuming, since a huge number of collisions between particles must be explicitly simulated. We proposed a "crowder-free" algorithm which treats the crowders implicitly (under the assumption that they are uniformly distributed in space), allowing us to eliminate them from the explicit simulation steps. The resulting algorithm was several orders of magnitude faster the traditional algorithms, thus enabling BD simulations with biochemical realism on a large scale.

In chapter 6 we took a different approach and addressed BD from an analytical perspective. We derived an advection-diffusion equation describing the motion of a small particle in the presence of a spatially heterogeneous distribution of crowder molecules. This equation predicted that diffusing molecules would be slowed in the presence of crowders, but would also experience a force directing them towards more dilute regions of space. This chapter therefore shows not only the analytical possibilities of BD, but also that BD can make testable predictions about biological behaviour.

Over all, the work in this thesis does not definitively favour RDME over BD, or vice-versa. As we have shown, the reality is more complicated. While BD certainly has a claim to greater physical accuracy, nonetheless the RDME is significantly more analytically tractable. Similarly, while the RDME has the advantage of being a generic model (we can apply it equally well to cells or tissues), BD provides substantially finer-grained spatial resolution without extreme computational costs.

The work in this thesis principally highlights the value of mathematical modelling of biology, beyond simply explaining what is already known. In chapters 4 and 6, we made testable predictions about real biological behaviour, which can be tested experimentally (indeed, in chapter 4 we *did* test our predictions on experimental data). This use of modelling in advance of experimentation is a highly attractive application of mathematical techniques to biology, which will likely only grow in popularity as computational power improves.

Bibliography

[1] Luonan Chen, Ruiqi Wang, Chunguang Li, and Kazuyuki Aihara. *Modeling biomolecular networks in cells: structures and dynamics*. Springer Science & Business Media, 2010.

[2] Daan Frenkel and Berend Smit. *Understanding molecular simulation: from algorithms to applications*, volume 1. Academic press, 2001.

[3] James D Murray. *Mathematical Biology. II Spatial Models and Biomedical Applications {Interdisciplinary Applied Mathematics V. 18}*. Springer-Verlag New York Incorporated, 2001.

[4] Daniel T Gillespie, Andreas Hellander, and Linda R Petzold. Perspective: Stochastic algorithms for chemical kinetics. *The Journal of chemical physics*, 138(17):05B201_1, 2013.

[5] Jacob D Durrant and J Andrew McCammon. Molecular dynamics simulations and drug discovery. *BMC biology*, 9(1):71, 2011.

[6] Daniel T Gillespie, Linda R Petzold, and Effrosyni Seitaridou. Validity conditions for stochastic chemical kinetics in diffusion-limited systems. *The Journal of chemical physics*, 140(5):02B604_1, 2014.

[7] Jana Lipková, Konstantinos C Zygalakis, S Jonathan Chapman, and Radek Erban. Analysis of brownian dynamics simulations of reversible bimolecular reactions. *SIAM Journal on Applied Mathematics*, 71(3):714–730, 2011.

[8] Michael Klann and Heinz Koeppl. Spatial simulations in systems biology: from molecules to cells. *International journal of molecular sciences*, 13(6):7798–7827, 2012.

[9] David Fange and Johan Elf. Noise-induced min phenotypes in e. coli. *PLoS computational biology*, 2(6):e80, 2006.

[10] Marc Sturrock, Andreas Hellander, Anastasios Matzavinos, and Mark AJ Chaplain. Spatial stochastic modelling of the hes1 gene regulatory network: intrinsic noise can explain heterogeneity in embryonic stem cell differentiation. *Journal of The Royal Society Interface*, 10(80):20120988, 2013.

[11] Karen Lipkow, Steven S Andrews, and Dennis Bray. Simulated diffusion of phosphorylated chey through the cytoplasm of escherichia coli. *Journal of bacteriology*, 187(1):45–53, 2005.

[12] Steven S Andrews, Nathan J Addy, Roger Brent, and Adam P Arkin. Detailed simulations of cell biology with smoldyn 2.1. *PLoS computational biology*, 6(3):e1000705, 2010.

[13] Péter Érdi and János Tóth. *Mathematical models of chemical reactions: theory and applications of deterministic and stochastic models*. Manchester University Press, 1989.

[14] John Charles Butcher. *Numerical methods for ordinary differential equations*. John Wiley & Sons, 2016.

[15] David Rickard. Kinetics of pyrite formation by the h 2 s oxidation of iron (ii) monosulfide in aqueous solutions between 25 and 125 c: The rate equation. *Geochimica et Cosmochimica Acta*, 61(1):115–134, 1997.

[16] S Schnell and C Mendoza. Closed form solution for time-dependent enzyme kinetics. *Journal of theoretical Biology*, 187(2):207–212, 1997.

[17] Peter Atkins, Julio De Paula, and James Keeler. *Atkins' physical chemistry*. Oxford university press, 2018.

[18] Daniel Thomas Gillespie and Effrosyni Seitaridou. *Simple Brownian diffusion: an introduction to the standard theoretical models*. Oxford University Press, 2012.

[19] M Loève. Elementary probability theory. In *Probability Theory I*, pages 1–52. Springer, 1977.

[20] Paul AM Dirac. The quantum theory of the emission and absorption of radiation. In *Proceedings of the Royal Society of London A: Mathematical, Physical and Engineering Sciences*, volume 114, pages 243–265. The Royal Society, 1927.

[21] Enrico Fermi. *Nuclear physics: a course given by Enrico Fermi at the University of Chicago*. University of Chicago Press, 1950.

[22] Nicolaas Godfried Van Kampen. *Stochastic processes in physics and chemistry*, volume 1. Elsevier, 1992.

[23] Brian Munsky and Mustafa Khammash. The finite state projection algorithm for the solution of the chemical master equation. *The Journal of chemical physics*, 124(4):044104, 2006.

[24] Stephen Smith and Vahid Shahrezaei. General transient solution of the one-step master equation in one dimension. *Physical Review E*, 91(6):062119, 2015.

[25] Vladimir Kazeev, Mustafa Khammash, Michael Nip, and Christoph Schwab. Direct solution of the chemical master equation using quantized tensor trains. *PLoS computational biology*, 10(3):e1003359, 2014.

[26] Shuohao Liao, Tomáš Vejchodskỳ, and Radek Erban. Tensor methods for parameter estimation and bifurcation analysis of stochastic reaction networks. *Journal of The Royal Society Interface*, 12(108):20150233, 2015.

[27] Simon L Cotter, Tomas Vejchodsky, and Radek Erban. Adaptive finite element method assisted by stochastic simulation of chemical systems. *SIAM Journal on Scientific Computing*, 35(1):B107–B131, 2013.

[28] Ivan G Darvey, BW Ninham, and PJ Staff. Stochastic models for second-order chemical reaction kinetics. the equilibrium state. *The journal of chemical physics*, 45(6):2145–2155, 1966.

[29] Chetan Gadgil, Chang Hyeong Lee, and Hans G Othmer. A stochastic analysis of first-order reaction networks. *Bulletin of mathematical biology*, 67(5):901–946, 2005.

[30] Tobias Jahnke and Wilhelm Huisinga. Solving the chemical master equation for monomolecular reaction systems analytically. *Journal of mathematical biology*, 54(1):1–26, 2007.

[31] Vahid Shahrezaei and Peter S Swain. Analytical distributions for stochastic gene expression. *Proceedings of the National Academy of Sciences*, 105(45):17256–17261, 2008.

[32] Ramon Grima, Deena R Schmidt, and Timothy J Newman. Steady-state fluctuations of a genetic feedback loop: An exact solution. *The Journal of chemical physics*, 137(3):035104, 2012.

[33] Nicolaas G Van Kampen. The equilibrium distribution of a chemical mixture. *Physics Letters A*, 59(5):333–334, 1976.

[34] Claudia Cianci, Stephen Smith, and Ramon Grima. Molecular finite-size effects in stochastic models of equilibrium chemical systems. *The Journal of chemical physics*, 144(8):084101, 2016.

[35] Philipp Thomas and Ramon Grima. Approximate probability distributions of the master equation. *Physical Review E*, 92(1):012120, 2015.

[36] Stephen Smith, Claudia Cianci, and Ramon Grima. Model reduction for stochastic chemical systems with abundant species. *The Journal of Chemical Physics*, 143(21):12B615_1, 2015.

[37] Alexander Andreychenko, Luca Bortolussi, Ramon Grima, Philipp Thomas, and Verena Wolf. Distribution approximations for the chemical master equation: comparison of the method of moments and the system size expansion. In *Modeling Cellular Systems*, pages 39–66. Springer, 2017.

[38] Stephen Smith and Ramon Grima. Model reduction for stochastic reaction systems. In *Stochastic Processes, Multiscale Modeling, and Numerical Methods for Computational Cellular Biology*, pages 143–158. Springer, 2017.

[39] Johan Elf and Måns Ehrenberg. Fast evaluation of fluctuations in biochemical networks with the linear noise approximation. *Genome research*, 13(11):2475–2484, 2003.

[40] Colin S Gillespie. Moment-closure approximations for mass-action models. *IET systems biology*, 3(1):52–58, 2009.

[41] Abhyudai Singh and Joao P Hespanha. Approximate moment dynamics for chemically reacting systems. *IEEE Transactions on Automatic Control*, 56(2):414–418, 2011.

[42] Ramon Grima. A study of the accuracy of moment-closure approximations for stochastic chemical kinetics. *The Journal of chemical physics*, 136(15):04B616, 2012.

[43] David Schnoerr, Guido Sanguinetti, and Ramon Grima. Validity conditions for moment closure approximations in stochastic chemical kinetics. *The Journal of chemical physics*, 141(8):08B616_1, 2014.

[44] David Schnoerr, Guido Sanguinetti, and Ramon Grima. Comparison of different moment-closure approximations for stochastic chemical kinetics. *The Journal of Chemical Physics*, 143(18):11B610_1, 2015.

[45] Daniel T Gillespie. The chemical langevin equation. *The Journal of Chemical Physics*, 113(1):297–306, 2000.

[46] David Schnoerr, Guido Sanguinetti, and Ramon Grima. The complex chemical langevin equation. *The Journal of chemical physics*, 141(2):07B606_1, 2014.

[47] David Schnoerr, Guido Sanguinetti, and Ramon Grima. Approximation and inference methods for stochastic biochemical kinetics—a tutorial review. *Journal of Physics A: Mathematical and Theoretical*, 50(9):093001, 2017.

[48] Pierre L'Écuyer. Random number generation. In *Handbook of Computational Statistics*, pages 35–71. Springer, 2012.

[49] Daniel T Gillespie. Exact stochastic simulation of coupled chemical reactions. *The journal of physical chemistry*, 81(25):2340–2361, 1977.

[50] Daniel T Gillespie. Approximate accelerated stochastic simulation of chemically reacting systems. *The Journal of Chemical Physics*, 115(4):1716–1733, 2001.

[51] Simon L Cotter, Konstantinos C Zygalakis, Ioannis G Kevrekidis, and Radek Erban. A constrained approach to multiscale stochastic simulation of chemically reacting systems. *The Journal of chemical physics*, 135(9):09B601, 2011.

[52] Andrew Duncan, Radek Erban, and Konstantinos Zygalakis. Hybrid framework for the simulation of stochastic chemical kinetics. *Journal of Computational Physics*, 326:398–419, 2016.

[53] Howard Salis and Yiannis Kaznessis. Accurate hybrid stochastic simulation of a system of coupled chemical or biochemical reactions. *The Journal of chemical physics*, 122(5):054103, 2005.

[54] Yang Cao, Daniel T Gillespie, and Linda R Petzold. The slow-scale stochastic simulation algorithm. *The Journal of chemical physics*, 122(1):014116, 2005.

[55] Anne Auger, Philippe Chatelain, and Petros Koumoutsakos. R-leaping: Accelerating the stochastic simulation algorithm by reaction leaps. *The Journal of chemical physics*, 125(8):084103, 2006.

[56] Tamas Szekely and Kevin Burrage. Stochastic simulation in systems biology. *Computational and structural biotechnology journal*, 12(20):14–25, 2014.

[57] Ramon Grima and Santiago Schnell. Modelling reaction kinetics inside cells. *Essays in biochemistry*, 45:41–56, 2008.

[58] JW Wojcieszyn, Robert A Schlegel, and Kenneth Alan Jacobson. Measurements of the diffusion of macromolecules injected into the cytoplasm of living cells. In *Cold Spring Harbor symposia on quantitative biology*, volume 46, pages 39–44. Cold Spring Harbor Laboratory Press, 1982.

[59] A M Turing. The Chemical Basis of Morphogenesis. *Philosophical transactions of the Royal Society of London. Series B, Biological sciences*, 237(641):37–72, 1952.

[60] Alfred Gierer and Hans Meinhardt. A theory of biological pattern formation. *Biological Cybernetics*, 12(1):30–39, 1972.

[61] Akiko Nakamasu, Go Takahashi, Akio Kanbe, and Shigeru Kondo. Interactions between zebrafish pigment cells responsible for the generation of turing patterns. *Proceedings of the National Academy of Sciences*, 106(21):8429–8434, 2009.

[62] Rushikesh Sheth, Luciano Marcon, M Félix Bastida, Marisa Junco, Laura Quintana, Randall Dahn, Marie Kmita, James Sharpe, and Maria A Ros. Hox genes regulate digit patterning by controlling the wavelength of a turing-type mechanism. *Science*, 338(6113):1476–1480, 2012.

[63] Jelena Raspopovic, Luciano Marcon, Laura Russo, and James Sharpe. Digit patterning is controlled by a bmp-sox9-wnt turing network modulated by morphogen gradients. *Science*, 345(6196):566–570, 2014.

[64] Masakatsu Watanabe and Shigeru Kondo. Is pigment patterning in fish skin determined by the turing mechanism? *Trends in Genetics*, 31(2):88–96, 2015.

[65] Istvan Lengyel and Irving R Epstein. A chemical approach to designing turing patterns in reaction-diffusion systems. *Proceedings of the National Academy of Sciences*, 89(9):3977–3979, 1992.

[66] Luis Diambra, Vivek Raj Senthivel, Diego Barcena Menendez, and Mark Isalan. Cooperativity to increase turing pattern space for synthetic biology. *ACS synthetic biology*, 4(2):177–186, 2014.

[67] Bartłomiej Borek, Jeff Hasty, and Lev Tsimring. Turing patterning using gene circuits with gas-induced degradation of quorum sensing molecules. *PloS one*, 11(5):e0153679, 2016.

[68] Natalie S Scholes and Mark Isalan. A three-step framework for programming pattern formation. *Current Opinion in Chemical Biology*, 40:1–7, 2017.

[69] Stephen Smith and Neil Dalchau. Model reduction permits turing instability analysis of arbitrary reaction-diffusion models. *bioRxiv*, page 213298, 2017.

[70] Stephen Smith and Neil Dalchau. Beyond activator-inhibitor networks: the generalised turing mechanism. *arXiv preprint arXiv:1803.07886*, 2018.

[71] Alan J McKane, Tommaso Biancalani, and Tim Rogers. Stochastic pattern formation and spontaneous polarisation: the linear noise approximation and beyond. *Bulletin of mathematical biology*, 76(4):895–921, 2014.

[72] Yang Cao and Radek Erban. Stochastic turing patterns: Analysis of compartment-based approaches. *Bulletin of mathematical biology*, 76(12):3051–3069, 2014.

[73] Stephen Smith, Claudia Cianci, and Ramon Grima. Analytical approximations for spatial stochastic gene expression in single cells and tissues. *Journal of The Royal Society Interface*, 13(118):20151051, 2016.

[74] Atiyo Ghosh, Andre Leier, and Tatiana T Marquez-Lago. The spatial chemical langevin equation and reaction diffusion master equations: moments and qualitative solutions. *Theoretical Biology and Medical Modelling*, 12(1):5, 2015.

[75] Audrius B Stundzia and Charles J Lumsden. Stochastic simulation of coupled reaction–diffusion processes. *Journal of computational physics*, 127(1):196–207, 1996.

[76] Johan Elf and Måns Ehrenberg. Spontaneous separation of bi-stable biochemical systems into spatial domains of opposite phases. *Systems biology*, 1(2):230–236, 2004.

[77] David Bernstein. Simulating mesoscopic reaction-diffusion systems using the gillespie algorithm. *Physical Review E*, 71(4):041103, 2005.

[78] David Fange, Anel Mahmutovic, and Johan Elf. Mesord 1.0: Stochastic reaction-diffusion simulations in the microscopic limit. *Bioinformatics*, 28(23):3155–3157, 2012.

[79] Johan Elf, Andreas Doncic, and Mans Ehrenberg. Mesoscopic reaction-diffusion in intracellular signaling. In *Fluctuations and Noise in Biological, Biophysical, and Biomedical Systems*, volume 5110, pages 114–125. International Society for Optics and Photonics, 2003.

[80] Brian Drawert, Michael J Lawson, Linda Petzold, and Mustafa Khammash. The diffusive finite state projection algorithm for efficient simulation of the stochastic reaction-diffusion master equation. *The Journal of chemical physics*, 132(7):074101, 2010.

[81] Elijah Roberts, John E Stone, and Zaida Luthey-Schulten. Lattice microbes: High-performance stochastic simulation method for the reaction-diffusion master equation. *Journal of computational chemistry*, 34(3):245–255, 2013.

[82] Jin Fu, Sheng Wu, Hong Li, and Linda R Petzold. The time dependent propensity function for acceleration of spatial stochastic simulation of reaction–diffusion systems. *Journal of computational physics*, 274:524–549, 2014.

[83] Sidney Redner. *A guide to first-passage processes*. Cambridge University Press, 2001.

[84] Samuel A Isaacson and Charles S Peskin. Incorporating diffusion in complex geometries into stochastic chemical kinetics simulations. *SIAM Journal on Scientific Computing*, 28(1):47–74, 2006.

[85] Stefan Engblom, Lars Ferm, Andreas Hellander, and Per Lötstedt. Simulation of stochastic reaction-diffusion processes on unstructured meshes. *SIAM Journal on Scientific Computing*, 31(3):1774–1797, 2009.

[86] Basil Bayati, Philippe Chatelain, and Petros Koumoutsakos. Adaptive mesh refinement for stochastic reaction–diffusion processes. *Journal of Computational Physics*, 230(1):13–26, 2011.

[87] Brian Drawert, Stefan Engblom, and Andreas Hellander. Urdme: a modular framework for stochastic simulation of reaction-transport processes in complex geometries. *BMC systems biology*, 6(1):76, 2012.

[88] Per Lötstedt and Lina Meinecke. Simulation of stochastic diffusion via first exit times. *Journal of computational physics*, 300:862–886, 2015.

[89] Lina Meinecke, Stefan Engblom, Andreas Hellander, and Per Lotstedt. Analysis and design of jump coefficients in discrete stochastic diffusion models. *SIAM Journal on Scientific Computing*, 38(1):A55–A83, 2016.

[90] Lina Meinecke and Per Lötstedt. Stochastic diffusion processes on cartesian meshes. *Journal of computational and applied mathematics*, 294:1–11, 2016.

[91] David Elderfield. Field theories for kinetic growth models. *Journal of Physics A: Mathematical and General*, 18(13):L773, 1985.

[92] Ruth E Baker, Christian A Yates, and Radek Erban. From microscopic to macroscopic descriptions of cell migration on growing domains. *Bulletin of mathematical biology*, 72(3):719–762, 2010.

[93] Duccio Fanelli and Alan J McKane. Diffusion in a crowded environment. *Physical Review E*, 82(2):021113, 2010.

[94] Lina Meinecke. Multiscale modeling of diffusion in a crowded environment. *Bulletin of mathematical biology*, 79(11):2672–2695, 2017.

[95] Claudia Cianci, Stephen Smith, and Ramon Grima. Capturing brownian dynamics with an on-lattice model of hard-sphere diffusion. *Physical Review E*, 95(5):052118, 2017.

[96] Stephen Smith, Claudia Cianci, and Ramon Grima. Macromolecular crowding directs the motion of small molecules inside cells. *Journal of The Royal Society Interface*, 14(131):20170047, 2017.

[97] PR Taylor, RE Baker, and CA Yates. Deriving appropriate boundary conditions, and accelerating position-jump simulations, of diffusion using non-local jumping. *Physical biology*, 12(1):016006, 2014.

[98] Florence Baras and M Malek Mansour. Reaction-diffusion master equation: A comparison with microscopic simulations. *Physical Review E*, 54(6):6139, 1996.

[99] Maciej Dobrzyński, Jordi Vidal Rodríguez, Jaap A Kaandorp, and Joke G Blom. Computational methods for diffusion-influenced biochemical reactions. *Bioinformatics*, 23(15):1969–1977, 2007.

[100] David Fange, Otto G Berg, Paul Sjöberg, and Johan Elf. Stochastic reaction-diffusion kinetics in the microscopic limit. *Proceedings of the National Academy of Sciences*, 107(46):19820–19825, 2010.

[101] Frank C Collins and George E Kimball. Diffusion-controlled reaction rates. *Journal of colloid science*, 4(4):425–437, 1949.

[102] Stefan Hellander, Andreas Hellander, and Linda Petzold. Reaction rates for mesoscopic reaction-diffusion kinetics. *Physical Review E*, 91(2):023312, 2015.

[103] Samuel A Isaacson. Relationship between the reaction–diffusion master equation and particle tracking models. *Journal of Physics A: Mathematical and Theoretical*, 41(6):065003, 2008.

[104] Samuel A Isaacson. The reaction-diffusion master equation as an asymptotic approximation of diffusion to a small target. *SIAM Journal on Applied Mathematics*, 70(1):77–111, 2009.

[105] Samuel A Isaacson. A convergent reaction-diffusion master equation. *The Journal of chemical physics*, 139(5):054101, 2013.

[106] MV Smoluchowski. Mathematical theory of the kinetics of the coagulation of colloidal solutions. *Z. Phys. Chem.*, 92:129–168, 1917.

[107] Stefan Hellander, Andreas Hellander, and Linda Petzold. Reaction-diffusion master equation in the microscopic limit. *Physical Review E*, 85(4):042901, 2012.

[108] Radek Erban and S Jonathan Chapman. Stochastic modelling of reaction–diffusion processes: algorithms for bimolecular reactions. *Physical biology*, 6(4):046001, 2009.

[109] J Andrew McCammon, Bruce R Gelin, and Martin Karplus. Dynamics of folded proteins. *Nature*, 267(5612):585–590, 1977.

[110] Alex D MacKerell Jr, Donald Bashford, MLDR Bellott, Roland Leslie Dunbrack Jr, Jeffrey D Evanseck, Martin J Field, Stefan Fischer, Jiali Gao, H Guo, Sookhee Ha, et al. All-atom empirical potential for molecular modeling and dynamics studies of proteins. *The journal of physical chemistry B*, 102(18):3586–3616, 1998.

[111] Ignasi Buch, Matt J Harvey, Toni Giorgino, David P Anderson, and Gianni De Fabritiis. High-throughput all-atom molecular dynamics simulations using distributed computing. *Journal of chemical information and modeling*, 50(3):397–403, 2010.

[112] Berni J Alder and T E Wainwright. Studies in molecular dynamics. i. general method. *The Journal of Chemical Physics*, 31(2):459–466, 1959.

[113] BJ Alder and TE Wainwright. Studies in molecular dynamics. ii. behavior of a small number of elastic spheres. *The Journal of Chemical Physics*, 33(5):1439–1451, 1960.

[114] Han Wang, Christoph Junghans, and Kurt Kremer. Comparative atomistic and coarse-grained study of water: What do we lose by coarse-graining? *The European Physical Journal E: Soft Matter and Biological Physics*, 28(2):221–229, 2009.

[115] Sereina Riniker and Wilfred F van Gunsteren. A simple, efficient polarizable coarse-grained water model for molecular dynamics simulations. *The Journal of chemical physics*, 134(8):084110, 2011.

[116] Anne Voegler Smith and Carol K Hall. Protein refolding versus aggregation: computer simulations on an intermediate-resolution protein model. *Journal of molecular biology*, 312(1):187–202, 2001.

[117] Feng Ding, Sergey V Buldyrev, and Nikolay V Dokholyan. Folding trp-cage to nmr resolution native structure using a coarse-grained protein model. *Biophysical journal*, 88(1):147–155, 2005.

[118] Valentina Tozzini. Coarse-grained models for proteins. *Current opinion in structural biology*, 15(2):144–150, 2005.

[119] Hao Hu and Weitao Yang. Free energies of chemical reactions in solution and in enzymes with ab initio quantum mechanics/molecular mechanics methods. *Annu. Rev. Phys. Chem.*, 59:573–601, 2008.

[120] John L Klepeis, Kresten Lindorff-Larsen, Ron O Dror, and David E Shaw. Long-timescale molecular dynamics simulations of protein structure and function. *Current opinion in structural biology*, 19(2):120–127, 2009.

[121] Radek Erban. From molecular dynamics to brownian dynamics. *Proc. R. Soc. A*, 470(2167):20140036, 2014.

[122] Radek Erban. Coupling all-atom molecular dynamics simulations of ions in water with brownian dynamics. *Proc. R. Soc. A*, 472(2186):20150556, 2016.

[123] Julija Zavadlav, Rudolf Podgornik, and Matej Praprotnik. Adaptive resolution simulation of a dna molecule in salt solution. *Journal of chemical theory and computation*, 11(10):5035–5044, 2015.

[124] Richard W Pastor, Bernard R Brooks, and Attila Szabo. An analysis of the accuracy of langevin and molecular dynamics algorithms. *Molecular Physics*, 65(6):1409–1419, 1988.

[125] Hyun Kyung Shin, Changho Kim, Peter Talkner, and Eok Kyun Lee. Brownian motion from molecular dynamics. *Chemical Physics*, 375(2-3):316–326, 2010.

[126] Donald L Ermak and JA McCammon. Brownian dynamics with hydrodynamic interactions. *The Journal of chemical physics*, 69(4):1352–1360, 1978.

[127] Amir Ba. Brownian motion and the central limit theorem. `https://www.weizmann.ac.il/complex/mukamel/sites/complex.mukamel/files/uploads/2013-brownian_motion.pdf`, note = Accessed: 2018-28-08.

[128] Hiromi Yamakawa. *Modern theory of polymer solutions*. Harper & Row, 1971.

[129] Jens Rotne and Stephen Prager. Variational treatment of hydrodynamic interaction in polymers. *The Journal of Chemical Physics*, 50(11):4831–4837, 1969.

[130] Linling Miao, Charles D Young, and Charles E Sing. An iterative method for hydrodynamic interactions in brownian dynamics simulations of polymer dynamics. *The Journal of chemical physics*, 147(2):024904, 2017.

[131] Marshall Fixman. Construction of langevin forces in the simulation of hydrodynamic interaction. *Macromolecules*, 19(4):1204–1207, 1986.

[132] Tadashi Ando, Edmond Chow, Yousef Saad, and Jeffrey Skolnick. Krylov subspace methods for computing hydrodynamic interactions in brownian dynamics simulations. *The Journal of chemical physics*, 137(6):064106, 2012.

[133] Tihamér Geyer and Uwe Winter. An o (n 2) approximation for hydrodynamic interactions in brownian dynamics simulations. *The Journal of chemical physics*, 130(11):114905, 2009.

[134] Edward Rolls and Radek Erban. Multi-resolution polymer brownian dynamics with hydrodynamic interactions. *The Journal of Chemical Physics*, 148(19):194111, 2018.

[135] Edward M Purcell. Life at low reynolds number. *American journal of physics*, 45(1):3–11, 1977.

[136] Albert Einstein. *Investigations on the Theory of the Brownian Movement*. Courier Corporation, 1956.

[137] Samuel Karlin. *A first course in stochastic processes*. Academic press, 2014.

[138] Steven B Zimmerman and Stefan O Trach. Estimation of macromolecule concentrations and excluded volume effects for the cytoplasm of escherichia coli. *Journal of molecular biology*, 222(3):599–620, 1991.

[139] Steven B Zimmerman and Allen P Minton. Macromolecular crowding: biochemical, biophysical, and physiological consequences. *Annual review of biophysics and biomolecular structure*, 22(1):27–65, 1993.

[140] R John Ellis. Macromolecular crowding: obvious but underappreciated. *Trends in biochemical sciences*, 26(10):597–604, 2001.

[141] Salvatore Torquato and Frank H Stillinger. Jammed hard-particle packings: From kepler to bernal and beyond. *Reviews of modern physics*, 82(3):2633, 2010.

[142] Felix Höfling and Thomas Franosch. Anomalous transport in the crowded world of biological cells. *Reports on Progress in Physics*, 76(4):046602, 2013.

[143] Cheemeng Tan, Saumya Saurabh, Marcel P Bruchez, Russell Schwartz, and Philip LeDuc. Molecular crowding shapes gene expression in synthetic cellular nanosystems. *Nature nanotechnology*, 8(8):602–608, 2013.

[144] Rafi Chapanian, David H Kwan, Iren Constantinescu, Fathima A Shaikh, Nicholas A A Rossi, Stephen G Withers, and Jayachandran N Kizhakkedathu. Enhancement of biological reactions on cell surfaces via macromolecular crowding. *Nature communications*, 5:4683, 2014.

[145] Sean R McGuffee and Adrian H Elcock. Diffusion, crowding & protein stability in a dynamic molecular model of the bacterial cytoplasm. *PLoS computational biology*, 6(3):e1000694, 2010.

[146] Maria Bruna and S Jonathan Chapman. Excluded-volume effects in the diffusion of hard spheres. *Physical Review E*, 85(1):011103, 2012.

[147] Stephen Smith and Ramon Grima. Fast simulation of brownian dynamics in a crowded environment. *The Journal of chemical physics*, 146(2):024105, 2017.

[148] Harold L Weissberg. Effective diffusion coefficient in porous media. *Journal of Applied Physics*, 34(9):2636–2639, 1963.

[149] JJ Blum, G Lawler, M Reed, and I Shin. Effect of cytoskeletal geometry on intracellular diffusion. *Biophysical journal*, 56(5):995–1005, 1989.

[150] Marta Galanti, Duccio Fanelli, Amos Maritan, and Francesco Piazza. Diffusion of tagged particles in a crowded medium. *EPL (Europhysics Letters)*, 107(2):20006, 2014.

[151] Michael J Saxton. Anomalous diffusion due to obstacles: a monte carlo study. *Biophysical journal*, 66(2):394–401, 1994.

[152] Michael T Klann, Alexei Lapin, and Matthias Reuss. Stochastic simulation of signal transduction: impact of the cellular architecture on diffusion. *Biophysical Journal*, 96(12):5122–5129, 2009.

[153] Matthias Weiss, Markus Elsner, Fredrik Kartberg, and Tommy Nilsson. Anomalous subdiffusion is a measure for cytoplasmic crowding in living cells. *Biophysical journal*, 87(5):3518–3524, 2004.

[154] Daniel S Banks and Cécile Fradin. Anomalous diffusion of proteins due to molecular crowding. *Biophysical journal*, 89(5):2960–2971, 2005.

[155] Emmanuel Dauty and AS Verkman. Molecular crowding reduces to a similar extent the diffusion of small solutes and macromolecules: measurement by fluorescence correlation spectroscopy. *Journal of molecular recognition*, 17(5):441–447, 2004.

[156] Julia F Reverey, Jae-Hyung Jeon, Han Bao, Matthias Leippe, Ralf Metzler, and Christine Selhuber-Unkel. Superdiffusion dominates intracellular particle motion in the supercrowded cytoplasm of pathogenic acanthamoeba castellanii. *Scientific reports*, 5:11690, 2015.

[157] Ralf Metzler and Joseph Klafter. The random walk's guide to anomalous diffusion: a fractional dynamics approach. *Physics reports*, 339(1):1–77, 2000.

[158] TT Marquez-Lago, Andre Leier, and Kevin Burrage. Anomalous diffusion and multifractional brownian motion: simulating molecular crowding and physical obstacles in systems biology. *IET systems biology*, 6(4):134–142, 2012.

[159] James A Dix and AS Verkman. Crowding effects on diffusion in solutions and cells. *Annu. Rev. Biophys.*, 37:247–263, 2008.

[160] B Cichocki and K Hinsen. Dynamic computer simulation of concentrated hard sphere suspensions: I. simulation technique and mean square displacement data. *Physica A: Statistical Mechanics and its Applications*, 166(3):473–491, 1990.

[161] Douglas Ridgway, Gordon Broderick, Ana Lopez-Campistrous, Melania Ru'aini, Philip Winter, Matthew Hamilton, Pierre Boulanger, Andriy Kovalenko, and Michael J Ellison. Coarse-grained molecular simulation of diffusion and reaction kinetics in a crowded virtual cytoplasm. *Biophysical journal*, 94(10):3748–3759, 2008.

[162] BU Felderhof. Diffusion of interacting brownian particles. *Journal of Physics A: Mathematical and General*, 11(5):929, 1978.

[163] Toshiya Ohtsuki and Koji Okano. Diffusion coefficients of interacting brownian particles. *The Journal of Chemical Physics*, 77(3):1443–1450, 1982.

[164] JM Deutch and BU Felderhof. Hydrodynamic effect in diffusion-controlled reaction. *The Journal of Chemical Physics*, 59(4):1669–1671, 1973.

[165] Steven S Andrews and Dennis Bray. Stochastic simulation of chemical reactions with spatial resolution and single molecule detail. *Physical biology*, 1(3):137, 2004.

[166] Marian Smoluchowski. Sur le chemin moyen parcouru par les molécules d'un gaz et sur son rapport avec la théorie de la diffusion. *Pisma Mariana Smoluchowskiego*, 1(1):479–489, 1924.

[167] Daniel T Gillespie. A diffusional bimolecular propensity function. *The Journal of chemical physics*, 131(16):164109, 2009.

[168] Masao Doi. Stochastic theory of diffusion-controlled reaction. *Journal of Physics A: Mathematical and General*, 9(9):1479, 1976.

[169] Ei Teramoto and Nanako Shigesada. Theory of bimolecular reaction processes in liquids. *Progress of Theoretical Physics*, 37(1):29–51, 1967.

[170] Ikemefuna C Agbanusi and Samuel A Isaacson. A comparison of bimolecular reaction models for stochastic reaction–diffusion systems. *Bulletin of mathematical biology*, 76(4):922–946, 2014.

[171] S Jonathan Chapman, Radek Erban, and Samuel A Isaacson. Reactive boundary conditions as limits of interaction potentials for brownian and langevin dynamics. *SIAM Journal on Applied Mathematics*, 76(1):368–390, 2016.

[172] Daniel T Gillespie. A rigorous derivation of the chemical master equation. *Physica A: Statistical Mechanics and its Applications*, 188(1-3):404–425, 1992.

[173] Ethan A Mastny, Eric L Haseltine, and James B Rawlings. Two classes of quasi-steady-state model reductions for stochastic kinetics. *The Journal of chemical physics*, 127(9):094106, 2007.

[174] John Goutsias. Quasiequilibrium approximation of fast reaction kinetics in stochastic biochemical systems. *The Journal of chemical physics*, 122(18):184102, 2005.

[175] Daniel T Gillespie. Stochastic simulation of chemical kinetics. *Annu. Rev. Phys. Chem.*, 58:35–55, 2007.

[176] Daniel T Gillespie. Deterministic limit of stochastic chemical kinetics. *The Journal of Physical Chemistry B*, 113(6):1640–1644, 2009.

[177] RB Potts. Note on the factorial moments of standard distributions. *Australian Journal of Physics*, 6(4):498–499, 1953.

[178] Crispin W Gardiner. *Handbook of stochastic methods for physics, chemistry and the natural sciences*. Springer-Verlag, Berlin,, 2004.

[179] Didier Gonze, José Halloy, and Albert Goldbeter. Deterministic versus stochastic models for circadian rhythms. *Journal of biological physics*, 28(4):637–653, 2002.

[180] Philipp Thomas, Arthur V Straube, and Ramon Grima. The slow-scale linear noise approximation: an accurate, reduced stochastic description of biochemical networks under timescale separation conditions. *BMC systems biology*, 6(1):39, 2012.

[181] Michael J Lawson, Linda Petzold, and Andreas Hellander. Accuracy of the michaelis–menten approximation when analysing effects of molecular noise. *Journal of The Royal Society Interface*, 12(106):20150054, 2015.

[182] Abhyudai Singh and Joao Pedro Hespanha. Lognormal moment closures for biochemical reactions. In *Decision and Control, 2006 45th IEEE Conference on*, pages 2063–2068. IEEE, 2006.

[183] Carlos A Gomez-Uribe and George C Verghese. Mass fluctuation kinetics: Capturing stochastic effects in systems of chemical reactions through coupled mean-variance computations. *The Journal of chemical physics*, 126(2):024109, 2007.

[184] R Grima. Noise-induced breakdown of the michaelis-menten equation in steady-state conditions. *Physical review letters*, 102(21):218103, 2009.

[185] Ramon Grima. An effective rate equation approach to reaction kinetics in small volumes: Theory and application to biochemical reactions in nonequilibrium steady-state conditions. *The Journal of chemical physics*, 133(3):07B604, 2010.

[186] Rajesh Ramaswamy, Nélido González-Segredo, Ivo F Sbalzarini, and Ramon Grima. Discreteness-induced concentration inversion in mesoscopic chemical systems. *Nature communications*, 3:779, 2012.

[187] Donald A McQuarrie. Stochastic approach to chemical kinetics. *Journal of applied probability*, 4(3):413–478, 1967.

[188] Ramon Grima. Linear-noise approximation and the chemical master equation agree up to second-order moments for a class of chemical systems. *Physical Review E*, 92(4):042124, 2015.

[189] Philipp Thomas, Hannes Matuschek, and Ramon Grima. Intrinsic noise analyzer: a software package for the exploration of stochastic biochemical kinetics using the system size expansion. *PloS one*, 7(6):e38518, 2012.

[190] Robert M Gray. Toeplitz and circulant matrices: A review. Technical report, STANFORD UNIV CALIF STANFORD ELECTRONICS LABS, 1971.

[191] Roberto Vescovo. Inversion of block-circulant matrices and circular array approach. *IEEE Transactions on Antennas and Propagation*, 45(10):1565–1567, 1997.

[192] Qian Chai, Bhupender Singh, Kristin Peisker, Nicole Metzendorf, Xueliang Ge, Santanu Dasgupta, and Suparna Sanyal. Organization of ribosomes and nucleoids in escherichia coli cells during growth and in quiescence. *Journal of Biological Chemistry*, 289(16):11342–11352, 2014.

[193] Stefanie Winkelmann and Christof Schütte. The spatiotemporal master equation: Approximation of reaction-diffusion dynamics via markov state modeling. *The Journal of Chemical Physics*, 145(21):214107, 2016.

[194] Stephen Smith and Ramon Grima. Single-cell variability in multicellular organisms. *Nature Communications*, 9(1):345, 2018.

[195] Ernst JM Helmreich. *The biochemistry of cell signalling*. Oxford University Press, USA, 2001.

[196] Katrina M Crawford and Patricia C Zambryski. Subcellular localization determines the availability of non-targeted proteins to plasmodesmatal transport. *Current Biology*, 10(17):1032–1040, 2000.

[197] Katrina M Crawford and Patricia C Zambryski. Non-targeted and targeted protein movement through plasmodesmata in leaves in different developmental and physiological states. *Plant Physiology*, 125(4):1802–1812, 2001.

[198] William J Lucas, Sabine Bouché-Pillon, David P Jackson, Lynda Nguyen, Lucian Baker, Biao Ding, and Sarah Hake. Selective trafficking of knotted1 homeodomain protein and its mrna through plasmodesmata. *Science*, 270(5244):1980–1983, 1995.

[199] Nalin M Kumar and Norton B Gilula. The gap junction communication channel. *Cell*, 84(3):381–388, 1996.

[200] Sami Ventelä, Jorma Toppari, and Martti Parvinen. Intercellular organelle traffic through cytoplasmic bridges in early spermatids of the rat: mechanisms of haploid gene product sharing. *Molecular biology of the cell*, 14(7):2768–2780, 2003.

[201] Xiang Wang, Margaret Lin Veruki, Nickolay V Bukoreshtliev, Espen Hartveit, and Hans-Hermann Gerdes. Animal cells connected by nanotubes can be electrically coupled through interposed gap-junction channels. *Proceedings of the National Academy of Sciences*, 107(40):17194–17199, 2010.

[202] Maciej H Swat, Gilberto L Thomas, Julio M Belmonte, Abbas Shirinifard, Dimitrij Hmeljak, and James A Glazier. Multi-scale modeling of tissues using compucell3d. *Methods in cell biology*, 110:325–366, 2012.

[203] Daniel L Barton, Silke Henkes, Cornelis J Weijer, and Rastko Sknepnek. Active vertex model for cell-resolution description of epithelial tissue mechanics. *PLoS computational biology*, 13(6):e1005569, 2017.

[204] Jamie Twycross, Leah R Band, Malcolm J Bennett, John R King, and Natalio Krasnogor. Stochastic and deterministic multiscale models for systems biology: an auxin-transport case study. *BMC systems biology*, 4(1):34, 2010.

[205] Thorsten Erdmann, Martin Howard, and Pieter Rein Ten Wolde. Role of spatial averaging in the precision of gene expression patterns. *Physical review letters*, 103(25):258101, 2009.

[206] Eric W Weisstein. Hypergeometric function. `http://mathworld.wolfram.com/HypergeometricFunction.html`, note = Accessed: 2018-01-04.

[207] Philipp Thomas, Nikola Popović, and Ramon Grima. Phenotypic switching in gene regulatory networks. *Proceedings of the National Academy of Sciences*, 111(19):6994–6999, 2014.

[208] Karen Featherstone, Kirsty Hey, Hiroshi Momiji, Anne V McNamara, Amanda L Patist, Joanna Woodburn, David G Spiller, Helen C Christian, Alan S McNeilly, John J Mullins, et al. Spatially coordinated dynamic gene transcription in living pituitary tissue. *Elife*, 5, 2016.

[209] Bénédicte Wenden, David LK Toner, Sarah K Hodge, Ramon Grima, and Andrew J Millar. Spontaneous spatiotemporal waves of gene expression from biological clocks in the leaf. *Proceedings of the National Academy of Sciences*, 109(17):6757–6762, 2012.

[210] Tanya L Leise, Connie W Wang, Paula J Gitis, and David K Welsh. Persistent cell-autonomous circadian oscillations in fibroblasts revealed by six-week single-cell imaging of per2:: Luc bioluminescence. *PloS one*, 7(3):e33334, 2012.

[211] Hartmut Löwen, Jean-Pierre Hansen, and Jean-Noël Roux. Brownian dynamics and kinetic glass transition in colloidal suspensions. *Physical Review A*, 44(2):1169, 1991.

[212] W Schaertl and H Sillescu. Brownian dynamics of polydisperse colloidal hard spheres: Equilibrium structures and random close packings. *Journal of Statistical Physics*, 77(5-6):1007–1025, 1994.

[213] B Cichocki, BU Felderhof, K Hinsen, E Wajnryb, and J Bl/awzdziewicz. Friction and mobility of many spheres in stokes flow. *The Journal of chemical physics*, 100(5):3780–3790, 1994.

[214] P Strating. Brownian dynamics simulation of a hard-sphere suspension. *Physical Review E*, 59(2):2175, 1999.

[215] B Doliwa and Andreas Heuer. Cage effect, local anisotropies, and dynamic heterogeneities at the glass transition: A computer study of hard spheres. *Physical review letters*, 80(22):4915, 1998.

[216] Stefan Auer and Daan Frenkel. Prediction of absolute crystal-nucleation rate in hard-sphere colloids. *Nature*, 409(6823):1020, 2001.

[217] Stefan Auer and Daan Frenkel. Numerical prediction of absolute crystallization rates in hard-sphere colloids. *The Journal of chemical physics*, 120(6):3015–3029, 2004.

[218] Grzegorz Wieczorek and Piotr Zielenkiewicz. Influence of macromolecular crowding on protein-protein association rates—a brownian dynamics study. *Biophysical journal*, 95(11):5030–5036, 2008.

[219] Justin R Houser, David J Busch, David R Bell, Brian Li, Pengyu Ren, and Jeanne C Stachowiak. The impact of physiological crowding on the diffusivity of membrane bound proteins. *Soft matter*, 12(7):2127–2134, 2016.

[220] Jason Seth Rothman, Laszlo Kocsis, Etienne Herzog, Zoltan Nusser, and Robin Angus Silver. Physical determinants of vesicle mobility and supply at a central synapse. *eLife*, 5, 2016.

[221] Christian L Vestergaard, Paul C Blainey, and Henrik Flyvbjerg. Optimal estimation of diffusion coefficients from single-particle trajectories. *Physical Review E*, 89(2):022726, 2014.

[222] R Grima. Intrinsic biochemical noise in crowded intracellular conditions. *The Journal of Chemical Physics*, 132(18):05B604, 2010.

[223] JA Valkenburg and CL Woldringh. Phase separation between nucleoid and cytoplasm in escherichia coli as defined by immersive refractometry. *Journal of bacteriology*, 160(3):1151–1157, 1984.

[224] Anne-Sophie Coquel, Jean-Pascal Jacob, Maël Primet, Alice Demarez, Mariella Dimiccoli, Thomas Julou, Lionel Moisan, Ariel B Lindner, and Hugues Berry. Localization of protein aggregation in escherichia coli is governed by diffusion and nucleoid macromolecular crowding effect. *PLoS computational biology*, 9(4):e1003038, 2013.

[225] Jacek T Mika and Bert Poolman. Macromolecule diffusion and confinement in prokaryotic cells. *Current opinion in biotechnology*, 22(1):117–126, 2011.

[226] Jay K Fisher, Aude Bourniquel, Guillaume Witz, Beth Weiner, Mara Prentiss, and Nancy Kleckner. Four-dimensional imaging of e. coli nucleoid organization and dynamics in living cells. *Cell*, 153(4):882–895, 2013.

[227] Harry Walter and Donald E Brooks. Phase separation in cytoplasm, due to macromolecular crowding, is the basis for microcompartmentation. *FEBS letters*, 361(2-3):135–139, 1995.

[228] Satya Nanda Vel Arjunan and Masaru Tomita. A new multicompartmental reaction-diffusion modeling method links transient membrane attachment of e. coli mine to e-ring formation. *Systems and synthetic biology*, 4(1):35–53, 2010.

[229] Catherine J Penington, Barry D Hughes, and Kerry A Landman. Building macroscale models from microscale probabilistic models: a general probabilistic approach for nonlinear diffusion and multispecies phenomena. *Physical Review E*, 84(4):041120, 2011.

[230] Angela Stevens and Hans G Othmer. Aggregation, blowup, and collapse: the abc's of taxis in reinforced random walks. *SIAM Journal on Applied Mathematics*, 57(4):1044–1081, 1997.

[231] Kevin J Painter and Thomas Hillen. Volume-filling and quorum-sensing in models for chemosensitive movement. *Can. Appl. Math. Quart*, 10(4):501–543, 2002.

[232] Maike MK Hansen, Lenny HH Meijer, Evan Spruijt, Roel JM Maas, Marta Ventosa Rosquelles, Joost Groen, Hans A Heus, and Wilhelm TS Huck. Macromolecular crowding creates heterogeneous environments of gene expression in picolitre droplets. *Nature nanotechnology*, 11(2):191, 2016.

[233] Paula Montero Llopis, Audrey F Jackson, Oleksii Sliusarenko, Ivan Surovtsev, Jennifer Heinritz, Thierry Emonet, and Christine Jacobs-Wagner. Spatial organization of the flow of genetic information in bacteria. *Nature*, 466(7302):77, 2010.

[234] Mark B Flegg. Smoluchowski reaction kinetics for reactions of any order. *SIAM Journal on Applied Mathematics*, 76(4):1403–1432, 2016.